AN ABSTRACT OF THE THESIS OF

Jeffery J. Ninnemann for the degree of Master of Science in Geology presented on March 16, 2005.

Title: A Study of Hyporheic Characteristics Along a Longitudinal Profile of Lookout Creek, Oregon

Abstract approved:

Roy D. Haggerty

The primary goal of this research project is to quantitatively measure the temporal scales of hyporheic exchange along a stream network. Our goal is to examine how hyporheic exchange varies with increasing stream size. Many previous studies focus on single stream reaches or on several reaches of similar sized streams, whereas we examine the residence time of water in the hyporheic zone over increasing length scales in a single stream. Prior work with tracer data and analysis using a transient storage model with an exponential residence time distribution (RTD) suggests that hyporheic parameters, primarily volume and mean residence time, are both spatially and temporally scale-dependent. However, recent work hypothesizes that the scale-dependence may be partially addressed by using a power-law RTD (Haggerty et al., 2002). Our research tests this hypothesis with multi-scale tracer tests.

A single, multi-scale tracer test was conducted in Lookout Creek, Oregon, to test the power-law RTD model and to examine hyporheic scaling relationships along the length of the stream, from its 2nd-order headwaters through its 5th-order mainstem. The longitudinal tracer test (LTT) involved an in-stream injection of Rhodamine WT (RWT) over 77 h, followed by monitoring at seven downstream locations for five months. Three additional intra-order tracer tests (IOTT's) were carried out, between each of the major stream confluences along Lookout Creek. The intra-order tests were conducted to quantify the behavior of the hyporheic RTD and to separate geomorphic variability from other possible scale-dependent factors.

The results from the longitudinal and IOTT's clearly demonstrate power-law RTDs, but not a "universal", basin-wide RTD. The use of a power-law RTD to

characterize the hyporheic zone reduced the scale-dependency of tracer tests results compared to an exponential RTD, but did not eliminate it. The exponent of the power-law characterizes the variance of the RTD and changes along the length of the stream, as do other parameters. The upper reaches of Lookout Cr. appear to have a distinct power-law RTD when compared to the lower reaches of the basin and may result from changes in geomorphology or the degree of geomorphic complexity. Larger 4th and 5th order streams exhibit a slightly longer delay before assuming a power-law distribution when compared to the smaller 2nd and 3rd order streams.

A Study of Hyporheic Characteristics Along a Longitudinal Profile of Lookout Creek, Oregon

by
Jeffery J. Ninnemann

A THESIS

submitted to

Oregon State University

in partial fulfillment of
the requirements for the
degree of

Master of Science

Presented March 16, 2005
Commencement June 2005

Master of Science thesis of Jeffery J. Ninnemann presented on March 16, 2005.

APPROVED:

Major Professor, representing Geology

Chair of the Department of Geosciences

Dean of Graduate School

I understand that my thesis will become part of the permanent collection of Oregon State University libraries. My signature below authorizes release of my thesis to any reader upon request.

Jeffery J. Ninnemann, Author

ACKNOWLEDGMENTS

Due to the large amount of technical assistance, field logistics, and the equipment needed to conduct my research, I owe a debt of gratitude to a number of people and organizations, including: Oregon State University, H.J. Andrews Experimental Forest, U.S. Forest Service Pacific Northwest Research Station, National Science Foundation, Roy Haggerty, Mike Gooseff, Steven Wondzell, Julia Jones, Stephen Lancaster, Jeff McDonnell, Kelly Falkner, John Selker, Jim Wigington, Justin LaNier, Fred Swanson, Charles Fardy, Laura Symmes, David Rupp, Jim Mayo, Becky Flitcroft, Louis Arighi, Scott English, Kevin McGuire, Mark Harmon, Sherri Johnson, Randy Wildman, Stan Gregory, Bonnie West, Jennifer Lupin, Willem Van Verseveld, John Faustini, and others that helped throughout the summer. This work was partially supported by the National Science Foundation through grant nos. EAR 99-09564 and DEB 0218088.

Any opinions, findings, and conclusions or recommendations expressed in this thesis are those of the author and do not necessarily reflect the views of the National Science Foundation.

Special thanks must go to my loving wife Kimberly and sons Elijahwa and Isaac, without which this thesis and much of my work would not be possible.

TABLE OF CONTENTS

TABLE OF CONTENTS (Continued)

Page

LIST OF TABLES

LIST OF FIGURES

LIST OF FIGURES (Continued)

LIST OF FIGURES (Continued)

LIST OF FIGURES (Continued)

LIST OF EQUATIONS

A STUDY OF HYPORHEIC CHARACTERISTICS ALONG A LONGITUDINAL PROFILE OF LOOKOUT CREEK, OREGON

1.0 INTRODUCTION

The "river continuum" and the "hyporheic corridor" concepts propose that the physical and ecological characteristics of a stream have definable qualities in relation to their position in the network and that the hyporheic zone is an extension of the stream continuum (Vannote et al., 1980; Stanford and Ward, 1993). As the river progresses from a small, steep gradient, constrained headwater stream to a large, shallow gradient meandering river, its characteristics gradually change. Some of a river's characteristics such as width, depth, velocity and mean hyporheic residence time change as a function of position and extent of observation within the river network (Blöschl and Sivapalan, 1995; Choi et al., 2000). By conducting longitudinal studies that characterize the physical processes of the river continuum over significant changes in stream size, scale dependent characteristics can be quantified and described.

Our understanding of the processes that are operating in natural systems is dependent on the spatial and temporal scales of study. Throughout this paper the term scaling refers to a reduction or increase in size. In the hydrologic context, scaling up and down refers to the transfer of information to a larger scale or smaller scale, respectively (Blöschl and Sivapalan, 1995). Scale-dependency of natural systems refers to the relationship that develops when the measurement of one physical value is dependent on the scale of measurement. Mandelbrot (1967) described a classic example of scale-dependency while explaining fractals and how they relate to the measurement of the length of the coastline of England. The length of the coastline of England is dependent on the scale of measurement: if one measures with a ruler that is 1 km long one gets a value that accounts for most of the large bays and inlets of the coastline. However, if one measures with a ruler 1 m long, the nooks, spits and beach curves are added in and yield a much longer coastline. As one increases the precision of the measuring instrument the

measured value also increases. The coastline can be considered a fractal system, which is a mathematical object that is "self-similar" over a range of scales (Mandelbrot, 1967). For example, the 1 km ruler measures the large bays and estuaries in the same way that the 1 m ruler measures the nooks, spits and beach curves. This fractal scaling of measured length with ruler length can be expressed mathematically using a power-law function, as represented in Equation 1 (Mandelbrot, 1982; Feder, 1988; Meakin, 1998).

Equation 1 (Power-law)

$$f(x) = y * x^k,$$

where x and y represent variables and k is a constant.

One of the physical features of the river continuum that appears scale dependent is the hyporheic zone. The hyporheic zone is the subsurface region below or adjacent to a stream, bounded by the flow paths that travel from the stream through the subsurface and eventually return to the stream (Bencala et al., 1993; Harvey and Bencala, 1993; Wagner and Harvey, 1997; Fernald et al., 2001). The flow paths of the hyporheic zone can be simulated with hyporheic residence time studies. Many hyporheic residence time studies have been conducted within individual stream reaches or grouped within one part of the river continuum. However, to our knowledge no hyporheic studies have been performed over reaches that exhibit significant increases in stream magnitude along the river continuum.

Our study of hyporheic exchange in a river continuum that increases in basin area from approximately 3.8 km^2 to 64 km^2 will help to understand how the physical processes of the hyporheic zone change, the influence that the stream network has on those changes, and how the changes will influence the ecology of the stream. The increases in stream magnitude will be quantified by up-slope contributing area and increases in stream order will be measured using Strahler's hierarchical classification system (Strahler, 1964).

Many geomorphic and hydrologic studies have examined the relationships between scale and process (Wolman and Miller, 1960; Pickens and Grisak, 1981; Neuman, 1990; Blöschl and Sivapalan, 1995; Choi et al., 2000; Jackson and Sturm, 2002). Some of the geomorphic studies have demonstrated that geomorphic features are principle factors in hyporheic exchange and these features tend to vary in size and spacing within stream networks (Wolman and Miller, 1960; Langbein and Leopold, 1964; Schumm and Lichty, 1965; Knighton, 1984; Swanson et al., 1986; Montgomery and Buffington, 1997; Nakamura et al., 2000; Kasahara and Wondzell, 2003). Further studies have shown that the complexities in depositional processes result in spatial variation in hydraulic conductivity, which causes dispersion in aquifer water to vary according to the size of the study domain (Pikens and Grisak, 1981; Neuman, 1990).

Several hyporheic studies have shown the hyporheic residence time is scale dependent while using the conventional methods (Harvey and Wagner, 2000; Harvey et al., 2000; Haggerty et al., 2002; Schummer et al., 2003; Haggerty et al., 2004). The conventional method for quantifying the hyporheic zone usually involves a solute tracer test, which is analyzed using an advection-dispersion-mass transfer model that assumes an exponential residence time distribution (Bencala et al., 1983; Bencala and Walters, 1983; Jackman et al., 1984; Triska et al., 1989; Stanford and Ward, 1993; Valett et al., 1993; White, 1993; Harvey et al., 1996 a; Harvey et al., 1996 b; Wondzell and Swanson, 1996 a; Wondzell and Swanson, 1996 b; Wondzell and Swanson, 1999; Fernald et al., 2001). The scale-dependence of hyporheic exchange may be explained by examining hyporheic flow over increasingly longer lengths of the stream. As the stream length increases, the water experiences a greater amount of geomorphic and depositional variability, which results in exposure to a greater amount of variation in hydrologic properties, such as hydraulic conductivity, effective porosity, flow-path length, recharge inputs, and others. In longer reaches, hyporheic flow experiences a wider range of hydraulic conductivities and, thus, greater dispersion and changes in effective hydraulic parameters (Pickens and Grisak, 1981; Neuman, 1990). In hydrology, as the length, area, or volume of the observed system is increased from a small scale,

ranging from 1 m^2 plots and 100 m^2 sub reaches, to a larger scale such as a basins on the order of 1 km^2, the fluid flow experiences continuous spatial variations in hydraulic properties which cause the hydraulic parameters to behave in a scale-dependent way (e.g., scale-dependent dispersion and dispersivity) (Pikens and Grisak, 1981; Neuman, 1990; Blöschl and Sivapalan, 1995). For example a tracer test conducted at the drainage basin scale, compared to a test completed at 1/10 of that basin length, may result in an increase in the dispersion of the tracer. Increased dispersion may stem from increases in the longest residence times as well as an increase in the mean residence time in the hyporheic zone.

We hypothesize that residence time distributions of hyporheic exchange in mountain streams are fractal and can be described with one power-law function over a small basin. Furthermore we hypothesize that the use of a power-law residence time distribution to characterize the hyporheic residence times will reduce or eliminate the scale-dependency associated with describing the hyporheic zone with an exponential residence time distribution. A basin-wide tracer test, which spans an increase in length from approximately 1,000 m to 14,300 m and advection time scales of 0.5 h to 48 h will test these hypotheses.

In this study, we conducted a longitudinal tracer test and numerous intra-order tracer tests within the main stem of Lookout Creek at the H.J. Andrews Experimental Research Forest, Oregon. The primary tracer test was a longitudinal test that began near the headwaters of Lookout Creek and extended to the outlet of the basin. The longitudinal tracer test (LTT) encompassed an increase in both drainage area and stream length. Three intra-order tracer tests (IOTT's) were conducted between each of the major confluences where Lookout Creek increased in stream order. Intra-order tracer tests were defined by being between the 2nd and 3rd order, 3rd and 4th order, and the 4th and 5th order as described by Strahler's hierarchical classification system (Strahler, 1964). These tracer tests allowed the RTDs of the stream to be measured. The information gained from concentration breakthrough curves and concentration profiles during the tests allowed the hyporheic parameters along the main stem of Lookout Creek to be estimated and

relationships between longitudinal residence times and basin areas ranging from 3.8 km^2 to 61 km^2 to be identified.

The IOTT's were conducted in addition to the LTT to allow us to corroborate the findings of the single LTT with separate injections. A power-law distribution at several stream sizes long the same stream would support a power-law RTD for the entire basin, if the distribution had the same descriptive power-law exponent. However, if the smaller tests did not display power-law behavior, it would indicate that the power-law did not appear until the water had traveled a longer distance than the intra-order reach lengths. Alternatively, observed power-law behavior along the entire 14 km reach length could have been the result of the influence of a particular portion of the stream in the upper reaches of the basin. In effect, an upstream reach with a strong power-law behavior may create a power law "echo" that is propagated downstream and recorded at lower monitoring sites during a single injection test. The IOTT tests helped to verify whether certain geomorphic stream types could exhibit a strong power-law behavior that controlled the downstream concentrations in the LTT. The smaller IOTT's further helped us to separate the behaviors of hyporheic exchange that are caused by spatial and temporal increases in the stream and the behavior that is caused by changes in geomorphology along Lookout Creek.

This study is a link in a larger effort to describe the movement of water through the entire Lookout Creek basin as well as mountain basins in general. Other researchers are trying to quantify basin-wide hillslope hydrologic processes to expand our understanding of these processes from the plot scale to the basin scale (McDonnell, 1990; Jones and Grant, 1996; Wemple et al., 1996; Cirmo and McDonnell, 1997; Jones et al., 2000; Jones, 2000; Bond et al., 2002; McGuire et al., 2002; Vitar et al., 2002; Bond, 2003; McDonnell, 2003; Seibert et al., 2003; Weiler et al., in press). A basin-wide hyporheic scaling relationship would complement the hillslope studies by linking stream hydrology to the watershed at the network scale.

This study will enable researchers to better relate data obtained from the stream at the basin outlet to processes in the basin as a whole. Researchers

looking at basin-wide ecological and anthropogenic processes have suggested that the transport properties of the stream have important implications to these systems. For example, several studies suggest that hydrologic properties of headwater basins may affect the downstream response to flooding and the water availability for people, plants, and wildlife (Swanson et al., 1986; Jones and Grant, 1996; Poff et al., 1997; Wondzell and Swanson, 1999; Nakamura et al., 2000; Wemple et al., 2001; Malcolm et al., 2002). Furthermore, basin-wide hyporheic exchange has been shown to influence a wide range of other processes including nutrient allocations, biotic refuges, pollution filtration, and temperature regimes of the stream, which can affect the local environment and/or have a cascading effect downstream (Triska et al., 1989; White, 1990; Stanford and Ward, 1993; Stanley and Boulton, 1993; Williams, 1993; Findlay, 1995; Jones et al., 1995;Valet et al., 1996; Fernald et al., 2000; Franken et al., 2001). Lastly, the stream is the integrator of all upstream processes. To use the stream to understand hillslope processes, it is critical that we understand the in-stream processes, which are the integrating function. By understanding how water behaves on a basin-wide scale we can better protect, preserve, conserve, and utilize our forest environments.

2.0 BACKGROUND

The hyporheic zone is a dynamic component of the river network both physically and ecologically. Tracer tests have been used to advance the understanding of the residence time, volume, and distribution of hydraulic flow paths through this zone (Bencala et al., 1983; Bencala and Walters, 1983; Jackman et al., 1984; Triska et al., 1989; Stanford and Ward, 1993; Valett et al., 1993; White, 1993; Harvey et al., 1996 a; Harvey et al., 1996 b; Wondzell and Swanson, 1996 a; Wondzell and Swanson, 1996 b; Wondzell and Swanson, 1999; Fernald et al., 2001; Haggerty et al., 2002). These tests have investigated a range of river sizes from small headwater streams to large, continent-draining rivers and have examined the stream network at scales ranging from less than 1 m to 78 km (Sanchez-Cabeza and Pujol, 1999; Hinkle et al., 2001; Laenen and Bencala, 2001;

Wörman et al., 2002; Kasahara and Wondzell, 2003; Storey et al., 2003). However, all of the tests have been conducted within reaches that do not increase significantly in stream magnitude.

It has been proposed that most physical characteristics of river networks approach a graded profile that is in a state of dynamic equilibrium with respect to time and location within the river network (Leopold and Maddock, 1953; Leopold and Langbein, 1962; Langbein and Leopold, 1964; Knighton, 1984; Merigliano, 1997). The river continuum concept expands on the stream's physical character and states that in extended river networks, biological communities should become established that approach equilibrium with the dynamic physical conditions of the channel (Vannote et al., 1980). If the hyporheic zone is part of this continuum, then it too should show a similar pattern of change in physical and ecological character. The hyporheic corridor concept addresses this issue by connecting the hyporheic zone to the river continuum through channel morphology and likens its character to a "bead necklace", expanding and contracting with geologic constraints (Stanford and Ward, 1993).

The hyporheic zone is a region of transient storage that is defined by flow paths that originate in the stream, travel through an aquifer adjacent to the stream, and then return to the stream (Bencala et al., 1983; Jackman et al., 1984; Bencala et al., 1993; Harvey et al., 1996 a; Harvey et al., 1996 b; Fernald et al., 2001). This zone of storage can extend vertically several meters and laterally from centimeters to kilometers, depending on the system (Stanford and Ward, 1993; Wondzell and Swanson, 1996 a; Wondzell and Swanson, 1999). Hyporheic exchange between the stream and the subsurface is controlled by surface topography, stream discharge, and hydraulic characteristics of the substrate, i.e. whether the substrate is bedrock or alluvium and the how much alluvium is present (Harvey and Bencala, 1993; Henry et al., 1994; Valettet al., 1996; Wondzell and Swanson, 1996 a; Fernald et al., 2001; Marion et al., 2002; White, 2002; Kasahara and Wondzell, 2003; Wondzell, in press). One of the standard practices in measuring the parameters of the hyporheic zone is to use a tracer test and an advection-dispersion-mass-transfer-model, which simulates transport and the exchange

between surface and subsurface flow (Bencala et al., 1993; Harvey et al., 1996 a; Harvey et al., 1996 b; Wagner and Harvey, 1997; Fernald et al., 2001). The most common model is the One-Dimensional Transport with Inflow and Storage (OTIS). OTIS solves standard transient storage equations using the properties of the stream and the conservation of mass through time as described in the equations below: (Bencala et al., 1983; Bencala et al., 1993)

Equation 2 (in-stream)

$$\frac{\partial C}{\partial t} = -\frac{Q}{A}\frac{\partial C}{\partial x} + D\frac{\partial^2 C}{\partial x^2} - \frac{A_s}{A}\frac{dC_s}{dt}$$

Equation 3 (in-storage zone)

$$\frac{\partial C_s}{\partial t} = \alpha\frac{A}{A_s}(C - C_s),$$

where C is the concentration (µg/L) of solute in the main channel, C_s is the concentration (µg/L) of solute in the storage zone, t is time, Q is the stream discharge (m^3/s), A is the cross sectional area of the stream (m^2), A_s is the cross sectional area of the storage zone (m^2), x is the downstream distance (m), D is the dispersion coefficient (m^2/s), and α is the first order storage zone exchange coefficient (1/s), which is inversely proportional to the mean residence time.

The conventional transient storage parameters are measured by injecting a conservative tracer and monitoring the concentrations at a designated distance downstream. The resulting concentration curves allow the volume and mean residence time of the hyporheic flow paths to be modeled. The tracer test method has been thought to represent the majority of hyporheic flow under low-discharge, steady-state conditions (Harvey et al., 1996 a; Harvey et al., 1996 b). However, the uncertainty in this technique increases when trying to measure longer flow paths, and the experimental methods must be tailored for the situation (Harvey et al.,

1996 a). High-discharge scenarios also increase the amount of uncertainty in the tracer test (Harvey et al., 1996 a).

The standard mass balance equations (Equations 2 and 3) assume that hyporheic residence times are exponentially distributed. Figure 1 shows a comparison of a breakthrough curve of a tracer test modeled with the conventional exponential distribution and the same tracer test modeled with power-law distribution that will be discussed later; both are shown in log-log space. Although the exponential distribution models the concentrations from breakthrough to peak accurately, relative error is much larger for late-time concentrations after the peak (Figure 1) (Gooseff et al., 2003). It has also been shown that the conventional exponential model estimates a mean hyporheic residence time that may be dependent on the mean channel residence time (Harvey et al., 2000; Haggerty et al., 2002; Schummer et al., 2003; Haggerty et al., 2004). In Figure 2 the relationship between mean channel residence time and the mean hyporheic residence time, which has been estimated using the conventional exponential models is presented using data from multiple tracer test results and compiled by Harvey and Wagner (2000). This relationship illustrates the sensitivity that the conventional exponential model has to scale. Depending on the size of the experimental reach the conventional model tends to give a different value. If a tracer test is conducted over a short reach, then shorter residence times are recorded with a relatively small mean residence time and conversely, if a tracer test is conducted over a long reach, then longer flow paths are measured with a larger mean residence time. This is may represent a fractal property, in that the value of the observed property depends on the size of the observation (Mandelbrot, 1967).

Figure 1. Observed concentration curves for RWT tracer test conducted on Lookout Creek below Mack Creek, A) fitted simulation curve using the conventional exponential model, B) fitted simulation curve using a power-law STAMMT-L model. (Gooseff et al., 2003)

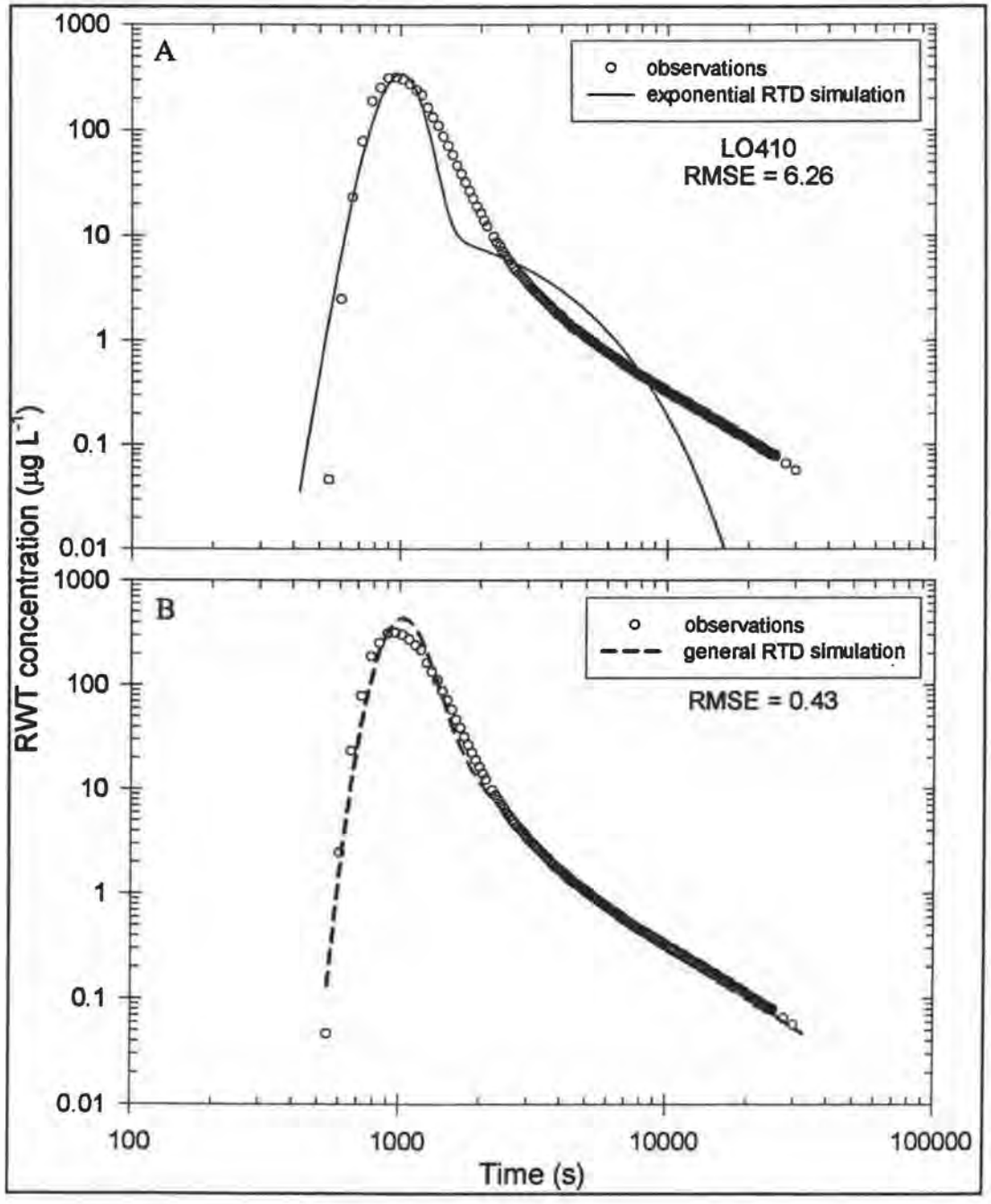

Figure 2. Scaling relationship between mean channel residence time and the mean hyporheic residence time estimated using the conventional exponential mass balance equation and presented by Harvey and Wagner (2000) using multiple tracer tests results.

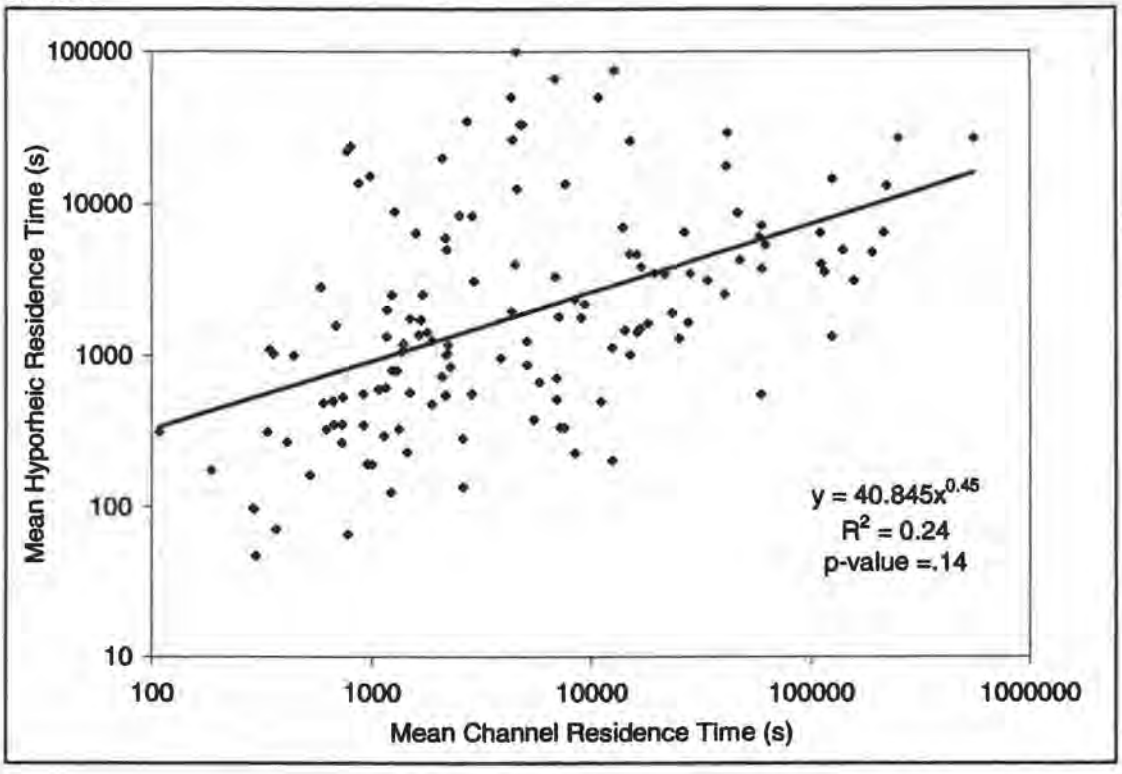

A new approach has been developed that allows the use of any density function in place of the exponential function. Use of a power-law function instead of the exponential function has been found to achieve a better late-time arrival fit (Figure 1) (Haggerty et al., 2002; Gooseff et al., 2003; Schummer et al., 2003; Haggerty et al., 2004), and should reduce scale-dependency if our hypothesis is correct. A new model, the Solute Transport and Multi-rate Mass Transfer-Linear coordinates model (STAMMT-L), allows the use of an exponential RTD, but also allows flexibility for other RTDs (Haggerty et al., 2000; Cvetkovic and Haggerty, 2002; Haggerty and Reeves, 2002; Haggerty et al., 2002). The density function (referred to as the hyporheic memory function, $g^*(t)$) that is embedded in STAMMT-L is the density probability that a molecule of water that enters the hyporheic zone at time $t = 0$ will remain in the subsurface at any later time t. This density function can take on the form of whatever function best represents the RTD. The equations

that describe the advection and dispersion with a general residence time in the STAMMT-L model are shown below (Haggerty et al., 2000):

Equation 4 (STAMMT-L in-Stream)

$$\frac{\partial C}{\partial t} = -v\frac{\partial C}{\partial x} + D\frac{\partial^2 C}{\partial x^2} - \beta_{tot}\frac{dC_s}{dt}$$

Equation 5 (STAMMT-L in-storage zone)

$$\frac{\partial C_s}{\partial t} = \int_0^t \frac{\partial C(t-\tau)}{\partial t} g^*(\tau) d\tau ,$$

where, v is the mean advection velocity (m/s) and equivalent to Q/A in Equation 2, β_{tot} is the ratio of storage to stream volume (m^3/m^3) and is equivalent to A_s/A in Equation 2, $g^*(t)$ (s^{-1}) is commonly defined as a exponential distribution of residence times, τ is a lag time (s). Equation 4 and Equation 5 are equivalent to Equation 2 and Equation 3, if Equation 6 is true:

Equation 6 (hyporheic memory function)

$$g^*(\tau) = \alpha^* \exp(-\alpha\tau)$$

The STAMMT-L model has the potential to increase the accuracy of modeling transient storage and improve spatial scaling if the correct hyporheic memory function is used. One possibility, advocated by Haggerty et al., 2002 (but also Schummer et al., 2003, and similar to Wörman et al., 2002, and others) is to employ a hyporheic memory function that gives some fractal properties to the model. Using a truncated power-law for the memory function is one way of giving some fractal properties to the model. In Equation 7 the memory function takes the form of a truncated power-law function by using a summation of exponential residence time distributions (Haggerty et al., 2002).

Equation 7 (Power-law hyporheic memory function)

$$g^*(\tau) = \int_{\alpha_{min}}^{\alpha_{max}} \frac{(k-2)\alpha^{k-2}e^{-\alpha \cdot t}}{\alpha_{max}^{k-2} - \alpha_{min}^{k-2}} d\alpha ,$$

where k is the characteristic slope of the breakthrough curve tail (after a pulse injection) in log-log space, α_{max} is the inverse of the minimum exchange time in the hyporheic zone, and α_{min} is the inverse of the maximum exchange time in the hyporheic zone. Note that to a first approximation Equation 7 has $g^*(t) \sim t^{1-k}$ for $\alpha_{max}^{-1} << \alpha_{min}^{-1}$. For a more complete description see Haggerty et al. (2002).

The power-law exponent that best fits the tail observed in concentration breakthrough curves can be used to characterize the power-law memory function. This power-law exponent can be easily observed in the slope (k) of the late-time breakthrough curve in log-log space. Throughout this paper the power-law exponent and the slope (k) will be discussed in terms of their absolute values. The slope of the power-law is a function of the large variance of residence times within the hyporheic zone at each location within the basin. Relative to each other a shallow slope to the power-law corresponds to a large variance of residence times and a steep slope signifies a small variance of residence times. A hyporheic system with a large amount of heterogeneity in substrate porosity, bedform, hydraulic gradients, geomorphology, etc. would be expected to have a shallow power-law slope (small power-law exponent). Likewise a hyporheic system that had relatively homogeneous physical hydrologic characteristics would be expected to have a steep power-law slope (large power-law exponent).

If the fractal relationship is manifest at one spatial scale, then it may be manifested at all spatial scales. However, fractal behavior may be limited to a critical spatial or temporal value that is controlled by the geomorphologic type or set of types within the basin. In order to evaluate these modeling issues a basin-wide longitudinal tracer test was conducted through multiple scales.

In several recent studies the new transient storage model, which uses a power-law memory function, was used to show that a power-law behavior explained the hyporheic residence time with greater accuracy than the exponential model (Figure

1) (Haggerty et al., 2002; Schummer et al., 2003). The use of the new transient storage model has been shown to be effective at estimating the late time behavior of RTDs for different geomorphic features and shows a greater sensitivity to longer residence times than the conventional model (Gooseff et al., 2003).

Rhodamine WT (RWT) was chosen for this study because of its low detection, low-toxicity, stability under environmental conditions, and its successful use and history in other tracer studies (Bencala et al., 1983; Derouane and Dassargues, 1998; Fox et al., 1991; Gooseff et al., 2003; Haggerty et al., 2000; Haggerty et al., 2002; Jensen and Kristensen, 1989; Kass, 1994; Pang et al., 1998; Pang and Close, 1999; Siton et al., 1997; Smart and Smith, 1976; Smart and Laidlaw, 1977; Stutter et al., 2001; Tai and Rathbun, 1988; Turner Designs, 1998a). The tendency for RWT to sorb to clay minerals, iron minerals and organic matter is a significant drawback to its use (Bencala et al., 1983; Stutter et al., 2001; Tai and Rathbun, 1988; Trudgill, 1987). However, the advantages to using RWT were judged to be greater than the drawbacks. For more details about the tracer dye, see Appendix I.

The tracer tests conducted for this study were completed in the H.J. Andrews Experimental Forest. The H.J. Andrews is located in the western Cascade Range of Oregon and encompasses the 6400-hectare drainage basin of Lookout Creek, a tributary of Blue River and the McKenzie River. Figure 3 below shows a map of the Lookout Creek basin and the locations on Lookout Creek of all of the monitoring and injection sites for this study. Ten gauged watersheds within the H.J. Andrews are shown in Figure 3, watershed #4 is considered the entire Lookout Cr. watershed and watershed #5 is called the Mack watershed. Elevations range from 410 m to 1630 m. The ecology is broadly representative of the region's conifer forests and associated wildlife. The forest structure is primarily Douglas fir (*Pseudotsuga menziesil*), Western Hemlock (*Tsuga heterophylla*), and Western Red Cedar (*Thuja plicata*) in the lower elevations and Noble fir (*Abies procera*), Pacific fir (*Abies amabilis*), Douglas fir (*Pseudotsuga menziesil*) and Western Hemlock (*Tsuga heterophylla*), in the upper elevations. Since its establishment in 1948, approximately 30% of the watershed has been harvested according to the practices of the day (Andrews Experimental Forest, 2003).

Figure 3. Map of the H.J. Andrews Experimental Research Forest, Oregon, illustrating the boundaries of the Lookout Creek Basin, the Lookout Cr. stream network, and the site location for the Longitudinal Tracer Test conducted during the summer of 2003.

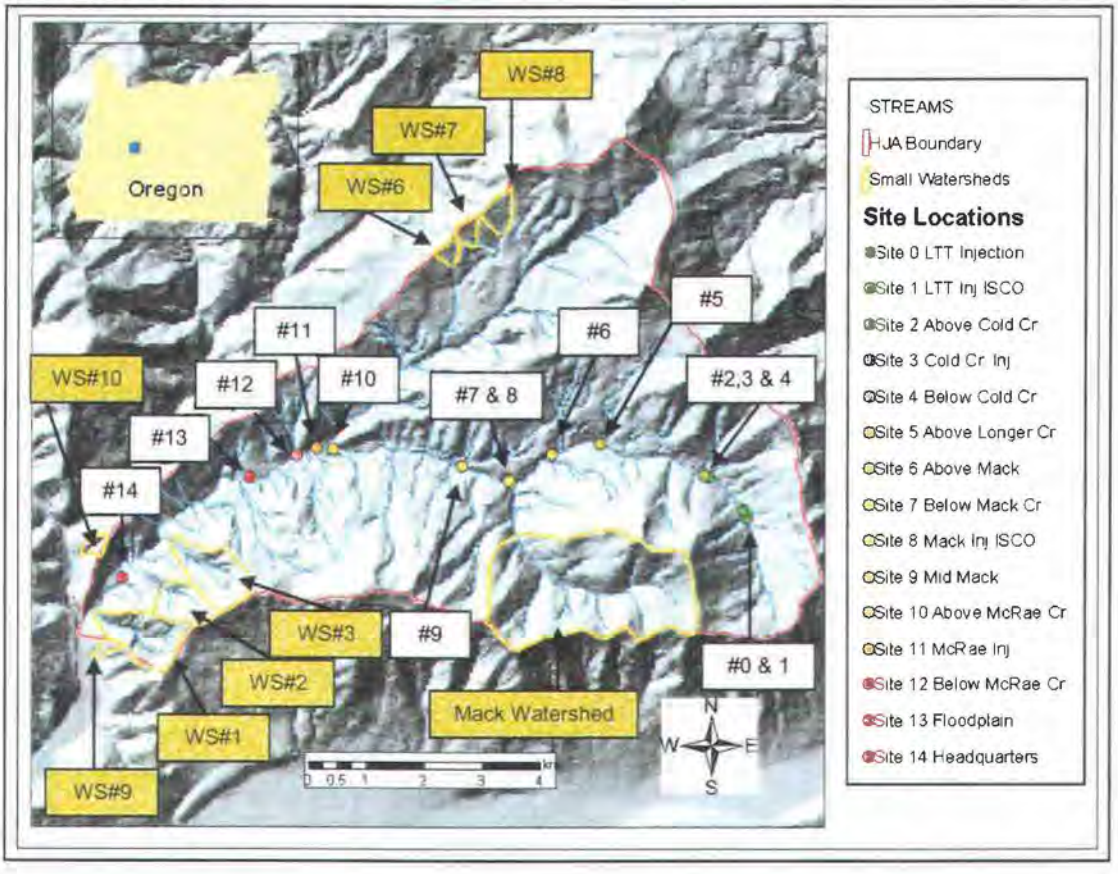

The geology below approximately 850 m elevation consists of Oligocene to Lower Miocene volcanic rocks composed of mudflows, ash flows, and stream deposits, and above 850 m the formations consist of andesite lava flows of Miocene age and more recent High Cascade volcanic rocks (Swanson and James, 1975; Andrews Experimental Forest, 2003). The landscape is generally mountainous terrain with stream erosion, landslides, and past glaciations influencing the stream geomorphology. Many of the tributaries to Lookout Cr., McRae Cr., and Mack Cr. have predominately steep valleys with narrow ridges carved by fluvial processes and have an average slope of 30-35° (Swanson and Jones, 2002). Several large earth flows, dozens of debris flows, and debris slides have given the basin a diverse geomorphic character. One large earth flow is

responsible for constricting the main stem of Lookout Creek approximately 1.5 km downstream from the McRae Cr. confluence. The constriction in the valley has contributed alluviation and concomitant valley widening that extends above McRae Cr. The general fluvial geomorphology varies according to location within the basin and position within the stream network. Some 1st and 2nd order tributaries are steep, narrow, and scoured by debris flows. In other parts of the basin, particularly in the 2nd, 3rd, 4th, and 5th order stream reaches, wide alluvial flood plains have accumulated behind debris dams and obstructions (Swanson and Jones, 2002). The dominant morphology of the stream network is the boulder/cobble-dominated stepped-pool sequence and steep channel units (Grant et al., 1990). The step-pool morphology dominates above Mack Cr. Below Mack Cr. the morphology gradually changes to a cobble-dominated cascade/riffle morphology.

The climate regime includes a wet and mild winter and dry and cool summer. The mean monthly temperature in the lower elevations (430 m) is 1 °C in January and 18 °C in July. Precipitation primarily occurs from fall to spring. The average precipitation is 230 cm at the lower elevations, falling mostly as rain, and 335 cm in the higher elevations, with a contribution coming from snow. Stream discharge averages 56% of the precipitation, but ranges from 40% to 70% (Swanson and Jones, 2002). The maximum discharge usually occurs during the winter and is three orders of magnitude larger than the summer minimums (Andrews Experimental Forest, 2003). The maximum and minimum recorded discharge at the USGS gauge located near the mouth of the basin on Lookout Cr. was ~226,500 L/s on February 7, 1996 and 136 L/s on September 16 and 17, 1981 respectively. The mean annual discharge at the Lookout Cr. gauge between 1950 and 2002 is ~3,400 L/s with a specific discharge of 54.5 L/s/km^2 (USGS, 2004).

3.0 METHODS

We initiated a LTT on Lookout Creek on June 14th, 2003. This involved injecting RWT at Site 1, shown in Figure 3. The RWT injections were held at an average in-stream concentration of 172 µg/L ± 24 µg/L, with an average pumping rate of 0.46 mL/s or 5786 µg /s for RWT for 77 h. The injection was facilitated by a Fluid Meter Inc. (FMI) DC injection pump (model # RHB1). The discharge in the stream was measured using a Marsh-McBirney, Inc. Flo-Mate™ flow meter and averaged 20.9 L/s ± 3 L/s over the duration of the injection. The concentration of RWT was measured longitudinally at eight locations using Turner Design™ model 10-AU fluorometers and Teledyne ISCO™ samplers (models 2900 and 3700 standard) (Figure 4). The fluorometers recorded RWT concentrations in real time using a pump that redirected stream water through a flow-through cell in the instrument. The ISCO samplers took discrete samples on programmed intervals, which were then returned to the laboratory for analysis using a fluorometer.

Three fluorometer sites were stationed on Lookout Creek, one immediately upstream of each tributary junction corresponding to at least a two-fold increase in discharge or an increase in stream order. The fluorometers were 1032 m (Site 2), 4145 m (Site 6), and 8,907 m (Site 10) downstream of the injection site (Table 1). The site positions were located using Global Positioning System (GPS) coordinates, aerial photographs, and physical features. The locations were then entered into an AcrHydro GIS™ data model and the distance between each site was measured in the GIS™ data layer (values reported in Table 1). The distances were later measured by counting my paces of the upper 9 km of stream length. The difference of GIS extrapolated distances and pacing distance was ± 20 m for the top 4 km and ± 100 m for the bottom 5 km. One ISCO sampler was located 84 m below the injection site (not shown on map). Four additional ISCO monitoring sites were established, one below each of the confluences and one near the outlet of the basin. The ISCO monitoring sites were 1,137 m (Site 4), 5,126 m (Site 7), 9,327 m (Site 12), and 14,274 m (Site 14) (Table 1).

During the test, stream discharge was measured three times at the injection site and once at each fluorometer site on the same day. Discharge was calculated by using the standard field methods of dividing a stream cross-section by >20 equally spaced intervals and measuring the depth and width at each location to calculate area. The mean velocity at each location was measured with a Marsh-McBirney, Inc. Flo-Mate™ flow meter. The area of the stream and the velocity were then multiplied together to estimate the discharge. For more details on methods used during the Longitudinal Tracer Test see Appendix I: Detailed Methods.

Table 1. Summary of site characteristics for the LTT conducted at the H.J. Andrews Experimental Forest, Oregon.

Site Name	Site #	Drainage Area (km^2)	Distance from Upstream Site (m)	Cumulative Distance From Injection Site LTT (m)	Basin Used in Regression LTT	Monitoring method	Stream Order	Peak concentration (µg/L)
LTT Injection	0	3.6	NA	0	-	NA	2nd	NA
LTT Inj ISCO	1	3.8	84	84	Observed	ISCO	2nd	242.400
Above Cold Cr.	2	5.4	948	1032	USGS	Fluorometer	2nd	91.700
Below Cold Cr.	4	6.2	105	1137	Mack	ISCO	3rd	22.500
Above Mack Cr.	6	15.0	3008	4145	USGS	Fluorometer	3rd	4.400
Below Mack Cr.	7	25.2	981	5126	Mack	ISCO	4th	1.410
Above McRae Cr.	10	33.9	3457	8583	WS03	Fluorometer	4th	0.936
Below McRae Cr.	12	51.7	744	9327	WS02	ISCO	5th	0.591
Headquarters	14	61.8	4947	14274	Direct USGS	Fluorometer	5th	0.265

Site Name	GPS UTM East	GPS UTM North	Time of start of Injection	Time of End of Injection	Total time of Injection (h)	Mass of RWT Injected (g)
LTT Injection	570580	4896687	7/14/03 2:20 PM	7/17/03 7:20 PM	77	1603.9
LTT Inj ISCO	570530	4896815				
Above Cold Cr.	569924	4897390				
Below Cold Cr.	569831	4897430				
Above Mack Cr.	567214	4897790				
Below Mack Cr.	566520	4897300				
Above McRae Cr.	563450	4897871				
Below McRae Cr.	562800	4897760				
Headquarters	559790	4895636				

Table 2. Summary of site characteristics for the IOTTs conducted at the H.J. Andrews Experimental Forest, Oregon.

Site Name	Site #	Drainage Area (km^2)	Distance From LTT Injection Site (m)	Cumulative Distance From Injection Site IOTT (m)	Basin Used in Regression IOTT	Monitoring method	Stream Order	Peak concentration (µg/L)
Cold Cr. Injection	3	6.2	1091	0		NA	3rd	NA
Below Cold Cr.	4	6.2	1137	46	Mack adjusted	ISCO	3rd	50.67
Above Longer Cr.	5	11.0	3196	2105	Mack adjusted	ISCO	3rd	6.04
Above Mack Cr.	6	15.0	4145	3054	USGS	Fluorometer	3rd	2.00
Mack Cr. Injection	7	25.2	5126	0		NA	4th	NA
Mack Injection ISCO	8	25.2	5151	25	Mack adjusted	ISCO	4th	27.08
Mid Mack	9	26.3	6127	1001	Mack adjusted	ISCO	4th	10.38
Above McRae Cr.	10	33.9	8583	3457	WS03	Fluorometer	4th	2.89
McRae Cr. Injection	11	50.0	8907	0		NA	5th	NA
Below McRae Cr.	12	51.7	9327	420	WSO2	ISCO	5th	7.58
Floodplain	13	53.9	10372	1465	USGS adjusted	ISCO	5th	4.13
Headquarters	14	61.8	14274	5367	Direct USGS	Fluorometer	5th	2.15

Table 3. Summary of site characteristics for the IOTTs conducted at the H.J. Andrews Experimental Forest, Oregon.

Site Name	GPS UTM East	GPS UTM North	Time of start of Injection	Time of End of Injection	Total time of Injection (h)	Mass of RWT Injected (g)
Cold Cr. Injection	569880	4897411	9/11/2003 10:30	9/12/2003 10:29	23.9	296.4
Below Cold Cr.	569831	4897430				
Above Longer Cr.	568040	4897970				
Above Mack Cr.	567214	4897790				
Mack Cr. Injection	566520	4897300	8/7/2003 12:32	8/8/2003 14:39	26.1	321.1
Mack Injection ISCO	566474	4897330				
Mid Mack	565650	4897590				
Above McRae Cr.	563450	4897871				
McRae Cr. Injection	563155	4897900	7/8/2003 23:53	7/9/2003 4:50	17.0	224.3
Below McRae Cr.	562800	4897760				
Floodplain	562008	4897378				
Headquarters	559790	4895636				

A synoptic concentration sampling test was conducted on June 17th, 2003 during the LTT on Lookout Cr. The synoptic samples were gathered by grab samples longitudinally starting at the LTT injection ISCO site and continuing downstream for the first 5,378 m of the LTT reach. The distance between each sample ranged from 26 m to 317 m and GPS coordinates were used to establish location along the river network. It took 8.5 h to gather the synoptic samples. The electrical conductivity of each sample was measured during collection. A portion of each sample was later analyzed in the laboratory for RWT concentration using a Turner Design™ model 10-AU fluorometers and laboratory methods described in detail in Appendix I Detailed Methods.

The second step of this project included three additional tracer tests between each major confluence within Lookout Creek. These intra-order tracer tests (IOTTs) encompassed changes in stream scale from a 3rd-order drainage basin to a 5th-order drainage basin.

The first IOTT was conducted between the confluence of McRae Creek and the H.J. Andrews headquarters. The McRae Cr. IOTT was conducted after Lookout Creek was shown to have returned to background concentrations. The injection occurred on July 8th, 2003 and continued at an average in-stream concentration of 6.9 µg/L ± 0.78 µg/L, and an average pumping rate of 0.28 mL/s or 3676 µg/s for approximately 17 h. The discharge in the stream was estimated to average 367 L/s ± 2.7 L/s over the duration of the injection. The injection technique used the same equipment and methods as the LTT. The discharge was estimated using a linear hydrograph regression with point discharges measured throughout the summer at the injection site and gauged watersheds in the H.J. Andrews (Figure 3). This tracer test was monitored 5,367 m downstream at the H.J. Andrews headquarters with a fluorometer. The concentration of dye was also monitored 1,465 m downstream by an ISCO™ sampler at a position in the stream where the valley morphology changes from wide and alluviated to constrained.

The second IOTT was conducted between the confluence of Mack Creek and McRae Creek. The Mack Cr. IOTT was conducted after Lookout Creek was shown to have returned to background concentrations. The injection occurred on

August 7th, 2003 and continued with an average concentration of 14.6 µg/L ± 2.5 µg/L, and an average pumping rate of 0.21 mL/s or 3415 µg/s of RWT for approximately 24 h. The discharge in the stream was estimated to average 223 L/s ± 1.4 L/s over the duration of the injection. The injection was conducted using a Fluid Meter Inc. AC injection pump (model # QG150, with a Q1CKC pump head). The discharge was calculated using the same methods and equipment as the McRae Cr. IOTT. This tracer test was monitored 3,457 m downstream above the McRae Cr. confluence with a fluorometer. It was also monitored 1,001 m downstream by an ISCO™ sampler at the largest tributary between Mack and McRae Cr. This tributary is a 1st order stream and is unnamed on the Blue River Ranger District H.J. Andrews Experimental Forest map.

The third IOTT was conducted between the confluence of Cold Creek and Mack Creek. The Cold Cr. IOTT was conducted after Lookout Creek was shown to have returned to background concentrations. The injection occurred on September 11th, 2003 and continued with a average concentration of 49.8 µg/L ± 0.58 µg/L, and an average pumping rate of 0.20 mL/s or 3433 µg/s of RWT for approximately 24 h. The discharge in the stream was estimated to average 73 L/s ± 0.5 L/s over the duration of the injection. The injection technique used the same equipment and methods as the Mack IOTT. The discharge was calculated using the same methods and equipment as the McRae Cr. IOTT. This tracer test was monitored 3,054 m downstream at a site above the Mack Cr. confluence with a fluorometer and 2,105 m downstream by an ISCO sampler at Longer Cr., the largest tributary between Mack and McRae Cr.

A fourth tracer test would have captured a replica of the 2nd order stream from the earlier LTT, but was canceled because the stream did not return to background concentrations until late November, after the onset of the winter storm season, at which time the stream discharges were no longer similar to the summer low-flow regime.

The final step for this project involved analyzing the concentration breakthrough curves. Because the long duration of the tracer tests made it infeasible to assume a constant discharge, we employed the RWT flux instead of

concentration. In order to calculate flux breakthrough curves we needed to have a continuous record of discharge for each site. The discharge hydrographs at each site were estimated with a paired watershed approach using linear hydrograph regression from gauged watersheds within the H.J. Andrews (Figure 3). The hydrograph regression used point discharges gathered throughout the summer and matched with one of the 10 gauged watersheds for a best-fit linear regression (Figure 3). The linear relationships established between individual site discharges and watershed gauge data were then used to estimate discharges for each monitoring site. The watershed that had the best fit for each site is reported in both Table 1 and Table 2.

The flux breakthrough curves allowed the hyporheic characteristics of each of our test reaches to be estimated. The STAMMT-L transient storage model was used to evaluate the flux breakthrough curves and estimate the hyporheic volume, dispersion coefficient, mass recovered, dilution coefficient, mean channel velocity, and power-law distribution (Haggerty and Reeves, 2002). In particular, the data were examined to determine if hyporheic residence times are described by a power-law distribution and if that relationship holds over several scales and through different stream morphologies. Relationships between parameters were analyzed using trend regressions and the regression analysis statistical package from the Excel data analysis tool kit. For a more detail reporting of all methods used in this thesis see Appendix I: Detailed Methods.

4.0 RESULTS

4.1. Longitudinal Tracer Test Power-Law Behavior

The concentration breakthrough curves for the LTT are shown in Figure 4 with concentration of RWT vs. time from injection in log-log space. Each monitoring site is shown in its own color with dark blue representing the Above Cold Creek Site #2, maroon representing the Below Cold Creek Site #4 and so forth down to the Headquarters Site #14 shown in yellow. The breakthrough curves in the top of

the graph represent the upper monitoring sites and the curves in the bottom of the graph show the lower monitoring sites. Going from the top of the graph to the bottom corresponds to going downstream from the injection site. Figure 4 shows that the first arrival times increased, the peak concentration decreased, and the total mass recovered decreased in the downstream direction. The late-time concentration data show power-law behavior. Concentrations at the Above Cold Creek and the Below Cold Creek sites showed increased rates of decline deviating from power-law behavior in the latest time of the tails of the breakthrough curves. These deviations from the power-laws began 90 days and 40 days from injections, respectively (Figure 4).

Figure 4. Concentration breakthrough curves for the monitoring sites in log-log space during the LTT, H.J. Andrews, summer, 2003.

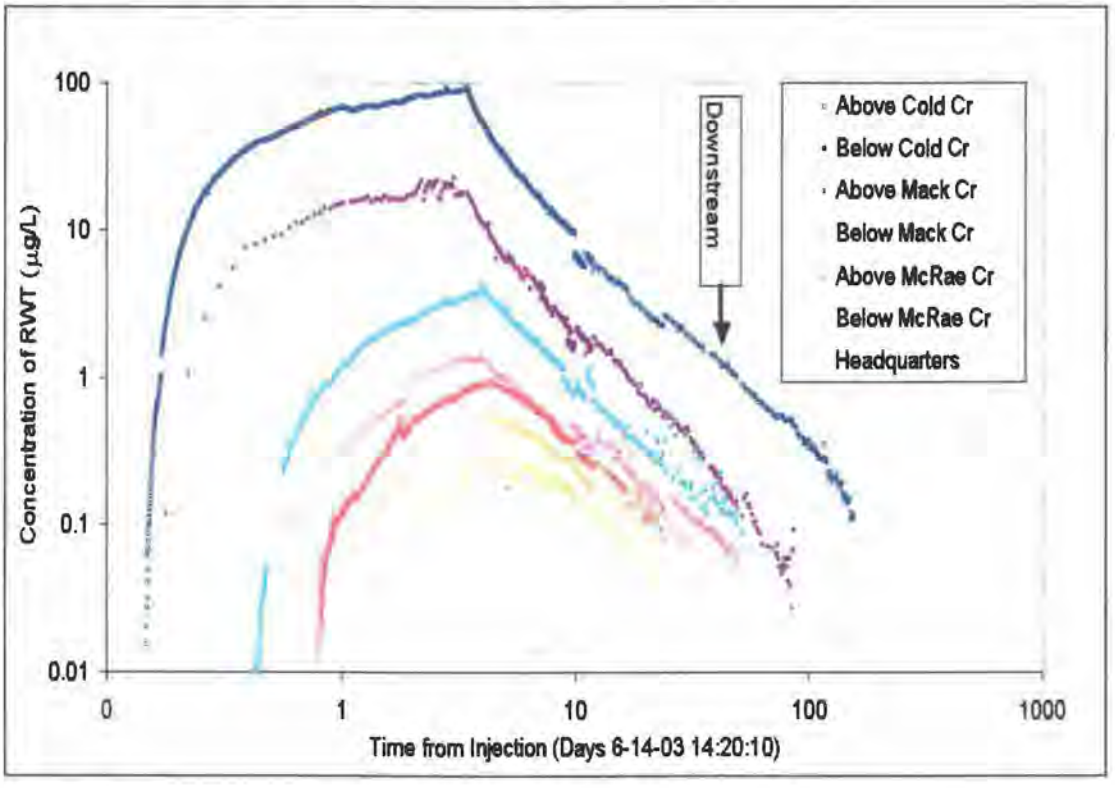

The concentration breakthrough curves for the LTT are shown in arithmetic space in Figure 5. The breakthrough curves in Figure 5 have been normalized to the individual peak concentration observed at each monitoring site (Table 1 and

Table 2). Normalization allows the data to be displayed together over a convenient scale and shows important features of the curves. The stagger of the breakthrough curves shown in this figure indicates that arrival times and peak concentrations were delayed in the downstream direction. The curves in Figure 5 appear to be shifted to the right depending on how far downstream each of their corresponding monitoring sites were located. The rising limbs of breakthrough curves were clustered closely together and the declining limbs were spread out (Figure 5). Total areas under the curves are greater in the downstream direction (Figure 5).

Figure 5. Concentration breakthrough curves normalized to the peak concentration (Table 1) for each of the monitoring sites in arithmetic space during the LTT.

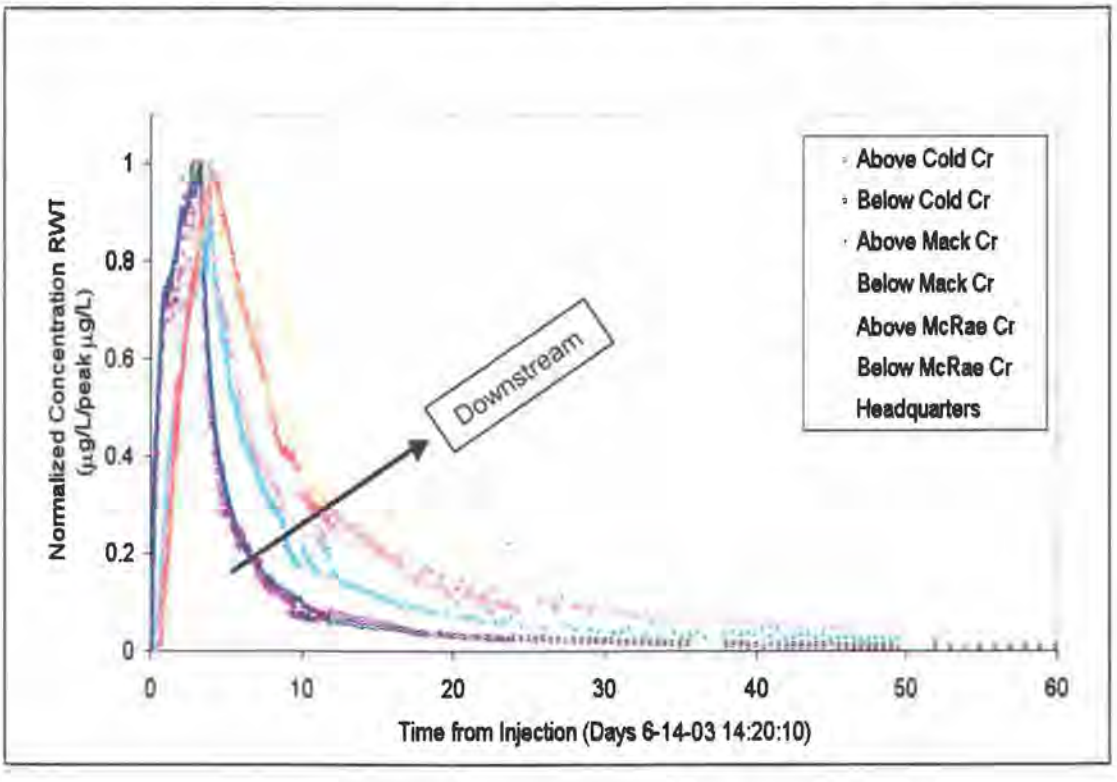

Figure 6 shows the RWT flux breakthrough curves vs. time from injection for all of the monitoring sites in log-log space during the LTT. The flux breakthrough curves have been normalized using the average rate of flux injected at the injection site during the LTT. Several of the flux breakthrough curves displayed larger

amounts of RWT flux in the lower sites than in the upper sites, especially during the later time periods of the test. The flux breakthrough curves exhibit power-law residence time distributions, as shown by the straightness of the late-time breakthrough curves in log-log space. The total area under the flux breakthrough curves decreases in the downstream direction.

Figure 6. Flux breakthrough curves normalized by the LTT's average injection flux rate in log-log space during the LTT.

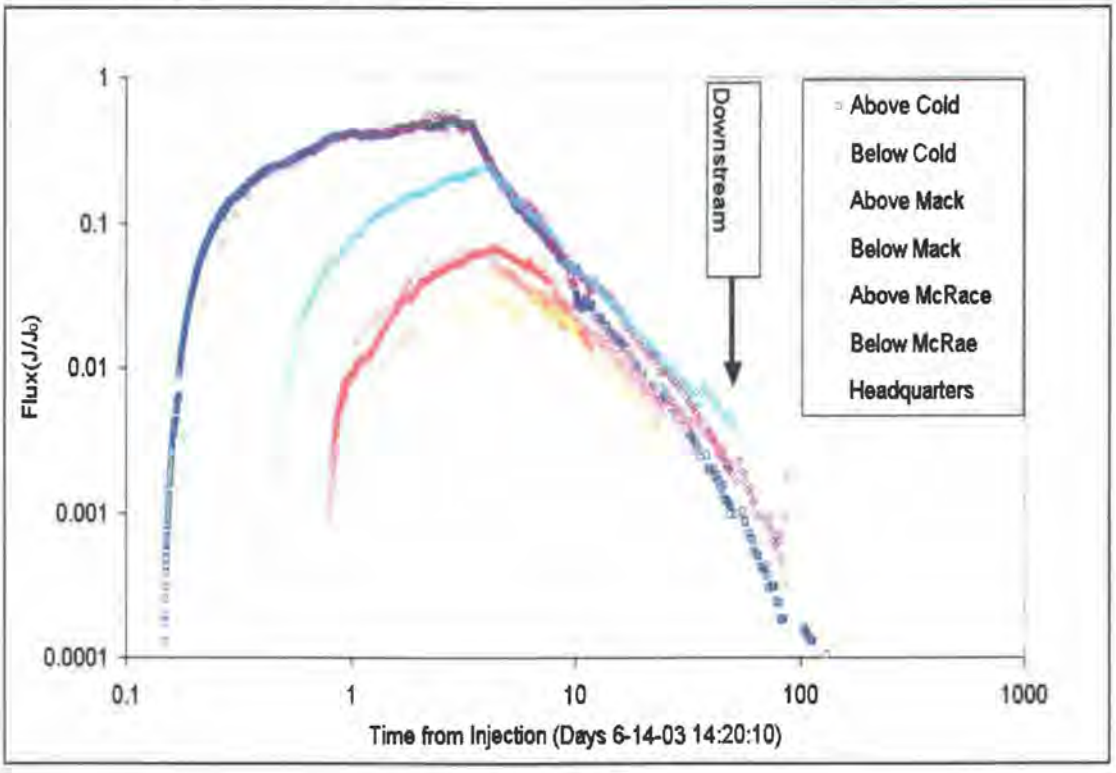

Figure 7 shows all of the flux breakthrough curves for the LTT that were shown in Figure 6; however in Figure 7 the axes are in arithmetic space. The arithmetic representation gives a more traditional view of breakthrough curves but does not show the differences in the late-time tails as clearly as the log-log representation in Figure 6.

Figure 7. Flux breakthrough curves normalized to the average flux injection rate for each of the monitoring sites in arithmetic space during the LTT.

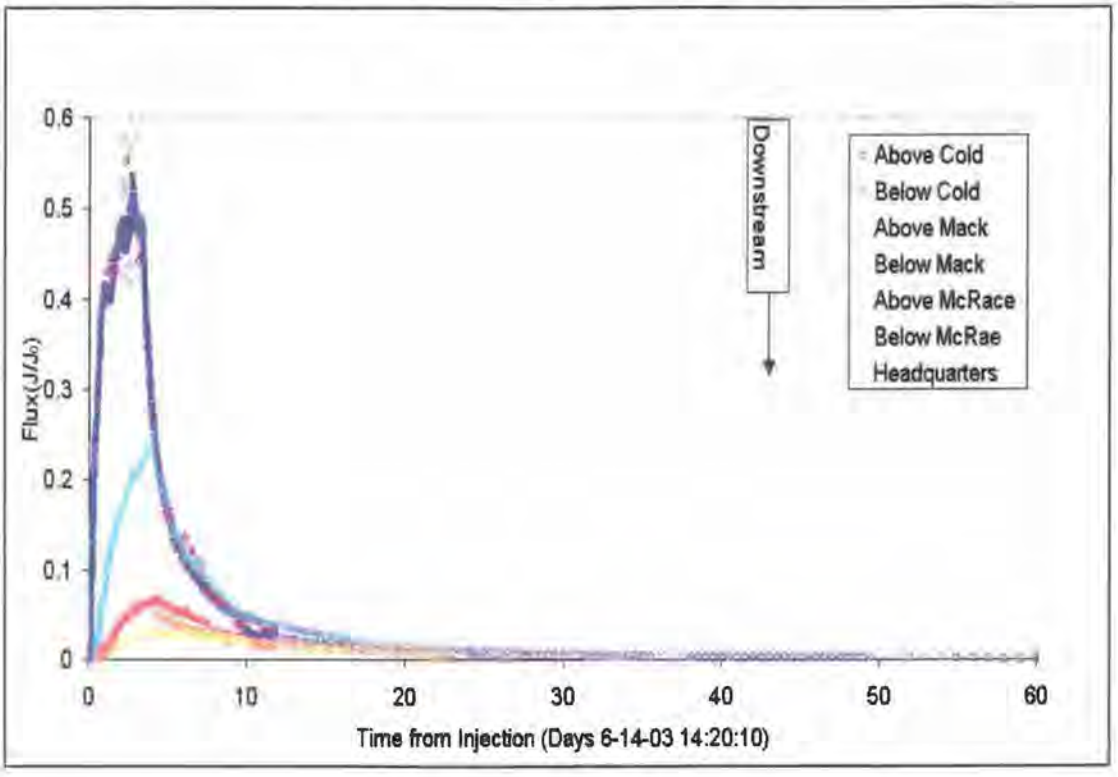

The STAMMT-L best-fit modeling results are shown in Figure 8 for the upper 4 monitoring sites for the LTT. The open circles in Figure 8 represent the flux breakthrough curve data points, which are the same points shown in Figure 6 and Figure 7. The solid lines represent the best fit model results for the data points with corresponding colors (Figure 8). Both the model and the data points have been normalized using the average flux injection rate of the LTT. The model simulated much of the flux curves fairly accurately, with the root mean square error (RMSE) less then 0.25. However, the rising limbs and peaks of the flux curves were often poorly modeled, while the tails were better represented (Figure 8). Each of the STAMMT-L models was fit using a power-law general residence time function (Figure 8).

The STAMMT-L best-fit modeling results for the lower three LTT monitoring sites are shown in Figure 9. Figure 9 is shown with the same axes and scale as Figure 8 to allow comparison of the two figures. The upper monitoring sites

displayed larger and more distinct peaks than the lower sites (Figure 8 & Figure 9). The model fits of the lower sites had a lower RMSE (<0.185) than the upper monitoring sites (Figure 9). Similar to the upper model fits in Figure 8, the lower model fits over represented the peaks of the curves while closely representing the tails (Figure 9).

Figure 8. Flux breakthrough curves and the STAMMT-L modeled best fits normalized to the average flux injection rate for the four upper monitoring sites in log-log space during the LTT.

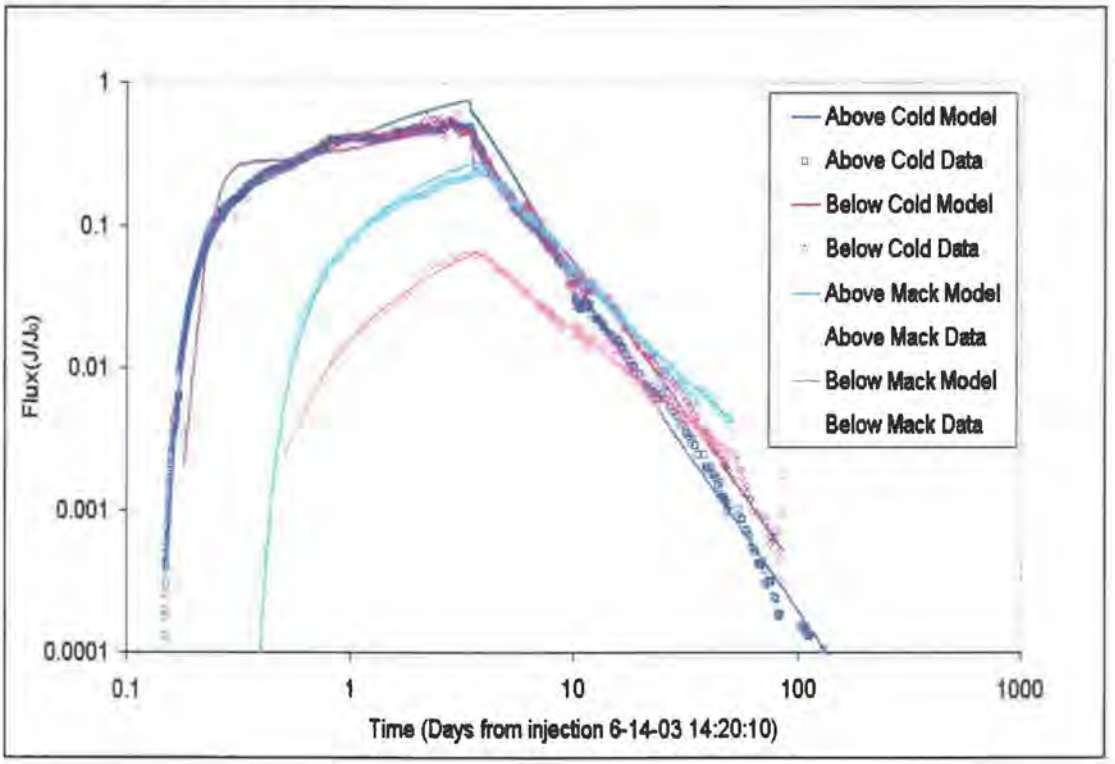

Figure 9. Flux breakthrough curves and the STAMMT-L modeled best fits normalized to the average flux injection rate for the three lower monitoring sites in log-log space during the LTT.

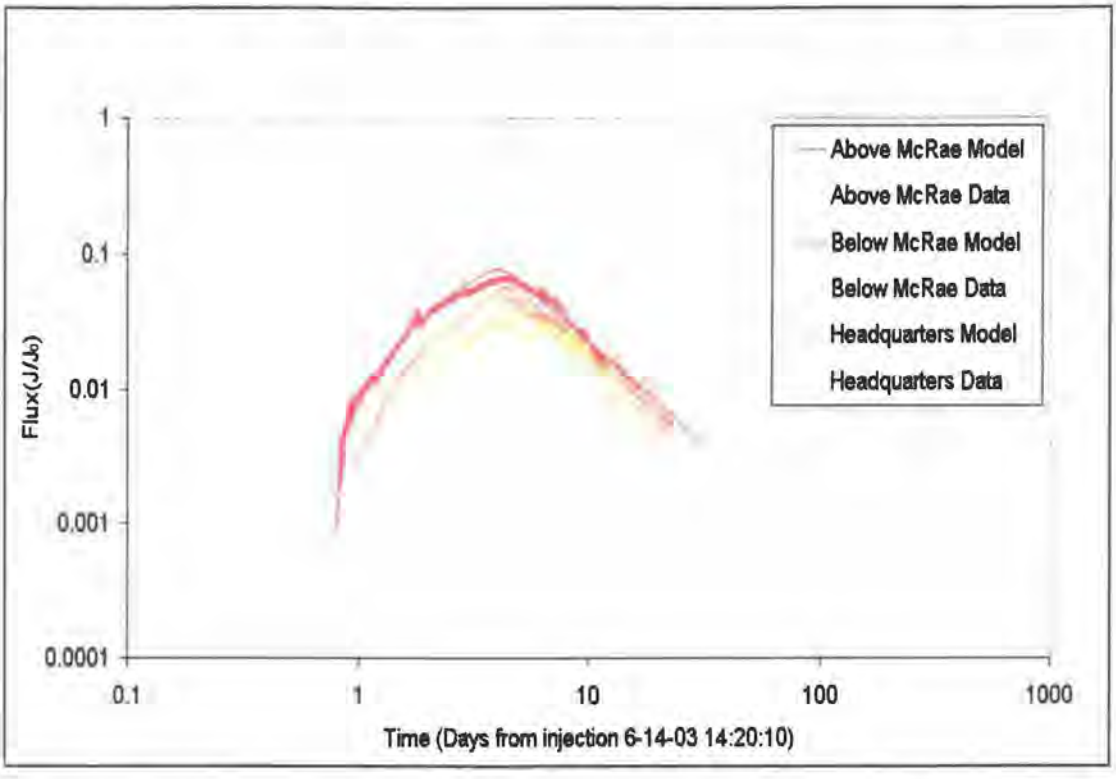

Figure 10 shows the best-fit model estimates for the power-law slope (k) vs. longitudinal distance from the LTT injection, for the LTT and IOTT's. Each data point represents a monitoring site on either the LTT or one of the IOTT's. The arrows between the data points indicate the downstream direction for the tracer tests (Figure 10). The model slopes for the LTT flux curves indicate that the slopes of the power-law were not consistent throughout the basin. The slopes of the power-law declined downstream until after the Mack Cr. confluence and then rose to the outlet (Figure 10). The slope pattern in the IOTT's will be discussed in the section below.

Figure 10. Power-law slopes (k) for the Longitudinal and Intra-Order tracer tests monitoring sites shown by longitudinal position on Lookout Creek.

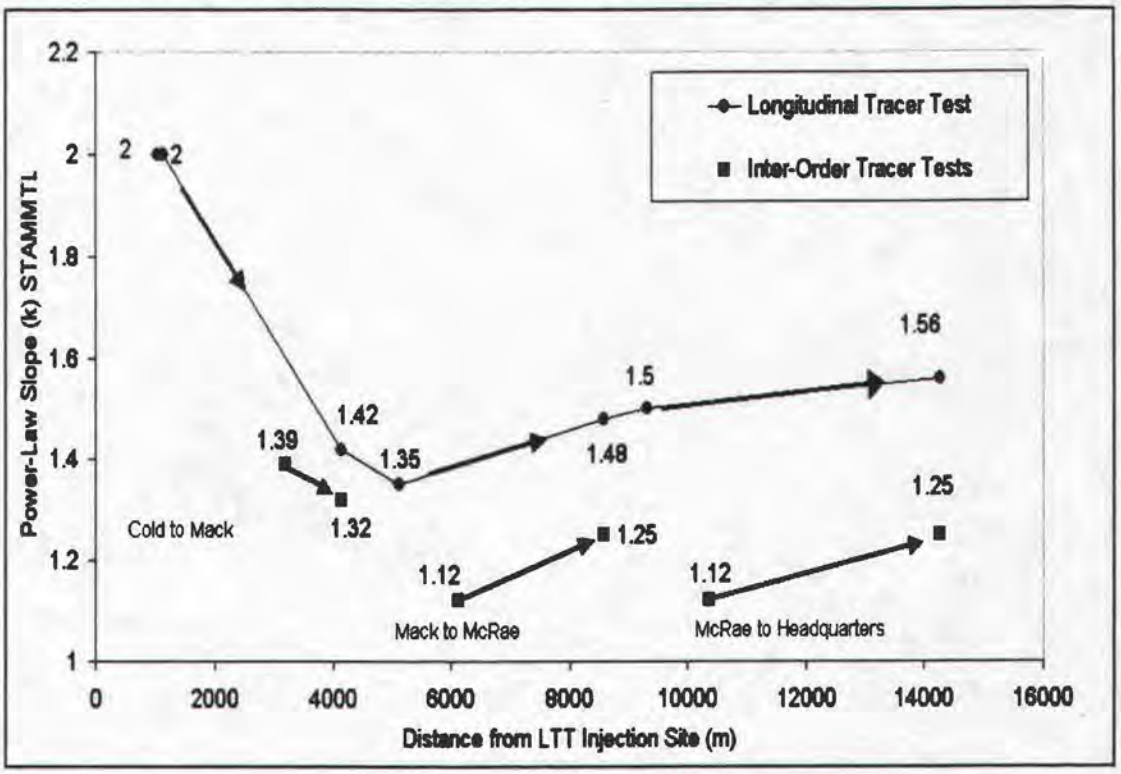

4.2. Intra-Order Tracer Tests Power-Law Behavior

The IOTT's conducted between the major confluences of Lookout Cr. showed power-law declines during the declining limb of the concentration and flux breakthrough curves. Figures 11, 12 and 13 show concentration vs. time for individual injections in log-log space for the Cold Cr., Mack Cr., and McRae Cr. IOTTs, respectively. Figure 11 shows the Cold Cr. IOTT with concentrations collected 46 m below the injection site in red, above Longer Cr. in dark blue, and above Mack Cr. in light blue. The injection breakthrough curve of the Cold Cr. IOTT showed small increases of concentration after 5 days and again after 12 days (Figure 11). The increase in the concentration observed after 5 days occurred during a rain event on September 16. The concentration increases after 12 days do not coincide with any rain events. The Longer Cr. breakthrough curve of the Cold Cr. IOTT showed some scatter and a drop off of concentration after 12 days

(Figure 11). The above Mack Cr. breakthrough curve of the Cold Cr. IOTT showed a small increase of concentration after 12 days (Figure 11). The concentration breakthrough curve of the Cold Cr. IOTT exhibits power-law behavior directly after the injection was stopped (Figure 11). The arithmetic representation of Figure 11 is shown in Figure 46 of Appendix II: Additional Parameter Information.

Figure 11. Concentration breakthrough curves for the monitoring sites in log-log space during the Cold Creek IOTT.

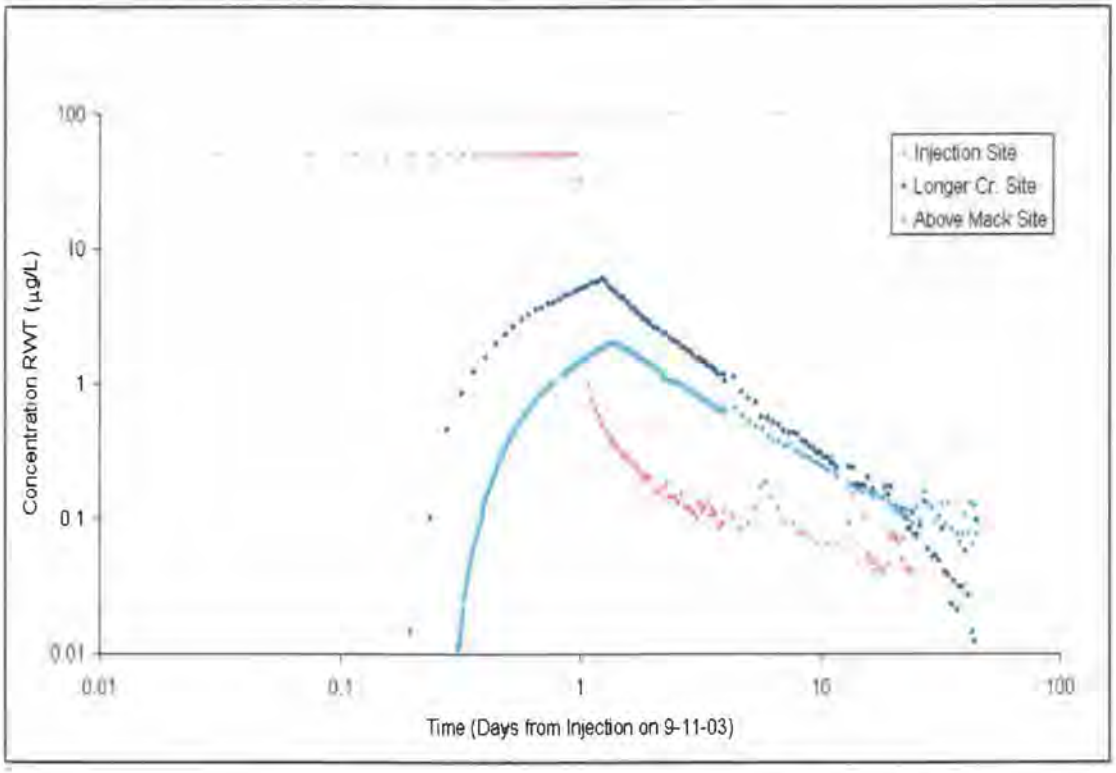

The concentration breakthrough curves of the Mack Cr. IOTT are shown in Figure 12. The red curve represents the injection-monitoring site, the yellow represents a monitoring site near a large unnamed tributary, and maroon represents the site above McRae Cr. in Figure 12. Power-law behavior developed approximately 1 day after the end of the injection (Figure 12). The arithmetic representation of Figure 12 is shown in Figure 43 of Appendix II: Additional Parameter Information

Figure 12. Concentration break through curves for the monitoring sites in log-log space during the Mack Creek IOTT.

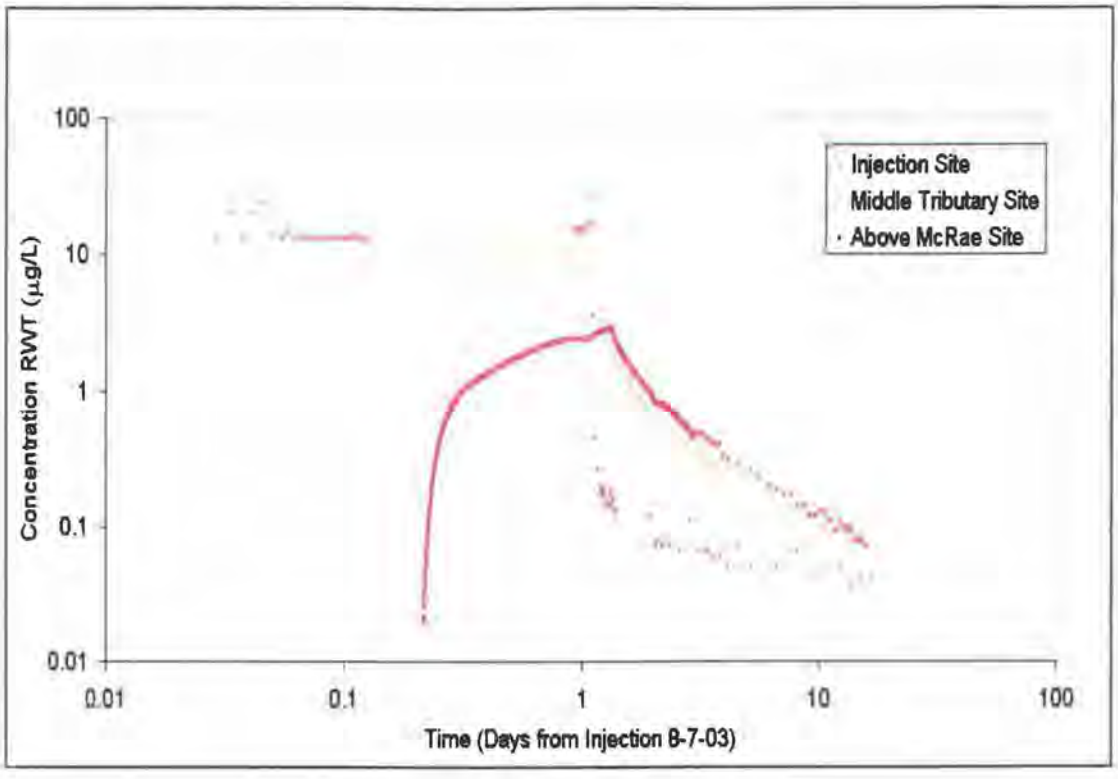

Figure 13 shows the concentration breakthrough curves of the McRae Cr. IOTT. The red curve represents the injection-monitoring site, the purple represents the monitoring site downstream of a large floodplain, and the light blue represents a site near the headquarters in Figure 13. Power-law behavior developed approximately 0.5 to 1 day after the end of the injection (Figure 13). Scatter was observed in all of the late time curves from the McRae Cr. IOTT (Figure 13). This scatter is attributed to small amounts of contamination in the ISCO sample bottles and lids. Contamination is believed to be the cause because the scatter is consistently in the upward direction and doesn't appear to drop below a certain line, which is equivalent to the power-law decline. Due to the general upward scatter, it is believed that the data are still useful, but the error in the model fits and parameter estimates were greater for this test. The arithmetic representation of Figure 13 is shown in Figure 40 of Appendix II: Additional Parameter Information.

Figure 13. Concentration breakthrough curves for the monitoring sites in log-log space during the McRae Creek IOTT.

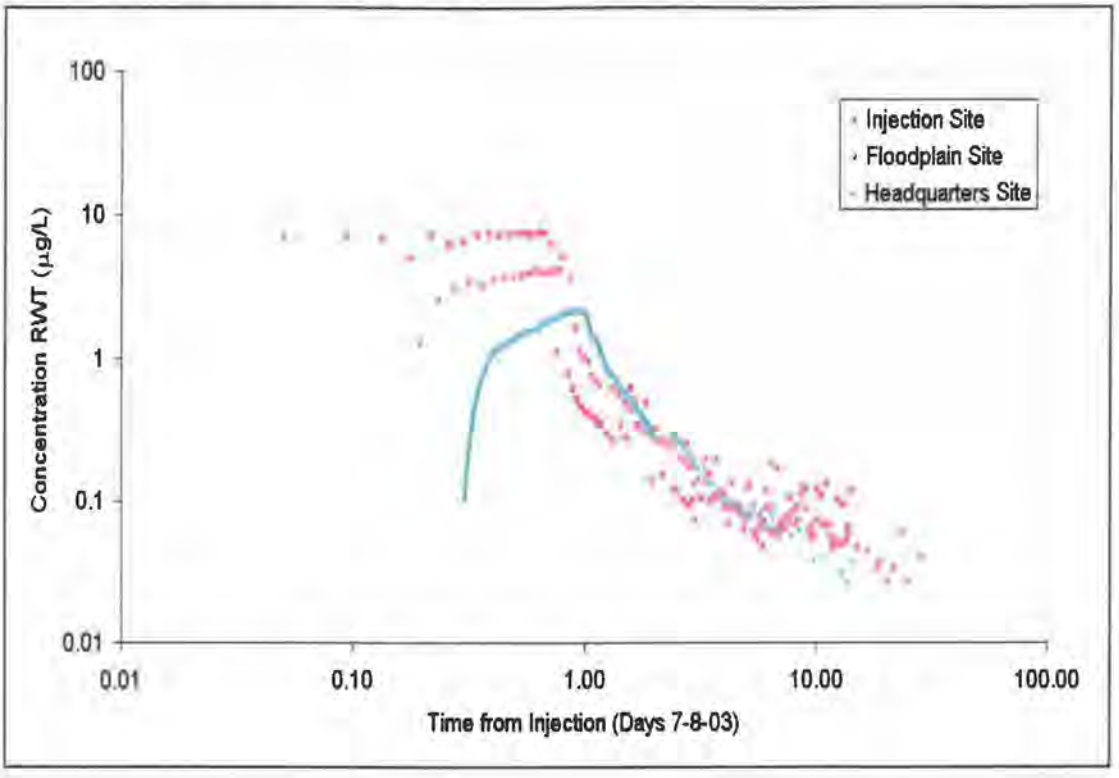

The flux breakthrough curves and the modeled simulations for Cold Cr., Mack Cr., and McRae Cr. are shown in Figures 14, 15, and 16, respectively. The flux curves are shown with normalized flux vs. time for individual injections in log-log space. The points on the graphs represent measured data and the lines represent the best-fit model results for the data points corresponding to the same color. Figure 14 shows power-law behavior directly after the end of the injection. A spike in the flux is observed 5 days after the start of the injection (Figure 14). A large amount of scatter is observed at the Longer Cr. site 25 days after the injection (Figure 14). The increase in the flux and late time scatter observed in Figure 14 occurred at the same times as rain events occurred in the basin. A comparison of the tracer concentrations and the stream hydrograph is discussed later in the Overview of Other Findings section and shown in Figures 20, 21, and 22.

Figure 14. Flux break through curves and STAMMT-L modeled best fits normalized to the average flux injection rate for the Cold Cr. IOTT monitoring sites in log-log space.

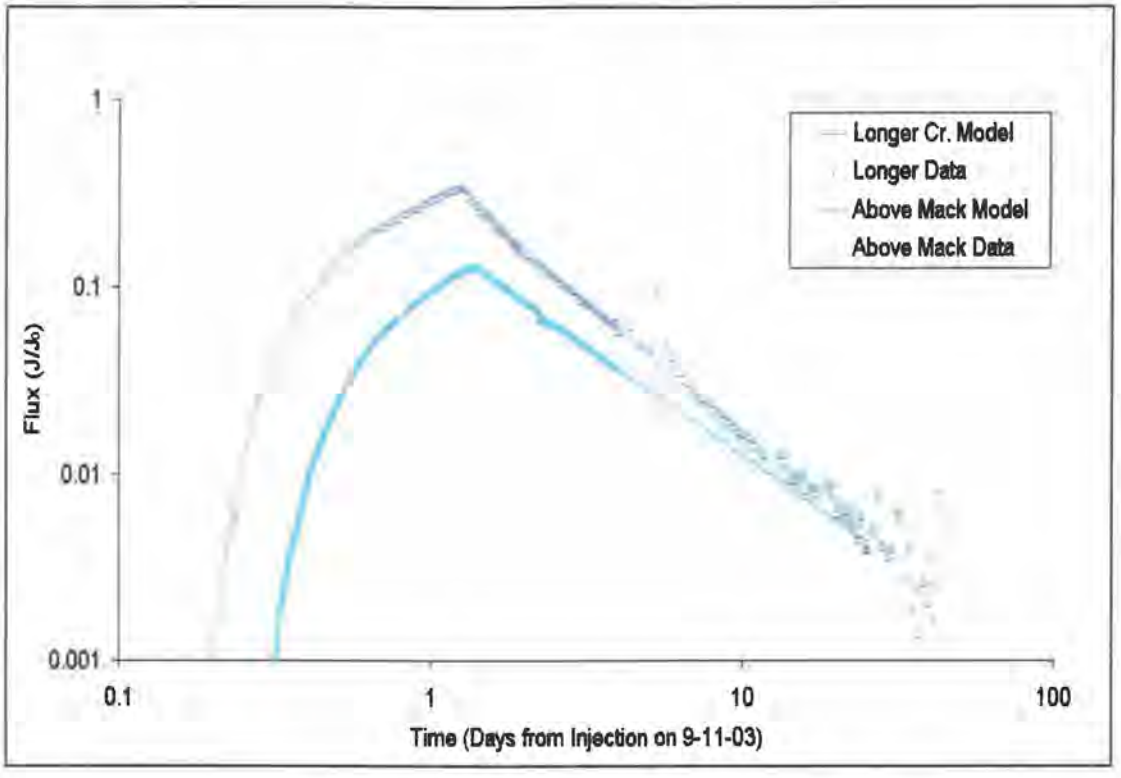

Figure 15, which represents the Mack Cr. IOTT flux curves, shows that power-law behavior took 0.5 to 1 day from the end of the injection to develop and little to no scatter was recorded.

The McRae Cr. IOTT flux curves are shown in Figure 16. Figure 16 indicates that the McRae Cr. IOTT flux curves developed a power-law behavior 0.5 to 1 day after the end of the injection. A large amount of scatter was observed at the Floodplain site and at the Headquarters site (Figure 16). The best-fit model of the Floodplain data over-estimated the flux at early arrival times (Figure 16). Figures 14, 15, and 16 are shown without model fits in arithmetic and log-log space in Figures 40,41,43,44,46 and 47 in Appendix II: Additional Parameter Information.

Figure 15. Flux break through curves and STAMMT-L modeled best fits normalized to the average flux injection rate for the Mack Cr. IOTT monitoring sites in log-log space.

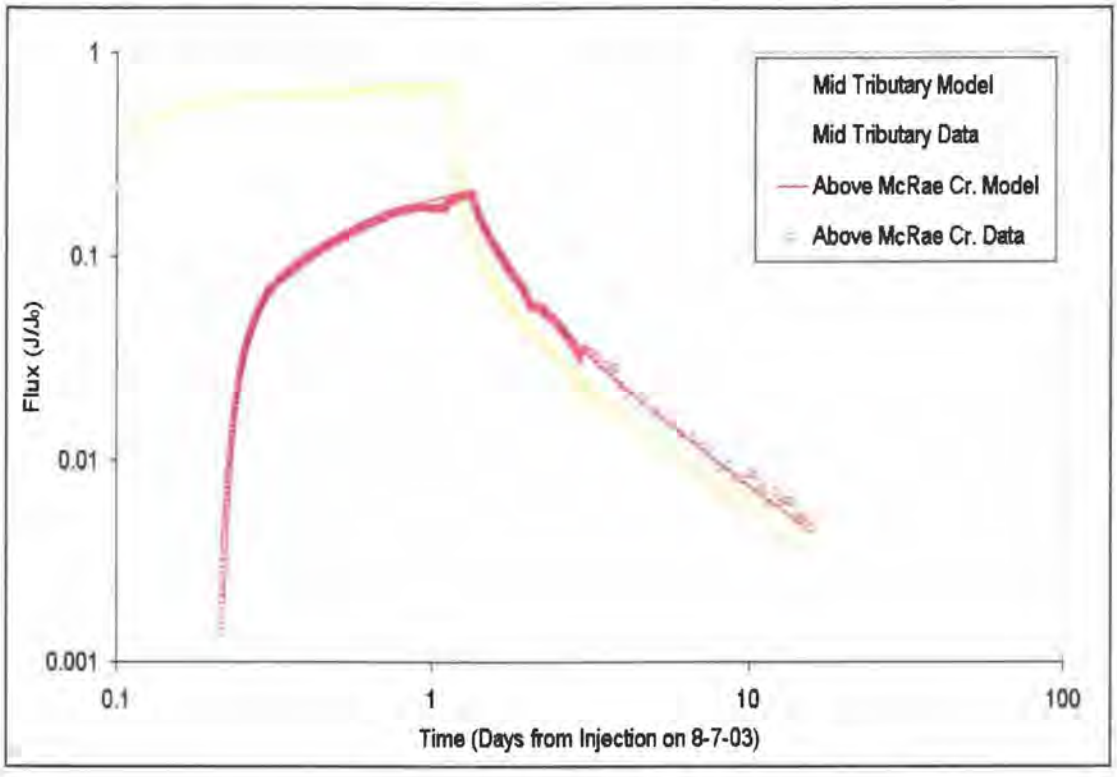

The power-law RTD of the McRae Cr. IOTT took a longer time to develop than the power-law RTD of Mack Cr. IOTT, which in turn took a greater amount of time to develop than the Cold Cr. IOTT RTD (Figures 11, Figure 12, Figure 13, Figure 14, Figure 15, and Figure 16).

Figure 16. Flux break through curves and STAMMT-L modeled best fits normalized to the average flux injection rate for the McRae Cr. IOTT monitoring sites in log-log space.

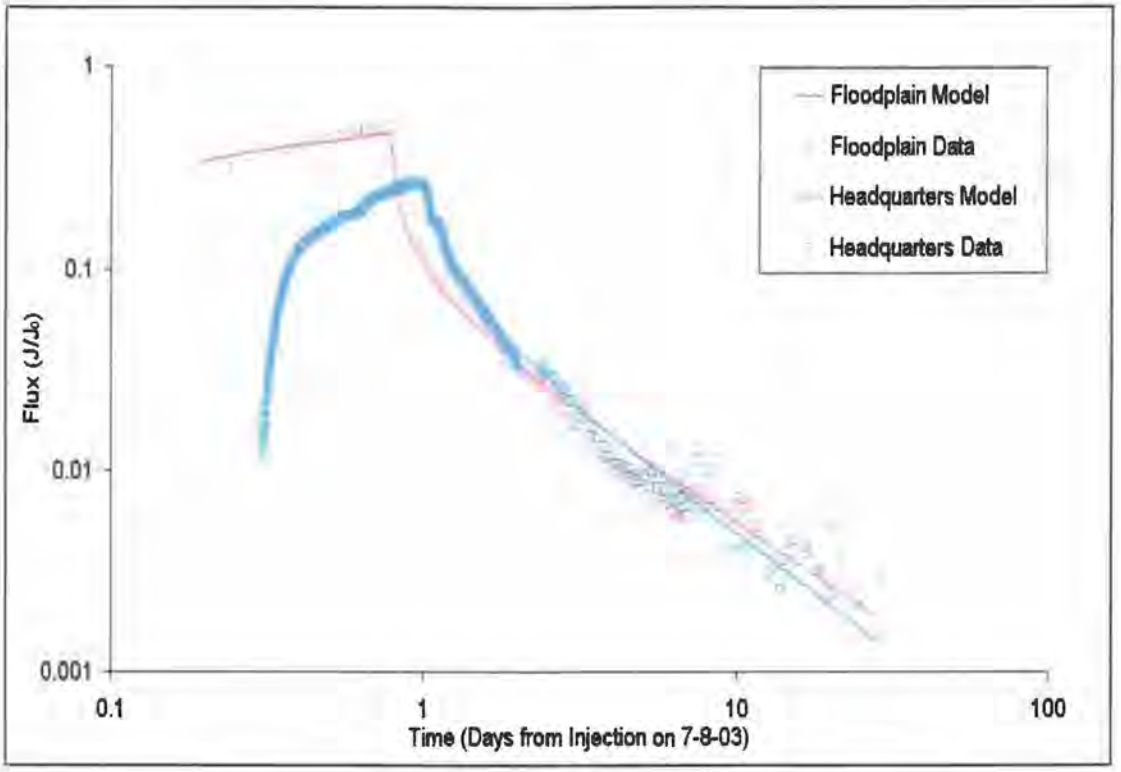

The best-fit model estimates for the power-law slope (k) vs. longitudinal distance from the LTT injection, for the IOTT's were shown previously in Figure 10. Each data point represents a monitoring site on either the LTT or one of the IOTT's. The arrows between the data points indicate the downstream direction for the tracer tests (Figure 10). The IOTT best-fit model slopes for the flux curves show a wide degree of variation when compared to the same longitudinal position of the LTT (Figure 10). The IOTT slopes are always shallower than the LTT slopes, but did not demonstrate a clear pattern of behavior (Figure 10). Upstream of the Below Mack Cr. site the power-law slopes appear to shallow with distance from the injection sites for both the LTT and the Cold Cr. IOTT (Figure 10). Downstream of the Below Mack Cr. site it appears that the power-law slopes steepen with distance from the injection sites for the LTT, Mack Cr. IOTT, and the McRae Cr. IOTT (Figure 10). Longitudinally, at least two distinct groups of slopes or power-law residence time distributions are present. The first group includes the

upper reaches of Lookout Creek (the Above and Below Cold Creek sites) and has a power-law exponent of –2. The second group includes all of the sites below Cold Creek (starting with the Longer Cr. site) and has a power law variable between –1.12 and –1.56 (Figure 10). This second group of values has an average power-law exponent of -1.46 for the LTT and -1.34 for all of the tracer tests (Figure 10).

Figure 17 displays the power-law slope (k) vs. the length from injection sites for individual tracer tests, in log-log space. The open circles represent all of the monitoring sites used in the LTT and the IOTT's. The plus (+) symbols represent all of the monitoring sites except the LTT's Above Cold Cr. site and the Below Cold Cr. site. The LTT Cold Cr. sites were excluded from the regression analysis in order to highlight the possibility that there are two distinct groupings of power-law exponents within the basin or that the Cold Cr. site data may be outliers. The regression line in Figure 17 shows a power-law relationship with steepening power-law slopes corresponding to increased distance from the individual injection sites. The R^2-value of the regression was 0.73 and p-value was >0.01.

Figure 17. Power-law slopes (k) at the different monitoring sites for the Longitudinal and Intra-Order Tracer Tests shown in total distance for individual injections on Lookout Creek in log-log space.

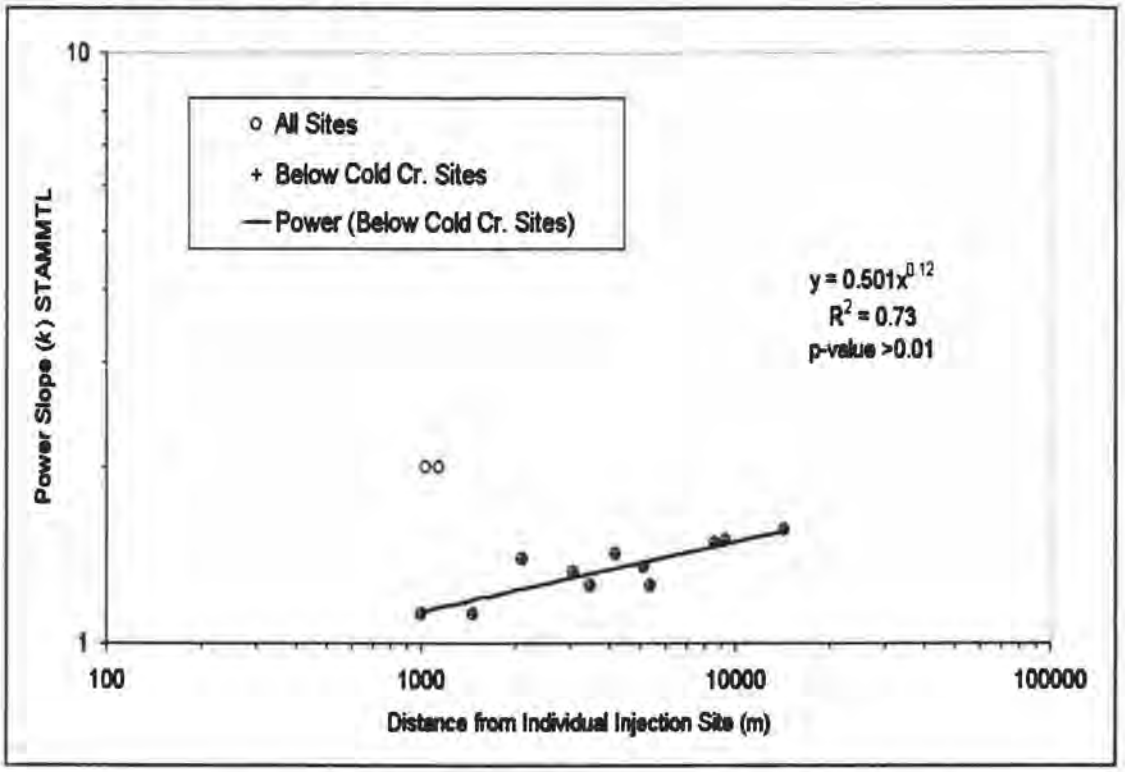

Figure 18 displays the power-law slope (k) on the left y-axis vs. mean channel residence time for individual injection sites, in log-log space. This graph also displays Harvey and Wagner's (2000) mean hyporheic residence time on the right y-axis vs. mean channel residence time to allow comparison with the current study's data. The LTT and IOTT data are displaced with Harvey and Wagner's data over one order of magnitude. The power-law slopes for the LTT and IOTT sites increase with increasing channel residence time (Figure 18). The relationship between increasing power-law slopes and increasing channel residence time is stronger, as shown by the higher r^2 values and lower p-values, if only the sites below Cold Cr. are included (Figure 18). The slope for the regression line, in log-log space, for the lower sites is smaller than the regression line with all of the sites included and Harvey and Wagner's regression line.

Figure 18. Power-law slopes (k) at the different monitoring sites for the Longitudinal and Intra-Order Tracer Tests vs. mean channel residence time in Lookout Creek shown in log-log space over 1 order of magnitude. Also shown is Harvey & Wagner's (2000) mean hyporheic residence time vs. mean channel residence time in log-log space over 1 order of magnitude.

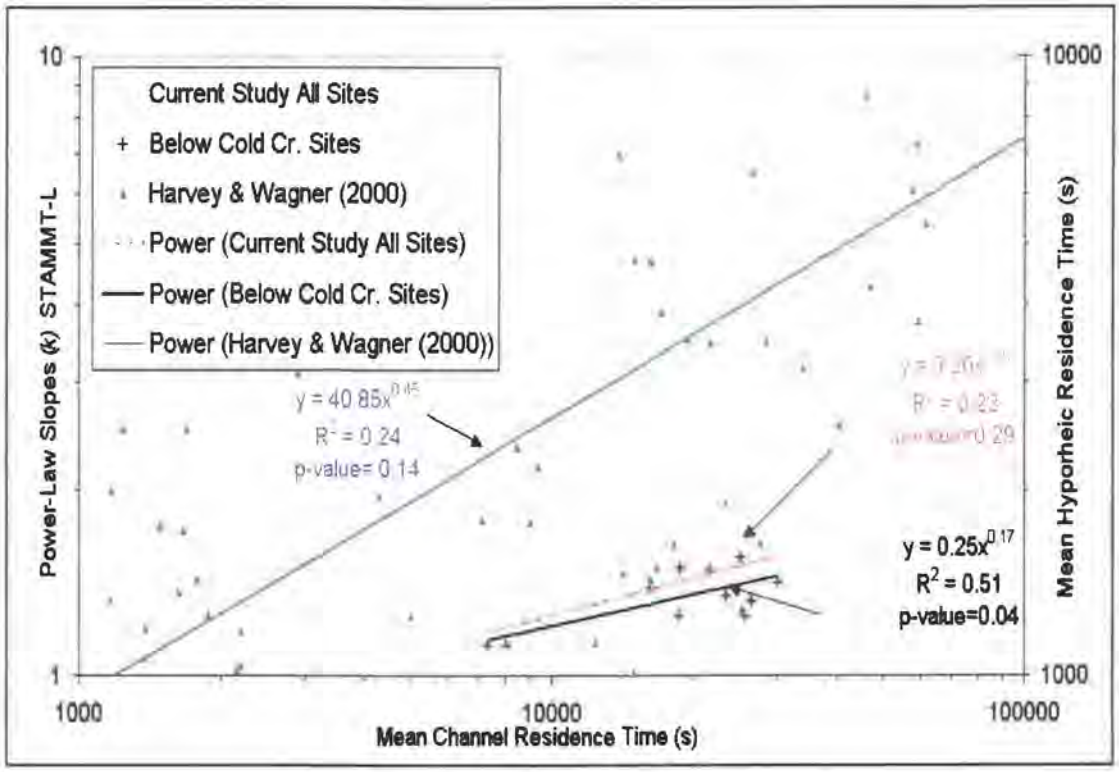

4.3. Overview of other findings

The estimated values for velocity, dispersion, dilution, β_{tot} (ratio of immobile area/mobile mass), percent mass recovered, minimum exchange time, and maximum exchange time are shown in Table 4 and Table 5 for the LTT, Cold Cr. IOTT, Mack Cr. IOTT, and the McRae Cr. IOTT. The estimated error and RMSE associated with the parameters and tracer tests are listed in Table 4 and Table 5. Due to a technical mathematical coding problem the estimated error of a power-law slope of 2 was unable to be calculated. The estimated in-channel volume and the estimated hyporheic volumes for the LTT and the IOTTs are shown in Table 6. In order to estimate the in-channel volume and hyporheic volume temporal and spatial assumptions had to be made about stream cross sectional area. As a result

of the assumptions, the values in Table 6 must be considered to have a large amount of error associated with them. Retardation has not been factored into the volume estimates shown in Table 6. Hyporheic retardation should reduce the volume estimates by some unknown amount; the largest estimates may be greater then 100 but it's more likely to be lower (Gooseff et al., in press). A detailed report of the estimated parameters is given in Appendix II.

Table 4. Summary of STAMMT-L estimated parameters and findings for the longitudinal stream tracer test.

Site Name LTT	Percent Mass Recovered (%) LTT	*Dilution* LTT	B_{tot} LTT	*Velocity* (m/s) LTT	*Dispersion* (D_L) (m^2/s) LTT	Power *RMSE*	Exponential *RMSE*
LTT INJ ISCO	65						
ABOVE COLD Cr.	78	*1±0.01*	*17.9±0.02*	*0.054±0.02*	*0.493±.na*	*0.25*	*1.03*
BELOW COLD Cr.	84	*1.23±0.01*	*26±0.01*	*0.052±0.01*	*0.52±.na*	*0.195*	*3.32*
ABOVE MACK Cr.	56	*1.42±0.08*	*62.2±0.01*	*0.138±0.01*	*0.454±.na*	*0.146*	*1.31*
BELOW MACK Cr.	19	*3.39±0.01*	*169±0.05*	*0.22±0.01*	*1.23±.na*	*0.118*	*0.87*
ABOVE MCRAE Cr.	18	*3.8±0.01*	*104±0.01*	*0.4 ±0.01*	*1.5±.na*	*0.115*	*0.95*
BELOW MCRAE Cr.	13	*4.89±0.01*	*111±0.01*	*0.5 ±0.01*	*1.5±.na*	*0.147*	*0.68*
HEADQUARTERS	9	*7.66±0.02*	*77.5±0.01*	*0.57 ±0.01*	*1.94±.na*	*0.185*	*0.74*

Site Name LTT	Slope (*k*) LTT	α_{min} LTT	α_{max} LTT	*Maximum Exchange Time*	*Minimum Exchange Time*
ABOVE COLD Cr.	*2 ±na*	$6.9*10^{-8}$	$4.0*10^{-5}$	$1.45*10^{+7}$	$2.5*10^{+4}$
BELOW COLD Cr.	*2±na*	$7.2*10^{-8}$	$1.0*10^{-5}$	$1.39*10^{+7}$	$1.0*10^{+5}$
ABOVE MACK Cr.	*1.42±0.003*	$6.8*10^{-8}$	$4.0*10^{-5}$	$1.47*10^{+7}$	$2.5*10^{+4}$
BELOW MACK Cr.	*1.35±0.001*	$6.8*10^{-8}$	$4.0*10^{-5}$	$1.47*10^{+7}$	$2.5*10^{+4}$
ABOVE MCRAE Cr.	*1.48±0.001*	$6.1*10^{-8}$	$4.0*10^{-5}$	$1.64*10^{+7}$	$2.5*10^{+4}$
BELOW MCRAE Cr.	*1.5±0.02*	$7.0*10^{-8}$	$4.0*10^{-5}$	$1.43*10^{+7}$	$2.5*10^{+4}$
HEADQUARTERS	*1.56±0.003*	$7.8*10^{-8}$	$4.0*10^{-5}$	$1.28*10^{+7}$	$2.5*10^{+4}$

Table 5. Summary of STAMMT-L estimated parameters and findings for the intra-order stream tracer tests.

Site Name IOTT	Percent Recovered (%) IOTT	*Dilution* IOTT	B_{tot} IOTT	*Velocity* (m/s) IOTT	*Dispersion* (m^2/s) IOTT	*Power RMSE*	*Exponential RMSE*
Cold Cr. IOTT							
BELOW COLD Cr.	101						
ABOVE LONGER Cr.	100	*0.8±0.02*	*192.6±0.12*	*0.131±0.11*	*1.21±.na*	*0.256*	*1.48*
ABOVE MACK Cr.	71	*1.11±0.002*	*283.1±0.003*	*0.116±0.004*	*1.48±.na*	*0.029*	*2.18*
Mack Cr. IOTT							
MACK INJ ISCO	98						
MID MACK TRIB	84	*0.75±0.05*	*72±0.8*	*0.125±0.02*	*1:625±.na*	*0.254*	*0.72*
ABOVE MCRAE Cr.	39	*1.45±0.05*	*33.7±0.07*	*0.187±0.01*	*0.499±.na*	*0.065*	*0.49*
McRae Cr. IOTT							
BELOW MCRAE Cr.	98						
FLOODPLAIN	76	*0.59±0.003*	*285±0.04*	*0.2±0.04*	*1.64±.na*	*0.265*	*1.01*
HEADQUARTERS	53	*1.29±0.001*	*106±0.001*	*0.21±0.004*	*0.5±.na*	*0.089*	*1.64*

Site Name IOTT	Slope (*k*) IOTT	α_{min} IOTT	α_{max} IOTT	*Max Exchange Time*	*Min Exchange Time*
Cold Cr. IOTT					
ABOVE LONGER Cr.	*1.39±0.001*	$5.0*10^{-5}$	$2.5*10^{-8}$	$4.0*10^{+7}$	$2.0*10^{-4}$
ABOVE MACK Cr.	*1.32±0.002*	$3.7*10^{-4}$	$2.2*10^{-8}$	$4.56*10^{+7}$	$2.7*10^{-3}$
Mack Cr. IOTT					
MID MACK TRIB	*1.12±0.002*	$4.2*10^{-4}$	$8.8*10^{-8}$	$1.14*10^{+7}$	$2.38*10^{-3}$
ABOVE MCRAE Cr.	*1.25±0.01*	$5.3*10^{-4}$	$6.0*10^{-7}$	$1.67*10^{+6}$	$1.89*10^{-3}$
McRae Cr. IOTT					
FLOODPLAIN	*1.12±0.003*	$2.0*10^{-3}$	$4.2*10^{-7}$	$2.38*10^{+6}$	$5.0*10^{-2}$
HEADQUARTERS	*1.25±0.001*	$3.8*10^{-4}$	$7.3*10^{-8}$	$1.37*10^{+7}$	$2.63*10^{-3}$

Table 6. Summary of estimated in channel and hyporheic volumes for the longitudinal and intra-order stream tracer tests.

LTT SITE	Average Stream Cross Section (m^2)	In Channel Volume Between Sites (m^3)	Volume of Hyporheic Zone Between Sites (m^3)	Total In Channel Volume for LTT (m^3)	Total Volume of Hyporheic Zone for LTT (m^3)
INJECTION SITE	0.298			$1.7*10^4$	$1.4*10^6$
ABOVE COLD	0.410	364±110	$6.5*10^3$±$2.0*10^3$	±5040	±$4.33*10^5$
BELOW COLD	0.457	45±14	$1.1*10^3$±350		
ABOVE MACK	0.920	$2.0*10^3$±610	$1.2*10^5$±$3.8*10^4$		
BELOW MACK	0.855	870±270	$1.5*10^5$±$4.42*10^4$		
ABOVE MCRAE	1.020	$3.2*10^3$±980	$3.4*10^5$±$1.1*10^5$		
BELOW MCRAE	1.250	850±260	$9.4*10^4$±$2.81*10^4$		
HEADQUARTERS	2.640	$9.4*10^3$ ±$2.8*10^4$	$7.3*10^5$±$2.2*10^5$		
IOTT Site	**Average Stream Cross Section (m^2)**	**In Channel Volume Between Sites (m^3)**	**Volume of Hyporheic Zone Between Sites (m^3)**	**Total In Channel Volume for IOTT (m^3)**	**Total Volume of Hyporheic Zone for IOTT (m^3)**
Cold Cr. IOTT					
BELOW COLD	0.410				
ABOVE LONGER	0.759	$1.2*10^3$±360	$2.3*10^5$±$6.9*10^4$	$2.0*10^3$	$4.5*10^5$
ABOVE MACK	0.920	800±240	$2.3*10^5$±$6.8*10^4$	±600	±$1.4*10^5$
Mack Cr. IOTT					
MACK INJ ISCO	0.920				
MID MACK TRIB	0.948	900±280	$6.6*10^4$±$2.0*10^4$	$3.3*10^3$	$1.5*10^5$
ABOVE MCRAE	1.020	$2.4*10^3$±730	$8.1*10^4$±$2.5*10^4$	±$1.0*10^3$	±$4.4*10^4$
McRae Cr. IOTT					
BELOW MCRAE	1.250				
FLOODPLAIN	1.649	$1.5*10^3$±450	$4.3*10^5$±$1.3*10^5$	$9.8*10^3$	$1.3*10^6$
HEADQUARTERS	2.640	$8.3*10^3$ ±$2.5*10^3$	$8.8*10^5$±$2.7*10^5$	±$2.9*10^3$	±$4.0*10^5$

The β_{tot} values reported in Table 4 and Table 5 may display a pattern that has significance in relation to the power-law RTD's. Figure 19 shows the β_{tot} values on the left y-axis vs. longitudinal distance on the x-axis with the power-law slope *k*-values on the right y-axis. The solid squares represent the estimates for β_{tot} during the LTT and the open squares show their corresponding power-law slope (*k*) values. The solid triangles represent the estimates for β_{tot} during the IOTTs and the open triangles show their corresponding power-law slope (*k*) values. This graph indicates that an inverse relationship between β_{tot} and the *k*-values is present. For example, if β_{tot} increases during a given tracer test, then the *k*-values generally decrease and visa versa (Figure 19).

Figure 19. Comparison of the β_{tot} estimates to the power-law slopes (*k*) at the different monitoring sites for the Longitudinal and Intra-Order tracer tests shown by longitudinal distance on Lookout Creek in arithmetic space.

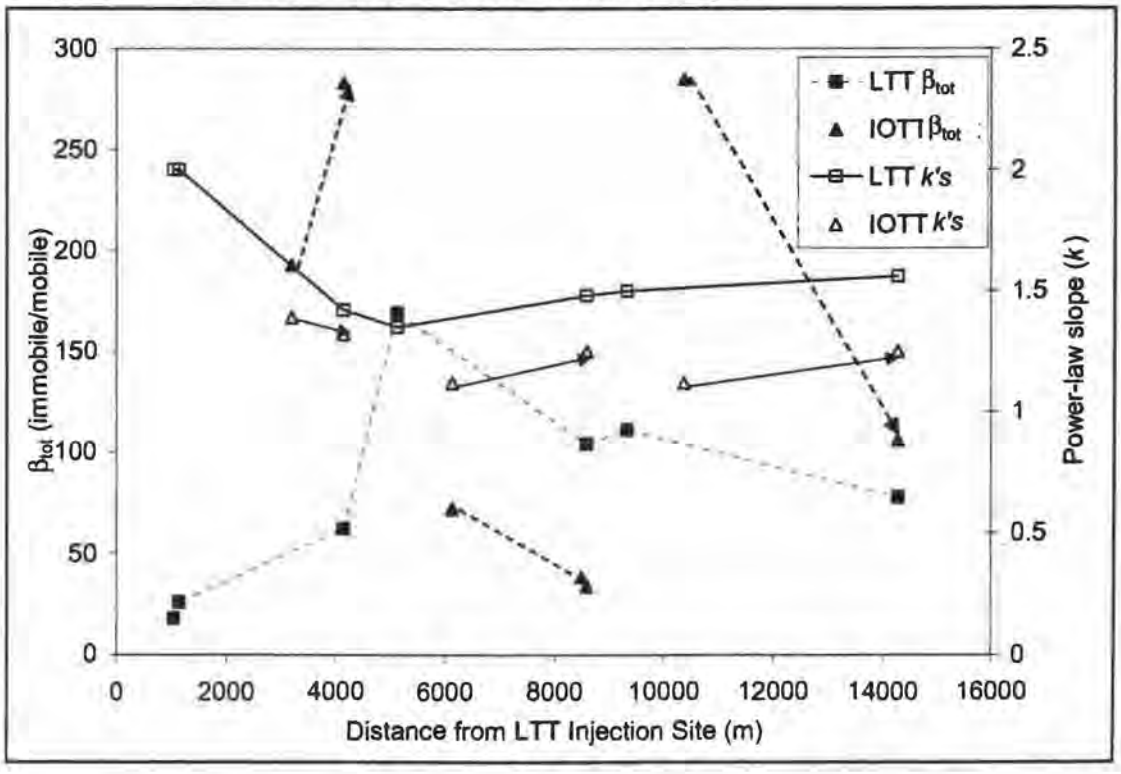

Figure 20 shows the relationship between the decreasing power-law slopes and the increasing β_{tot}. In Figure 20 the power-law slope values for each of the monitoring sites during the LTT and the IOTTs are shown on the y-axis and the corresponding β_{tot} values are shown on the x-axis. Open circles represent all of the

monitoring sites. All of the sites below the Cold Cr. sites are represented by plus signs (+). The relationship for all of the monitoring sites is shown with the dotted line. The r^2 value between this relationship is low with 0.28 in a linear regression, however the p-value is 0.06 (Figure 20). The relationship between power-law slope and β_{tot} values without the LTT Cold Cr. sites is shown to be weak with a low R^2 value of 0.07 and a high p-value of 0.43 and is represented with the black line.

Figure 20. Comparison of the β_{tot} estimates vs. the power-law slopes (k) estimates for the Longitudinal and Intra-Order tracer tests.

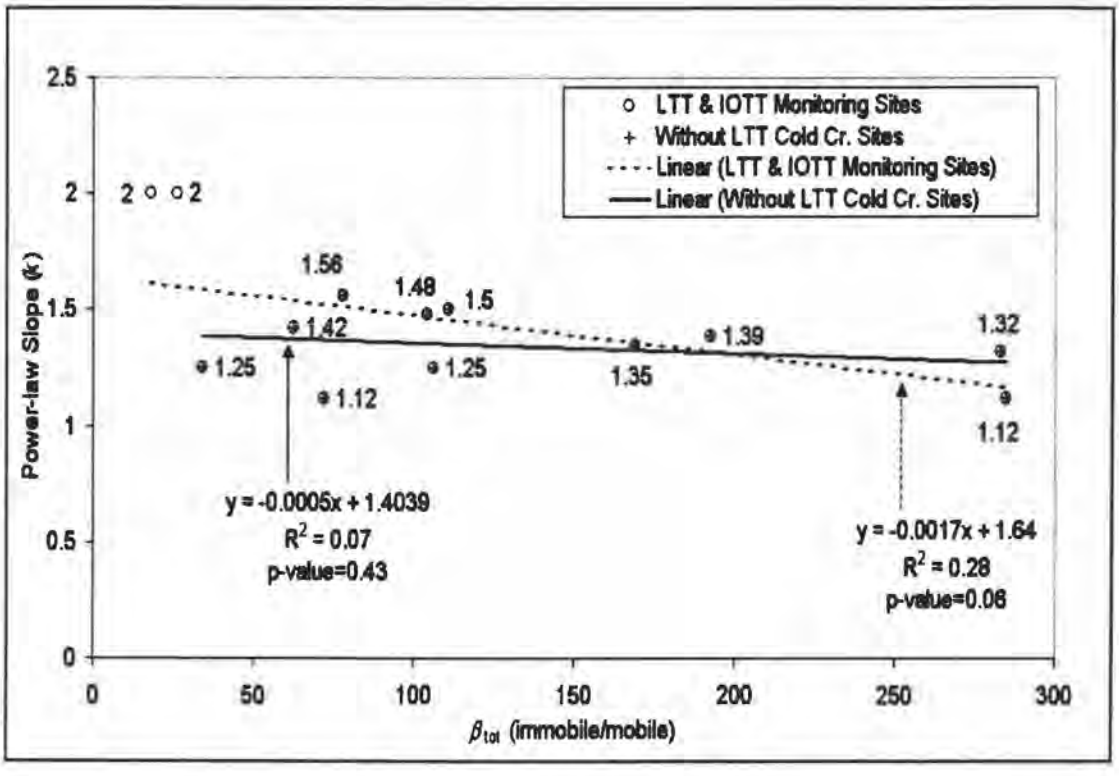

A delayed or retarded concentration decline after several large fall rainstorm events was observed in the declining concentration tails of the above Cold Cr. LTT site, as well as the Longer Cr. site and the Above Mack Cr. site during the Cold Cr. IOTT. Figure 21 shows the discharge on the left y-axis vs. time from the LTT injection, along with the corresponding RWT concentrations on the right y-axis for the Cold Cr. LTT site. Only the tail of the breakthrough curve is shown on Figure 21. Individual fall storms are labeled on Figure 21. During the September 9th and

September 16th rain events a short leveling off of concentration was observed followed by a small drop in concentration after the storm, after the October 11th rain event a larger drop in concentration is recorded (Figure 21). The small drops in concentration after each rain event are less than expected due to the sizes of each event (Figure 21).

Figure 21. The concentration (right y-axis) and the hydrograph (left y-axis) vs. time from injection at the above Cold Cr. site, during the LTT.

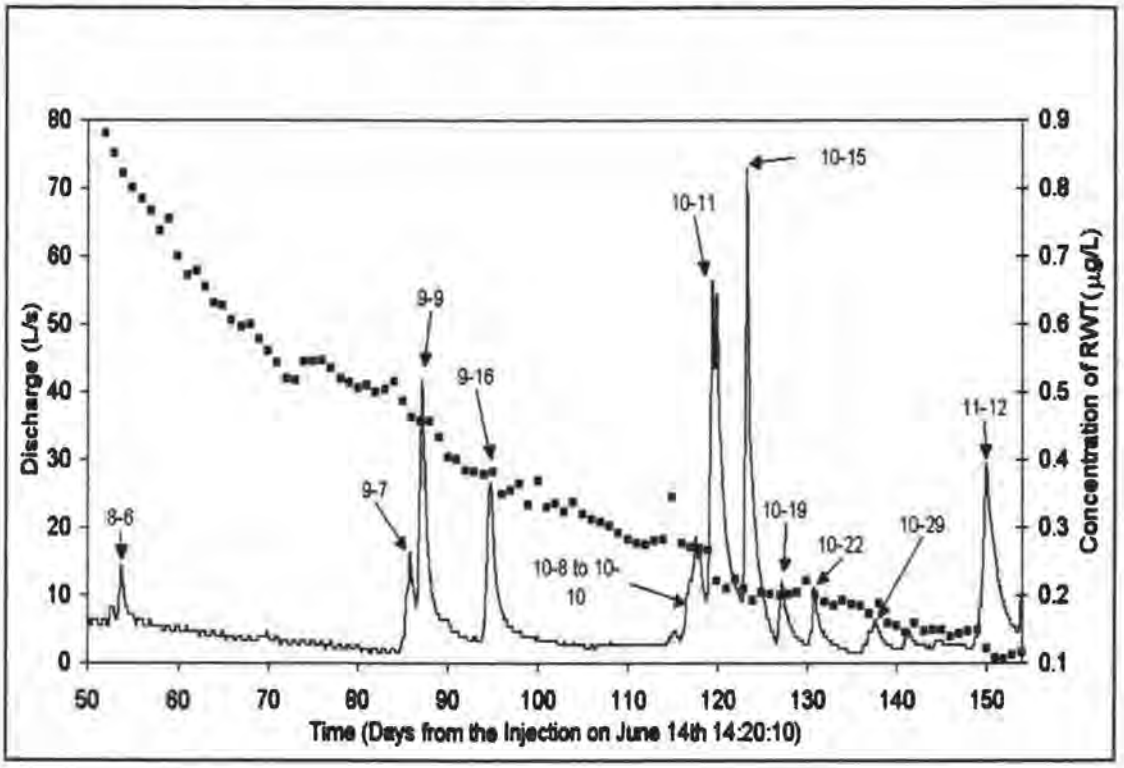

Figures 22 and 23 show discharge on the left y-axis vs. time from the Cold Cr. IOTT injection, as well as the corresponding RWT concentrations on the right y-axis for the respective sites. Figure 22 shows the discharge and concentrations taken at the Longer Cr. site with only the declining tail after 2 days from injection shown. Figure 23 shows the discharge and concentrations taken at the Above Mack Cr. site with only the declining tail after 2 days from injection shown. Little to no decrease in concentration after fall rainstorms was observed at both the Longer Cr. monitoring site and the above Mack Cr. monitoring site during the

Cold Cr. IOTT (Figure 22 & Figure 23). A detailed assessment of the RWT concentration storm response is presented in Appendix III.

Figure 22. The concentration (right y-axis) and the hydrograph (left y-axis) vs. time from injection at the Longer Cr. site, during the Cold Cr. IOTT.

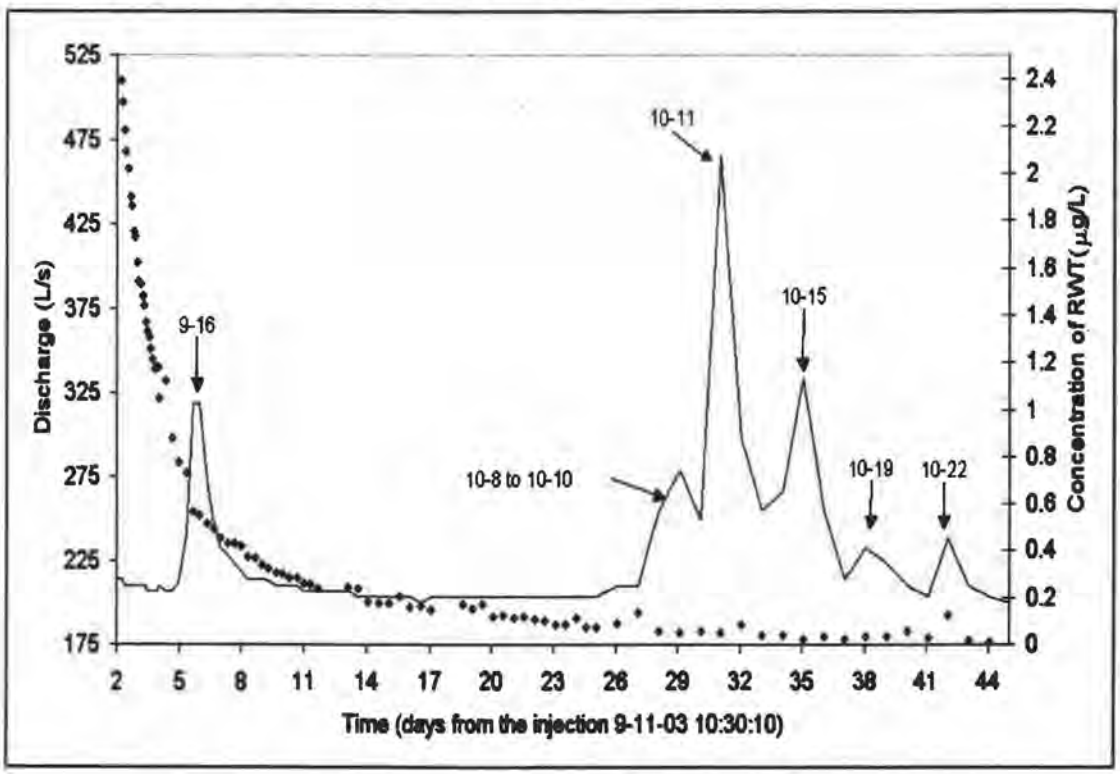

Figure 23. The concentration (right y-axis) and the hydrograph (left y-axis) vs. time from injection at the Above Mack Cr. site, during the Cold Cr. IOTT.

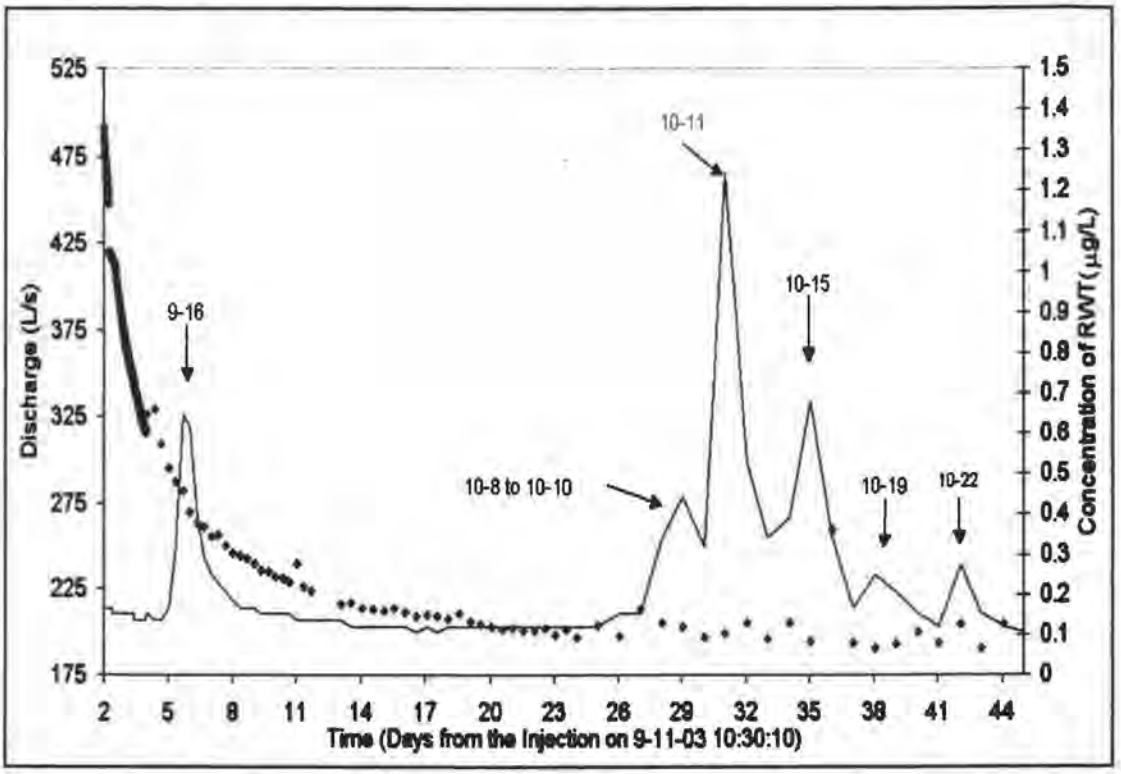

Figure 24 shows the result of a synoptic sampling exercise conducted on the 17th of June, the third day of the LTT injection. The graph has RWT concentration multiplied by upslope contributing basin area vs. longitudinal distance from the injection site shown in semi-log space. Contributing basin area was used in this graph as a surrogate for discharge. By multiplying concentration by basin area Figure 24 shows an estimate value that is linearly proportional to flux for the synoptic sample sites. Direct flux measurements could not be calculated because of a lack of real discharge values between synoptic sample sites. Solid diamonds represent the synoptic samples. The tributaries that correspond to large drops in concentration are labeled in the figure (Figure 24). The concentrations observed at the Injection ISCO site, Above Cold Cr. site, Below Cold Cr. ISCO site, and the Above Mack Cr. site are labeled with open triangles (Figure 24). The synoptic samples show a distinct decline in concentrations after each major confluence (Figure 24). If contributing areas were a perfect surrogate for discharge, there were no mass loss and the streams were at steady state then the expect sample values

would not be expected to change longitudinally and a horizontal line would appear in Figure 24. The concentrations measured during the synoptic sampling matched the monitoring sites closely, with the exception of the Above Cold Cr. site (Figure 24). The Above Cold Cr. site reported a RWT concentration of 473 $(\mu g/L)/km^2$ at the same time that the synoptic sampling reported a RWT concentration of 337 $(\mu g/L)/km^2$ (Figure 24). The reason for the discrepancy between the fluorometer and the hand sample at the Above Cold Cr. site is unknown. For a detailed review of the synoptic sampling results and discussion see Appendix IV.

Figure 24. The concentrations of the synoptic samples and concentration at the upper monitoring sites take during the injection of the LTT normalized to the upslope contributing basin area vs. longitudinal distance in semi-log space, June 17th 2003.

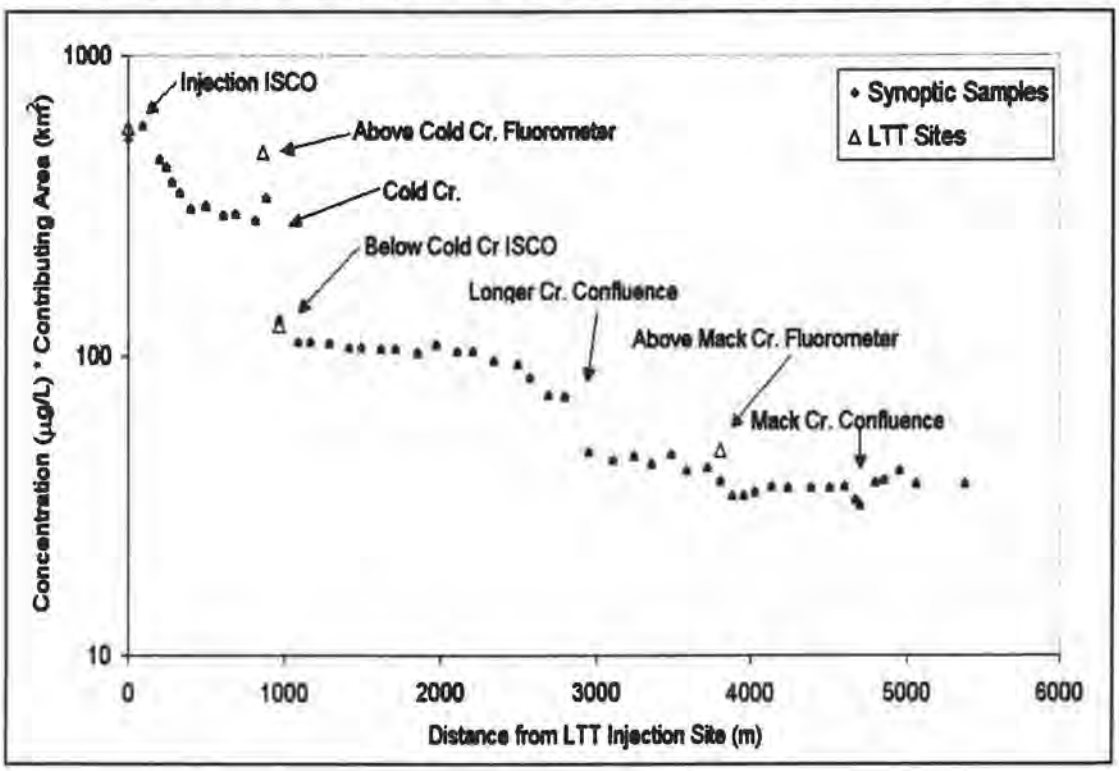

5.0 DISCUSSION

5.1. Behavior of Hyporheic Exchange in the LTT and the IOTTs

The behavior of flow paths through the hyporheic zone is commonly determined by evaluating the concentration breakthrough curves or flux

breakthrough curves of solute tracer tests. The curves are compared to hyporheic exchange models in an attempt to find the closest mathematical model to represent the hyporheic residence time distributions, which represents the distribution of flow paths. The most commonly used model is the conventional exponential model, which uses an exponential function to describe the mass transfer rates between the stream and hyporheic zone. Unfortunately, the exponential model does not accurately replicate the mass transfer in late time as shown in Figure 1. The dependency of the exponential models on a limited range of timescales of mass transfer has resulted in a scale-dependency of the hyporheic characteristics estimated by these models (Harvey et al., 2000; Harvey & Wagner, 2000; Haggerty et al., 2002; Schummer et al., 2003; Haggerty et al., 2004). In an effort to solve the scale-dependency issue we have employed a second type of mass transfer model. This second type of model, STAMMT-L, which is described in the background section of this report, uses a mass transfer function that is a power law and accounts for a wide range mass transfer timescales.

The power-law RTD has important characteristics that make it appropriate for the problem of parameter scale-dependency in modeling the hyporheic exchange. First of all, power-law functions are generally not dependent on scale and remain consistent over most scales. Secondly, several studies have shown that the tails of breakthrough curves of tracer test behave as power-laws if enough late-time data is collected (Haggerty et al., 2002; Gooseff et al., 2003; Schummer et al., 2003; Haggerty et al., 2004). This current study has strengthened the argument that power-law RTDs describe the normal behavior of the hyporheic zone in mountain streams better than the exponential RTD. The four different tracer tests analyzed in this study all showed power-law RTDs. The breakthrough curves for the four different tracer tests are shown in Figures 4, 6, 8, 9 & 11-16, and all of them have a straight line or nearly straight line in their tails, which indicates power-law behavior. Furthermore, the STAMMT-L model results confirmed that the best fits are achieved by general residence time distributions that used power-laws. Model simulations that used the conventional exponential model failed to represent the late-time data as accurately and had RMSEs that were always higher than the

power-law models (Table 4 and Table 5). Therefore, this study has shown that the hyporheic zone is dominated by power-law residence time distributions in the Lookout Creek basin in the Oregon Cascades.

The nature of a power-law residence time distribution conveys vital information about the characteristics of the hyporheic zone. A power-law distribution indicates that the hyporheic zone has a wide range of flow path lengths and numerous flow paths within that range. Hyporheic flow paths are driven by geomorphic characteristics and hydraulic gradients in the streambed, therefore different power-law distributions may indicate differences in the driving forces of hyporheic exchange. This study has shown that power-law RTDs were prevalent in the Lookout Cr. basin, but the behavior could be quantified in greater detail. The STAMMT-L model fits that were used to simulate the breakthrough curves also estimated the power-law exponents for the declining breakthrough curve. Each of these power-law exponents can be used as a signature or a fingerprint that characterizes a particular RTD. The exponent provides information on the variance of flow paths and exchange rates within the hyporheic zone. The STAMMT-L model results for the LTT and the IOTTs show that a range of power-law exponents (k) exist in the Lookout Cr. basin and therefore a range of RTDs exist. The range for our tracer tests was between –2 and –1.12 (Figure 10 and Table 4 and Table 5). These k-values create a relatively shallow slope for the breakthrough curve tail and indicate a wide distribution of hyporheic flow path lengths (Haggerty et al., 2002).

The LTT showed a constant k-value of -2 in the 2nd order reaches above Cold Cr. and k-values of -1.35 to -1.56 below (Figure 10). The larger k-values observed in the upper reaches compared to the lower reaches would seem to indicate that there is greater variance in residence times in the lower sections. The consistent –2 k-values in the 2nd order reaches may indicate homogeneous hydraulic conductivities or flow paths, which may be a reflection of homogeneous geomorphic characteristics in the upper reach and a smaller variance of residence time distributions. The k-values of -1.35 to -1.56 estimated for the lower reaches of the LTT may indicate a more heterogeneous geomorphic setting, hydraulic

conductivities, and larger variance of residence time distributions. This study did not quantify the geomorphology of the tracer test reaches in enough detail to prove or disprove the role that geomorphology may play on the *k*-values. However, it is likely that changes in geomorphology cause changes in RTDs. For example the lower *k*-values seem to correspond to portions of Lookout Cr. that are alluviated with a wide valley floor, where as the higher *k*-values seem to occur around Cold Cr. were there is less alluvium and the valley is more constrained.

One potential error in the power-law RTD findings in the LTT may have resulted from a power-law "echo". Power-law behavior could have been propagated downstream and observed at the downstream sites because of the hyporheic characteristics in the upper reaches. However, the k-values from the IOTTs tell us that the power-law distributions of flow paths in the hyporheic zone in the lower reaches are independent of the upper reaches, therefore strengthening the argument for power-law behavior throughout the basin. The IOTTs displayed similar traits in *k*-values as the LTT, although slightly lower. The range of *k*-values for the IOTTs' was from –1.12 to –1.39 (Figure10). Because of time, weather, and high concentrations there was no IOTT that duplicated the LTT reach above Cold Creek so no comparison of the 2nd order *k*-values was possible. However, the IOTTs' confirm that even at smaller scales, the reaches between the confluences have their own power-law RTD and a wide spread of distributions as shown by the low *k*-values (Haggerty et al., 2002).

5.2. Development of Power-Law Behavior

Development of the power-law behavior in the hyporheic zone did not occur at the same time after the end of the injection during each of the tracer tests, as indicated in Figures 11-16. Other studies have shown that, as the size of the stream increases, a decreased percentage of water is traveling through the hyporheic zone (Kasahara and Wondzell, 2003). By this rationale, a small stream with the same hyporheic flow paths will develop into a power-law RTD faster than a larger stream because a larger fraction of the water in the small stream will enter and exit the hyporheic zone before the larger stream can do the same.

The IOTTs indicate that as the size of the stream increases, the time it takes to develop the power-law behavior observed in the hyporheic zone increases (Figures 14-16). For example the Cold Cr. IOTT developed power-law behavior directly after the end of the injection as shown by the immediate straight line of both breakthrough curves after the peak in Figure 14. The delayed behavior is shown by the curves of the Mack Cr. IOTT, which took between 12 and 24 h to develop into straight lines and show signs of the power-law RTD (Figure 15).

The LTT did not show the same pattern of delayed development of the power-law RTD as the IOTTs. All of the monitoring sites in the LTT showed power-law behavior from immediately after the peak of the breakthrough curve (Figure 4, 6, 8-9). This pattern can be explained by the influence of the above sites on the lower sites. Once the power-law is developed in the upper reaches it is propagated down to the lower reaches and the lower reaches sense a power-law RTD sooner than they may have developed without the upper reaches' input.

The ratio between the size of the stream and the size of the hyporheic zone (β_{tot}) is another important factor. The larger the hyporheic zone, the longer the time needed for the tracer to exchange with the hyporheic zone and return to the stream. The water must experience enough flow path variance to develop a power-law RTD. The estimates for β_{tot} during this study should not be given too much significance due to the influence of sorption on the numbers, which will be discussed below, however the β_{tot} can be used as a rough estimate of the size of the hyporheic zone. Based on the general relationships of the β_{tot} values, Mack Cr. IOTT (4^{th} order) took a longer time to become a power-law than the McRae Cr. IOTT (5^{th} order). This can partly be explained because the hyporheic zone along the McRae Cr. reach is almost three times as large as the same distance along Mack Cr. reach.

Increasing or decreasing the velocity of the stream or the exchange rate between the stream and the hyporheic zone reduces or increases the development time of a power-law behavior. The velocity of a stream will generally increase with increasing size, but it is possible for two streams with the same discharge to have different mean velocities depending on the slope, roughness, or geomorphic

complexity of stream. Likewise, the exchange rate of two similar streams could differ depending on the slope, roughness, geomorphic complexity, and porosity of the substrate. The data from this study indicate that the greater the discharge of the stream, the longer time it takes for the power-law RTD to develop, or power-law RTD develops more slowly farther downstream.

5.3. Effects of Sorption on Breakthrough Curves and β_{tot} Estimates

The effects of sorption on the breakthrough curves of this study cannot be overlooked. Rhodamine WT was chosen as a tracer for this study because of its many advantages, however RWT has a significant disadvantage in the fact that it sorbs to clay minerals, iron minerals, and organic matter (Bencala et al., 1983; Stutter et al., 2001; Tai and Rathbun, 1988; Trudgill, 1987). The amount of sorption of RWT for the typical tracer test, which usually tests over a reach length of 100's of m, is usually small enough to overlook or make minor adjustments to account for the loss. However, the LTT and the IOTTs were all conducted over 1,000's of m and the amount of exposure to sorbing material was increased with distance. The loss or retardation due to sorption was significant during these tests, as indicated by the decline of mass recovered in Table 4 and Table 5.

The sorption of RWT to clays, irons, and organics has been shown to be linear with respect to concentration in a sub-basin within the Lookout Cr. basin (Gooseff et al., in press). Gooseff et al. (in press) showed that in watershed 3 (WS03) the concentration of Rhodamine WT (CRWT) sorption isotherm had an dissociation constant (K_d) of 0.0332 L/g and was represented by Equation 8.

Equation 8 (RWT sorption isotherm)

$$S = K_d * CRWT,$$

where S is the sorbed mass of RWT per mass of sediment in µg/g and CRWT is the aqueous concentration of Rhodamine WT in µg/L. The estimated isotherm is

thought to be an over estimation of the natural sorption of RWT in WS03, because the calculation was conducted in a laboratory and used sediment smaller then 2mm (Gooseff et al., in press). The isotherm was calculated using concentrations between 0.025 µg/L to 70 µg/L, which is appropriate for all of our tracer tests except for the LTT injection ISCO™ site and the peak of the Above Cold Cr. site during the LTT (Gooseff et al., in press).

Because the sorption of RWT is linear, it is also released in a linear fashion and therefore has a retarding effect on the tracer plume as it moves downstream. The retardation of the plume by sorption shifts the tails of the breakthrough curves up and to the right. This shift in the tails increases the estimated size of the hyporheic zone. Although the sorption shifts the breakthrough curves it does not alter the shapes of the curves, and therefore does not affect our analysis of the power-law RTD. The linearity of the RWT sorption isotherm in the Lookout Cr. basin allows our power-law RTD analysis to proceed, but does raise questions about the accuracy of our β_{tot} estimates. In all likelihood the β_{tot} results shown in Table 4 and Table 5 and in Figure 19 are over-estimates that increase in error as the length of the test reach increases.

5.4. Can a Single Power-Law RTD be Scaled to the Entire Lookout Creek?

A major goal of this study was to investigate whether there was a characteristic power-law RTD that could represent the entire Lookout Creek basin. Power-law functions are independent of scale and therefore allow a convenient method for scaling up tracer results. If a single power law existed for Lookout Cr., a scaling relationship could be developed to extrapolate hyporheic characteristics from small reaches to the entire basin.

The LTT and IOTTs results are more complicated than a simple single power-law RTD in Lookout Cr. (Figure 10). Throughout all of the tracer tests no two monitoring sites had the same power-law exponent (k), but several patterns did emerge that may have significance. A comparison of the modeled slopes of the IOTTs to the slope found at the same location during the LTT indicates significant

variability as well as a possible pattern (Figure 10). The LTT showed an average *k*-value of -1.46 for the reaches below Cold Cr. and the IOTT had an average *k*-value of –1.24, to create a combined average of –1.34. The IOTT *k*-values were smaller than the LTT *k*-values, which indicates that the shorter tracer test has a larger distribution of residence times. This difference may result from lower discharges during the IOTTs, which affects the amount of hyporheic zone that the tracer test is interrogating or may reflect an actual change in the size of hyporheic zone that the tracer test is sensing. The LTT and the IOTT data indicate that, as the β_{tot} increases, the distribution of the residence times widens, and as the β_{tot} decreases, the residence time distribution narrows (Table 4 and Table 5 and Figure 19). Therefore, the changes in *k*-values are likely responding to changes in the hyporheic zone. Several other relationships were observed when the *k*-values for LTT and IOTT were compared to each other. The direction of change observed in the *k*-values for the LTT and IOTT may show a basin wide pattern. The upper reaches of Lookout Cr. showed a decrease in *k*-values between sites, in the downstream direction, during the LTT and the Cold Cr. IOTT. During the Cold Cr. IOTT, *k*-values deceased from -1.39 (site 5) to -1.32 (site 6) (Figure 10). The LLT showed deceases in *k*-values from -2 (site 4) to -1.42 (site 6) for the same longitudinal positions as the Cold Cr. IOTT (Figure 10). The decrease in *k*-values continued until below the Mack Cr. confluence. Below the Mack Cr. confluence the *k*-values increased all the way to the last monitoring site at the headquarters. The Mack Cr. IOTT, McRae Cr. IOTTs and lower sites of the LTT showed increases in *k*-values downstream. The Mack Cr. IOTT showed *k*-values increasing going from –1.12 (site 9) to –1.25 (site 10) and the LTT showed increase from –1.35 (site 7) to -1.48 (site 10) (Figure 10). The McRae Cr. IOTT showed increasing values of *k* going from –1.12 (site 13) to –1.25 (site 14) and the same stretch of stream showed an increase in the LTT from *k*-values of -1.5 (site 10) to –1.54 (site 14) (Figure 10). The longitudinal changes in *k*-values could be showing variability around a local mean *k*-value. The average *k*-value of all of the *k*-values below Cold Cr. was -1.34. If the *k*-values are centered on a local mean in the lower reaches, then the average value may be the best representation of a basin

wide residence time distribution. Another reason for the fluctuations in the *k*-values longitudinally may be explained by changes in the characteristics of the hyporheic zone between each reach, which may be driven by changes in geomorphic characteristics (Anderson et al., 2004; Kasahara and Wondzell, 2003).

If the *k*-values are centering on an average value or if they are reflecting a particular type of geomorphology it could allow a characteristic value to be developed for use in other Oregon Cascade basins. For example if a relationship can be established between low *k*-values and alluviated reaches then those low k-values could then be used to characterize the hyporheic properties of other alluviated reaches in different basins. This study is an attempt at quantifying a basin wide RTD, and further studies need to be completed to solidify the relationship between power-law RTDs and geomorphology.

5.5. Is the Power-Law RTD in Lookout Creek Scale Invariant?

Part of the original hypothesis of this study was to use a mass transfer model to characterize the hyporheic tail and see if the scale-dependency of tracer tests parameters could be eliminated. The scale-dependency of reach length to the tracer parameter estimates has been a problem when using the conventional exponential model (Harvey et al., 2000; Haggerty et al., 2002; Gooseff et al., 2003; Schummer et al., 2003; Haggerty et al., 2004). The development of a method of model analysis that is more accurate in modeling the multitude of flow paths and exchange rates that typically exist in a mountain hyporheic zone should increase our accuracy in predicting hyporheic parameters. Physical evidence indicates that hyporheic exchange behaves in a fractal or power-law manner, with a variety of fast and slow flow paths on all scales (Figure 8-9, 14-16). Using a power-law distribution of flow paths is a convenient way to develop a new model that accounts for the variety of flow paths and at the same time is less dependent on the scale of the test reach. The new model, if RTD's are scale independent, would allow parameter estimates to be applied to a larger section of the stream than was covered by the tracer test.

The finding of this study partially supports the goal of building a new scale-independent mass transfer model. Figure 18 shows that the scale-dependency was reduced by using a power-law RTD instead of the conventional exponential RTD but not eliminated. The scale-dependency of the tracer tests was hinged upon the relationship between the size of the power-law exponent and the length of the stream. The reduction of scale-dependency is shown in Figure 18. For comparison, Figure 18 shows the results of Harvey and Wagner's (2000) conventional exponential model analysis compared to our power-law model results. By comparing the power-law regression fit for Harvey and Wagner's (2000) data to the current study's power-law regression fit we can see that the scale-dependency of the model parameters is reduced by the power-law RTD model (Figure 18). The reduction of scale-dependency is shown in the slope of the regression lines in log-log space, which is 0.45 for Harvey and Wagner's (2000) data and 0.2 for the current study's data with all of the sites and 0.16 when only the lower reaches were included.

This study's data indicate that the power-law exponent increases as mean channel residence time increases (Figure 18). This relationship was also observed when power-law exponents vs. test reach length were graphed for the below Cold Cr. sites 2 and 4 (Figure 17). The fact that the Cold Cr. sites did not match the pattern of the lower sites may indicate that they are just anomalies. However, the Cold Cr. sites could also indicate that there is something significantly different about the upper reaches of Lookout Cr. that causes the power-law exponents to change. The power-law exponents represent the slope of the breakthrough tail and therefore the distribution of flow paths in the hyporheic zone. Increased power-law exponents indicate that the distribution of hyporheic flow paths is decreased with longer test lengths. If the Cold Cr. sites are not included in the analysis, the r^2 values go from 0.22 to 0.51, the p-values go from 0.29 to 0.04 and the scale-dependency of the power-law exponents is further decreased, but not eliminated (Figure 18).

The separation of the Cold Cr. data from the rest of the sites may be justified by the different geomorphologies that are driving the changes in hyporheic

exchange. While this study did not include an extensive geomorphic survey, a rough visual survey was conducted and differences were noted between all of the confluences. Cobble/boulder beds with numerous logjam steps dominated the upper reaches of Lookout Creek down to Mack Creek. Cobble beds with cascade/riffle morphology dominated the lower reaches. Other studies have shown that the hyporheic exchange in the H.J. Andrew is partially driven by geomorphic characteristics such as stream gradient breaks, sizes of drops, spacing between geomorphic features like pools and drops, and amounts of sediment behind drops (Anderson et al., 2004; Kasahara and Wondzell, 2003). A basin the size of Lookout Creek may have enough change in geomorphology to create several different and distinct power-law residence time distributions. It is probable that each power-law may hold a unique scaling relationship within its unique geomorphic setting and that smaller tracer tests within that geomorphic regime could be scaled up to the furthest extent of that regime. However, in order to conclusively prove that statement, more research and testing must be done and power-law exponents would have to be matched with geomorphic regimes. This study indicated that a "universal" residence time distribution for the basin does not exist.

5.6. Other Findings and Observations

During the LTT and IOTT several findings did not involve our hypothesis and power-law RTDs, but are of interest in hyporheic research and are therefore reported in this section.

First of all, several irregularities were observed in the behavior of the concentrations in the late time breakthrough curves. A series of spikes and rises are evident in the concentration and flux curves for the Cold Cr. IOTT (Figure 11 & Figure 14). These spikes and rises coincide with several storms that occurred during this test and they are believed to be the cause of the observed anomalies. The spikes and rises are of particular interest here because they seem to indicate a release of RWT into the stream. One possible mechanism of such a release may be

related to the rise in stage of the stream associated with the storm events. The Cold Cr. IOTT was conducted over a reach length that was earlier used in the LTT, but had since returned to background concentrations of RWT. During the LTT the stage and discharge of the stream were higher than during the Cold Cr. IOTT. The increase in stage during the Cold Cr. IOTT exposed surfaces that had been abandoned after the decline in discharge during the LTT. The abandoned LTT surfaces may have had higher concentrations of sorbed RWT that were re-exposed and allowed to reenter the stream with the consequence of a measurable spike during the Cold Cr. IOTT. The largest spike was observed at the Cold Cr. IOTT injection site (Figure 11). The Longer Cr. and Above Mack Cr. site didn't show as much change in concentration during the rain events, but the flux curves registered a spike, which indicates that mass was being added to the system even if it didn't show as an increase in concentration (Figure 14).

Another irregularity involved the early fall rain events and the breakthrough curves during the LTT and IOTT. As mentioned above, the Cold Cr. Injection site showed an increase in concentration during the rain event on 9-16-03, however the Above Cold Cr., Longer Cr. and Above Mack Cr. sites did not show a significant increase or decease in concentration (Figure 21-22). The spike of concentration at the Cold Cr. Injection site adds an unexplained complexity to the problem. It was first thought that the extra rise at the Injection site was a result of the stream being exposed to higher concentration of RWT during the LTT, however the Above Cold Cr. site did not respond with changes in concentration as expected, since it was exposed to an even higher concentration than the Cold Cr. Injection site during the LTT (Figure 11, 20-22). The Above Cold Cr., Longer Cr. and Above Mack Cr. sites did not show much change in concentration during several rain events, however the lack of change in concentration still indicates that RWT mass was entering the stream to offset the increase in stream discharge. Also significant is that the water that entered the stream had the right amounts of RWT to maintain a near constant concentration with only a gradual decline of concentration after the rain event (Figure 21-22). For further information on the concentration storm response in the LTT and IOTTs see Appendix III: Storm Response.

Secondly, other parameters measured by the LTT and the IOTTs present further evidence that the tracer tests are sensitive to the specific reach and the flow conditions during the test. Large variability was observed in parameters such as β_{tot} and dispersion, which may indicate the susceptibility of these two parameters to sensing the differences in test reaches. The parameter estimates for the velocity, dilution, and mass recovered displayed much more regular longitudinal patterns. These longitudinal patterns were generally explained by position in the basin and total distance from the injection sites. A more in-depth discussion is given in Appendix II: Additional Parameter Information.

6.0 CONCLUSIONS

Four major conclusions were developed from the longitudinal and intra-order tracer tests that were conducted on Lookout Creek in the H.J. Andrews Experimental Forest, a small mountain basin in the Oregon Cascades, during the summer of 2003.

First, power-law residence time distributions were observed at 13 different monitoring sites during four tracer tests that covered 14 km of Lookout Cr. and account for 61.8 km^2 of the contributing area of the 64 km^2 basin. This study indicates that power-law residence time distributions dominate the behavior of hyporheic exchange in the H.J. Andrews.

Second, this study found that power-law exponents of the RTD change longitudinally along Lookout Creek and within individual tracer tests. The distribution of hyporheic flow paths has a lower amount of variability in the upper reaches of Lookout Cr. compared to the lower reaches. The difference between power-law RTDs observed at the same location during different tests may be the result of variance around a common average or the result of changes in stream discharge. The longitudinal change in power-law RTD's within individual tracer tests cannot be explained by scale-dependency alone and it is our assumption that geomorphic differences in the study reaches cause the differences in the observed power-law RTD.

Third, no single power-law RTD was identified that characterized the entire basin. The use of a power-law RTD to characterize the hyporheic exchange did not eliminate the scale-dependency of tracer test parameters, but did significantly reduced the dependency compared to the conventional RTD exponential model. More detailed studies are needed to determine if a given power-law RTD can be associated with a type of geomorphology. If this relationship can be established, it may be possible to use a small tracer test to quantify the hyporheic characteristics in a stream and use a scaling up relationship to extend the characteristics to the extent of the specific type of geomorphology.

Finally, it takes a larger amount of time to develop a power-law RTD as the stream size increases longitudinally. Increases in discharge, hyporheic volume, and velocity likely were responsible for the increased delay in developing a power-law RTD by increasing the travel distance that is necessary for the stream water to experience enough variability in flow paths to acquire a power-law distribution.

Future studies could add valuable information to our understanding of power-law behavior in mountain rivers. The prevalence of power-law behavior in other settings, including other basins within the Oregon Cascades, Oregon Coast Range, as well as other mountain ranges is unknown and would provide valuable data. Longitudinal tracer tests that extend over 3 orders of magnitude of distance, 5 orders of magnitude of time and measure continuous discharge would also be valuable for future hyporheic flow understanding. Other tracer tests may help to establish whether power-law behavior breaks down at specific distances or in certain types of geomorphology. A quantitative study exploring the relationship between power-law RTD's and specific geomorphic types would also have many benefits for the practical application of the power-law RTD's in other fields like ecology and watershed analysis.

7.0 APPENDIX I: DETAILED METHODS

7.1. Longitudinal Tracer Test

The Longitudinal Tracer Test (LTT) consisted of a basin wide longitudinal tracer test on Lookout Creek, located in the Western Cascades of Oregon (Figure 3). The test was conducted to study the behavior of hyporheic exchange and the distribution of flow paths within the hyporheic zone at multiple scales. More specifically, this test was investigating whether the residence time distribution of the hyporheic zone behaved in a fractal manner. If fractal behavior was observed on the tracer test scale, a power-law function would be tested to see if the behavior could be scaled to the entire basin.

The LTT encompassed 14,274 km of Lookout Creek. Monitoring sites recorded solute tracer concentrations above and below major confluences, including Cold Cr., Mack Cr., McRae Cr., as well as a monitoring station at the H.J. Andrews headquarters near the mouth of Lookout Cr. basin. In this tracer test 1603.9 g of Rhodamine WT (RWT) was injected near the upper portions of Lookout Creek as indicated in Figure 3. Lookout Cr. is a 2^{nd} order stream at the injection site. The injection lasted 78 h and concentrations were collected at the monitoring stations until the stream reached background levels of Rhodamine. Data was collected for 5 months at the Above Cold Cr. site. The general site characteristics and Universal Transverse Mercator (UTM) positions of all the LTT sites are presented in Table 1 of the Methods section of this thesis.

The choice of RWT as tracer for this study was a result of the advantages that RWT provides for a field study. RWT has many desirable qualities for use in ecologically sensitive mountain streams, and has been successfully used in many tracer studies (Derouane and Dassargues, 1998; Gooseff et al., 2003; Haggerty et al., 2000; Haggerty et al., 2002; Kass, 1994; Pang et al., 1998; Pang and Close, 1999; Siton et al., 1997; Smart and Smith, 1976; Smart and Laidlaw, 1977; Stutter et al., 2001; Turner Designs, 1998a). The qualities that make RWT a useful tracer include a low detection threshold of <0.1 μg/L, it is more stable than other

fluorescent dyes, changes in pH above 6 have little affect on its fluorescence, it is considered by the U.S. Environmental Protection Agency to be non-toxic if used in according to the national sanitation guidelines, and shown to be non-toxic at concentration of 1-2 μg/L for 24 h (Federal Register; Field et al., 1995; Smart and Laidlaw, 1977; Stutter et al., 2001; Turner Designs, 1998a).

Various studies have shown that photochemical decay, reactions in solution, volatilization, and uptake by organisms of RWT is small or insignificant (Bencala et al., 1983; Fox et al., 1991; Jensen and Kristensen, 1989; Tai and Rathbun, 1988; Turner et al., 1991; Smart and Smith, 1976; Smart and Laidlaw, 1977). The main disadvantage of RWT is sorbtion to clays minerals, iron minerals, and organic matter, which has been found to be significant in several studies (Bencala et al., 1983; Stutter et al., 2001; Tai and Rathbun, 1988; Trudgill, 1987). Additionally, RWT has 2 different isomers, which have been found to have different absorption rates and fluorescence emissions (Stutter et al., 2001). The differences in isomers have been shown to contribute to significant error in interpreting chromatographs and mass recovery (Stutter et al., 2001). Despite the drawbacks, the advantages have allowed RWT to be considered a conservative tracer in many studies with successful results (Derouane and Dassargues, 1998; Gooseff et al., 2003; Haggerty et al., 2000; Haggerty et al., 2002; Kass, 1994; Pang et al., 1998; Pang and Close, 1999; Siton et al., 1997; Smart and Smith, 1976; Smart and Laidlaw, 1977; Stutter et al., 2001).

The Universal Transverse Mercator (UTM) positions were established by acquiring global positioning system (GPS) direct satellite feed information or by using ArcGIS to establish approximate positions. The approximate positions were estimated by using a stream layer, a digital elevation model, and recent aerial photos. By using known physical features such as confluences, point bars, stream meanders, and the proximity to roads, sites were identified from aerial photographs in ArcGIS and the UTM coordinates were then extracted from the GIS map.

7.1.1. Longitudinal Tracer Test Injection Site

The LLT injection site was located ~10m downstream of the bridge for the upper old growth trail, ~0.4 km from Road 1506. Originally the injection was planned to take place ~2 km upstream, but due to low discharge and inaccessibility, the top of the old growth trail site was chosen.

The injection site consisted of a DC injection pump connected to six 12 V DC batteries with a generator backup. Dilute RWT was pumped from a large plastic tub into the stream using ¼" rigid vinyl tubing. The pump was a 260 mL/min Fluid Meter Inc. (FMI) DC injection pump (model # RHB1), manufactured by Fluid Meter Inc. in Syosset, New York. The six batteries were various 12 V deep-cycle DC Trojan models, manufactured in Lithonia, Georgia. The bank of six 12 V deep-cycle batteries were employed to stabilize the FMI pumping rate by reducing the decline of DC power over time. Each of the batteries was connected in parallel to boost the power storage capacity. We further attempted to augment the power loss by monitoring the power drain. When the batteries reached ~12.45 V we turned the generator on for ~2 hrs. The generator was connected to one end of the battery line and the FMI pump was connected to the other end of the line. We monitored the voltage with a multi-meter from the FMI end of the battery line.

A critical drawback to using a DC powered pump is the fluctuation in the power source over long periods of time. It was observed prior to the injection, that as the power of the 12 V DC battery declined, the pumping rate also declined. Originally it was thought that the battery bank and the generator recharging the batteries would be enough to maintain a steady enough power source that would not affect the injection rates. Unfortunately, this technique of power control caused its own problems. The generator caused a quick power spike and initially accelerated the pumping rates when it was turned on and then the pumping rate slowly declined after the generator was turned off. The resulting injection was unstable (Figure 25).

On the day of the injection, we measured a discharge of 24.6 L/s 40 m downstream of the injection site, using a Flo-Mate™ flow meter. Using this

discharge we calculated that we would need 1620 g of RWT to achieve a target concentration of 250µg/L, for a 72 hr injection. We then mixed an injection solution that consisted of 33,530 mL of 0.05% RWT (model # 106053 FWT Red 50) from Bright Dyes Miamisburg, Ohio, and 100,590 mL of water from the stream, resulting in a concentration of 12.5 g/L RWT. Next we calibrated the FMI pump to pump at a rate of 0.5 mL/s at 12.65 V. Optimally, this would have allowed a 74.51 h injection at 250 µg/L.

The actual injection concentration during the tracer test was lower and the test injection lasted longer than originally calculated. Several factors contributed to this problem. First of all, it is believed that the original discharge measurement underestimated the flow rate, possibly due to underflow or instrument error in measuring small streams. Secondly, the average operating voltage of the FMI pump was <12.58 V, instead of the initially estimated 12.65 V. The consequences of the lower pumping rate in combination with underestimating the stream's discharge resulted in an average stream concentration of 172 µg/ L ± 24 µg/ L over 78 h (Figure 25). The RWT injection continued at a varying rate for 78 hours and at the conclusion of the injection, 5,808 mL of solution remained. A total of 1603.9 g of RWT was injected into Lookout Creek during the LTT.

Figure 25 shows the concentrations of Lookout Cr. taken from an ISCO™ sampler, manufactured by Teledyne in Los Angeles, California. The sampler was located 84 m downstream of the injection site for 7 days after the start of the LTT injection. The average daily concentration during the injection is shown in Figure 25 by a red line with the individual daily values labeled and a red arrow pointing to their corresponding day. A blue line shows the overall average injection concentration and its value is displayed with a blue arrow (Figure 25).

Figure 25. Concentrations for the Longitudinal Tracer Test taken from the injection site ISCO™, HJA 2003.

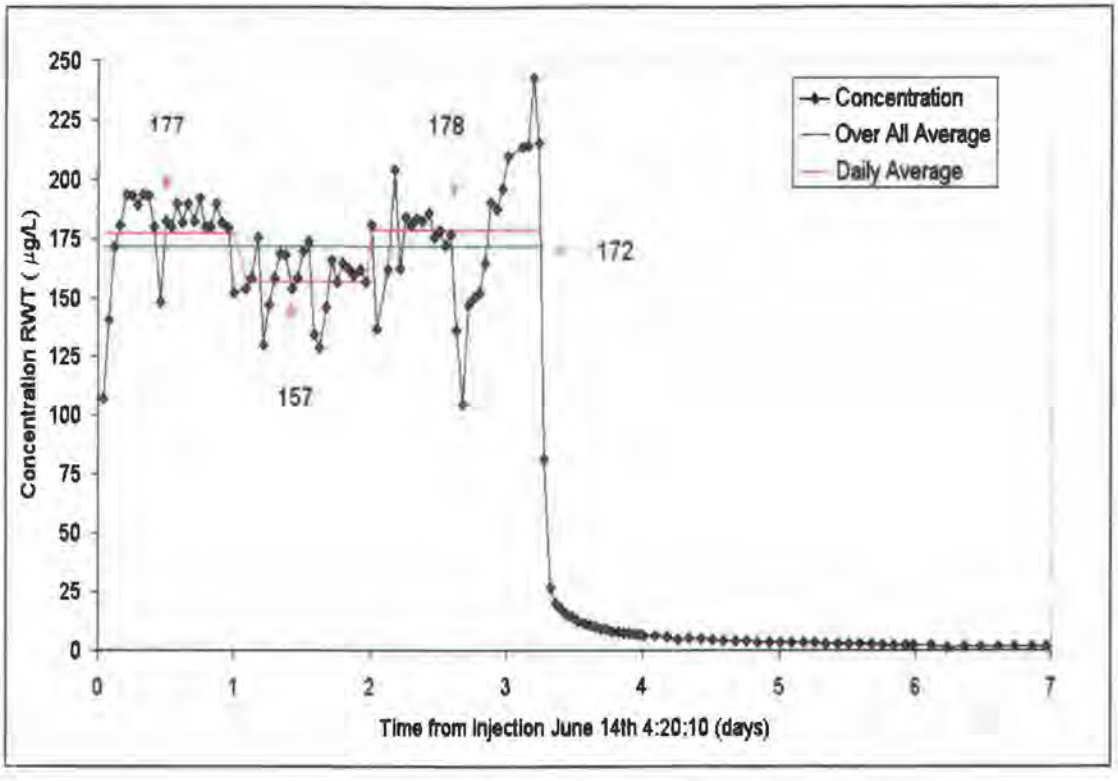

The general set up of the injection site is shown in Figure 26 with arrow and labels marking the equipment used during the injection. The injection solution was stored in a 170 L polypropylene plastic tub made by Sterilite Corporation in Townsend, Massachusetts. A lid was placed over the top of the tub but was not sealed completely to allow access for the pump intake hose. The solution was stirred several times per day. The injection pump was placed near the edge of the stream, next to the tub, and was mounted on a chemistry stand with clamps and wire (Figure 26). The influent line was rigid vinyl tubing that was 1.5 m long with a ¼" inner diameter. The tubing was carefully clamped to the edge of the tub to prevent movement, accidental removal, and keep the tubing slightly above the bottom of the tub. Originally the tubing was kept from the bottom of the tub in order to prevent the tubing from being suctioned onto the bottom, however this also helped to prevent material that may have settled out of solution from being sucked up. The tub was placed on a slight incline to make one corner slightly

deeper during the later portions of the draw down. The effluent hose was rigid vinyl tubing, 4.6 m long with a ¼" inner diameter, and extended from the pump to the center of the stream. Figure 27 shows the release of RWT from the end of the effluent hose into the thalweg of the stream. The injection site was staffed almost continuously for the first 48 h, occasionally for the next 18 h, and continuously for the final 6 h.

Despite the occasional stirring of the injection solution at the completion of the test, sediment was observed in the bottom of the tub. This sediment is believed to be a combination of silt blown into the solution and the settling of the RWT out of solution. Grab samples gathered on July 16, 2003 at 10:48 had an average concentration of 10.7 g/L RWT. The concentration of the grab samples was lower than the original injection solution (12.5 g/L RWT), which seems to indicate that settling reduced the concentration of the RWT in solution through time.

Figure 26. Picture of the injection site set up for the longitudinal tracer test, HJA, 2003.

Figure 27. Picture of Rhodamine WT being released into the thalweg of Lookout Cr. during the longitudinal tracer test, HJA 2003.

7.1.2. Longitudinal Tracer Test Monitoring Sites

The concentration of Rhodamine WT was measured longitudinally at eight locations using fluorometers (model# 10-AU) manufactured by Turner Design™ in Sunnyvale California and ISCO™ samplers (models 2900 and 3700 standard) (Figure 3 and Table 1). Three fluorometers were equipped with flow-through cell systems to directly measure the fluorescence of the stream water. One fluorometer was equipped with a cuvette holder for measuring discrete ISCO™ samples in the lab. The three fluorometer sites were stationed on Lookout Creek upstream of each tributary junction corresponding to at least a two-fold increase in discharge related to an increase in stream order. These tributaries were Cold Creek, Mack Creek, and McRae Creek (Figure 3 & Table 1).

The three stream monitoring fluorometers were calibrated together for consistency. The calibration of the fluorometers was accomplished by placing all of the fluorometers inline with each other so that the effluent of the first became the influent of the second fluorometer and the effluent of the second became the influent of the third. Standard solutions were mixed using the stream water from Lookout Creek near the H.J. Andrews Headquarters. Every time a standard or a blank was run, adequate time was given to flush the hoses and fluorometers of the previous solution. The sensitivity dials of the fluorometers were set to FS = 75% of 90.00 μg/L at medium, with a 20 μg/L standard. The fluorometers were then set to zero by using the H.J. Andrews Headquarters water as a blank and calibrated using a standard of 50 μg/L. The span of the fluorometers was set at 49% (Haggerty fluorometer), 49% (Gooseff fluorometer), 49% (McDonnell fluorometer), and 43% (Washington State Forest Service Lab fluorometer). The span of the fluorometer is a way of adjusting the range and sensitivity of the fluorometer to a calibrated fluoresce of RWT. The resulting ranges included High= 0 to 313, Medium= 0 to 31, Low= 0 to 2.7. The fluorometers were also set to account for temperature changes using the Turner Design™ specifications for RWT of exponential coefficient of 0.026 /^{0}C (Turner Designs™, 1999). The calibration of the laboratory fluorometer is discussed later in this section.

The general setup of a fluorometer monitoring site is shown in Figure 28. Each monitoring sites was equipped with one fluorometer with a flow through cell powered by two 12 V deep cycle batteries. The stream water was brought to the fluorometer by a peristaltic pump powered by two 12 V deep cycle batteries. The influent and effluent lines shown in Figure 28 are made of 3/8" ID clear flexible vinyl tubing.

Figure 28. The Above Cold Cr. monitoring site showing the standard fluorometer set-up during the Longitudinal Tracer Test.

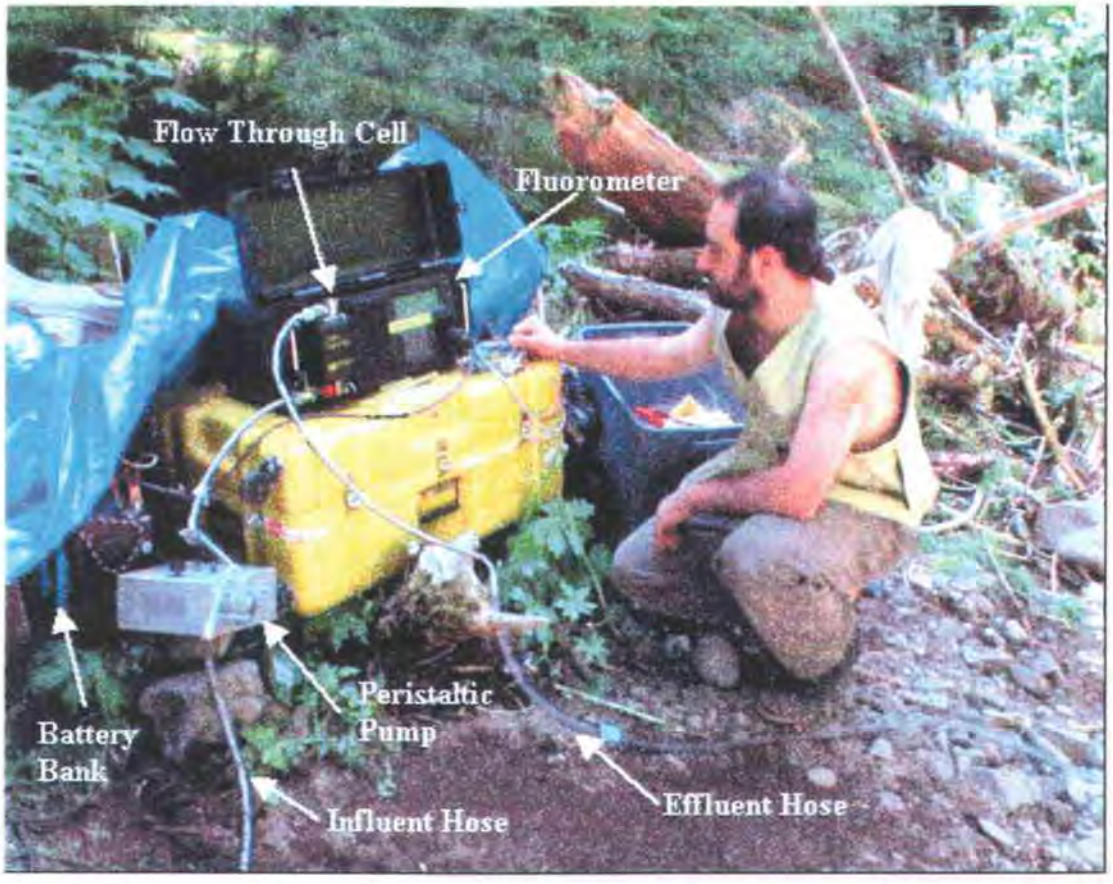

The two 12 V deep cycle batteries attached to the fluorometer were connected in parallel to boost the storage capacity of the battery bank. One battery was removed every 24 hours and a recharged battery was added. This method of battery rotation guaranteed power to the fluorometer and pump for the duration of the experiment. Each time the battery was replaced the data logger in the fluorometer was turned off and the fluorometer was allowed to sit for at least 5 minutes before shutting down. This shut down procedure allowed the computer analog to write an end of file code, and prevented the data from being corrupted.

A system of hoses and a peristaltic pump delivered the stream water to and from the fluorometer. The influent hose consisted of a 3/8" ID clear flexible vinyl tubing with a plastic strainer attached at the intake. The intake was set in or near the thalweg of the stream and anchored with stones. Temperature fluctuations

between the stream and the fluorometer have potential to cause air bubbles to be created in the hose. Increased water temperature reduces the air solubility in the water, which may result in air bubbles in the line and flow-through cell. In order to reduce the amount of temperature change in the intake system, the hose was submerged and anchored in the stream until it reached the shore. Upon reaching the shore the hose was covered with a tarp or bark in order to block direct sunlight. This cover also prevented solar decay of the RWT. A peristaltic pump was placed as close as possible to the same elevation of the stream. By setting the pump near the same elevation (<0.6 m) it reduced the hydraulic pull by the pump and reduced bubbles caused by the pumping action. A length of peristaltic tubing, manufactured by Masterflex™ in Vernon Hills, Illinois, P/N BH-96420-24 Platinum-cured Silicone ¼" ID, approximately 1 m long was attached to the influent line at the pump. Due to unexplained reasons, this tubing was prone to wearing through after approximately 32 h. The tubing continued to wear out even after the pump head was replaced and new tubing was added. As a remedy to this problem, the tubing in the pump head was moved every 24 h to an unworn section. It is believed that the tubing itself was weak and it is recommended that further studies include a higher grade of tubing. After leaving the pump, the influent tubing went directly into the bottom of the flow-through cell of the fluorometer. The first approximately 2 m of tubing near the fluorometer, both on the influent and effluent sides, was covered with duct tape to reduce sun exposure and light degradation of the dye. The pump was also covered with a tarp to reduce sun exposure. The pump was powered by a two-battery system identical to the fluorometer power system. A small hose clamp was fastened at each of the locations where the tubing connected to another tube, the fluorometer, or the strainer to prevent air from entering. A small amount of duct tape was wrapped around the tubing at the point where the clamp was applied; this allowed the clamp to be tightened without cutting into the tube. The effluent line was always placed to rise at least 0.6 m above the fluorometer before returning to the stream. If air bubbles entered the line, the rise in the tubing allowed them to accumulate at the

highest point and not in the flow-through cell. The outlet of the effluent line was always downstream of the inlet of the influent line.

The fluorometers were manned constantly for at least the first 24 h of the injection until such attention was unnecessary. The sites were then visited 2 to 5 times per day during the injection. The frequency of the visits to the injection site was based on the status of the breakthrough curve. The fluorometers were originally set in the low sensitivity range and left in manual mode. As the concentration of RWT in the stream increased, the fluorometer was manually switched to medium at ~2.7 μg/L and to high at 31 μg/L, if needed. The manual switching was necessary because of an error in the programming of the fluorometer, which does not allow automated range switching while it is being powered by DC power. This process was reversed on the declining limb of the breakthrough curve. Both on the rise and fall of the breakthrough curve, the rate of change was slow enough that periodic attention was enough to catch the transitions.

The fluorometers began recording background concentrations of the stream several hours before the injection started. Each fluorometer was programmed to record sample concentrations, and collect temperature data every 30 seconds. The clocks on all the fluorometers were synchronized. A notebook was kept at each site to record all major occurrences, as well as a field box equipped with a fluorometer manual, duct tape, extra clamps, extra hoses, a screwdriver, a wrench, emergency amber sample bottles, and pencils.

The set up and staffing of the monitoring and injection site during the course of the tracer tests was accomplished by a number of volunteers ranging from 1 to 12. Before the LTT started I did a week of equipment gathering, site location reconnaissance, and planning in the field at the H.J. Andrews. Fluorometers were deployed above McRae Cr. and at the Headquarters by myself on June 11th, 2003, in order to collect background and practice site set up. On June 13th, 2003, seven volunteers retrieved the fluorometers in the field, gathered background water, and various other tasks. The day of the injection 12 volunteers were used to set up all of the sites and injections sites. During the first 24 hrs of the injection each of the

fluorometer monitoring sites was staffed by at least 1 person. For the first nine days after the start of the injection a staff of 2 to 6 people maintained the monitoring sites, replacing batteries, replacing peristaltic tubing, collected ISCO™ samples, and analyzed the ISCO™. After the first six days the above McRae Fluorometer was removed and after the first 9 days the above Mack fluorometer was removed. Both fluorometers were replaced with ISCO™ auto samplers. From June 23rd, 2003 to November 15th,2003; the LTT was maintained primarily by one person.

The McRae Cr. IOTT had 3 volunteers that helped with set up and the injection. After the injection one person maintained the McRae Cr. IOTT. The Mack Cr. IOTT had 2 volunteers that helped with set up and the injection and was maintained after the injection by one person. The final Cold Cr. IOTT was performed completely by one person.

Four additional ISCO™ monitoring sites were established below each of the confluences, near the base of the basin, and below the injection site (Figure 3 & Table 2). Figure 29 show the general setup of an ISCO™ monitoring site. Each ISCO™ sampler had a 12 V battery power source, 3.05 m to 7.62 m of 3/8" ID clear flexible vinyl tubing intake hose, and a plastic screen attached at the intake. The fluorometers monitoring sites were replaced with ISCO™ samplers during the late time decline of the concentration curve. The replacement occurred within 10 days of the beginning of the injection but varied between sites depending on the rate of decline.

The ISCO™ samplers were set at various sampling intervals throughout the test. The different intervals included a 6-minute integrated hourly sampling below the injection site for the first 96 h, and a range of 1 h to 24 h sampling intervals at all of the other sites. ISCO™ samples were continually collected until the concentrations went below 0.1 μg/L or to background fluorescence.

Figure 29. The monitoring site at the Above Cold Cr. site after the fluorometer was replace with a ISCO showing the standard ISCO™ set-up during the Longitudinal Tracer Test.

The discreet ISCO™ samples were each labeled with an identifier and returned to the walk-in refrigerator at the H.J. Andrews headquarters for storage until processed. In some cases, the samples in the field were transferred from the ISCO™ sample bottles to 60 mL amber sample bottles. If the samples were transferred, the ISCO™ bottles were then carried to a nearby tributary of fresh water and rinsed three times and extra water was shaken out before being reset in the ISCO™. ISCO™ or amber bottles used for sampling were always rinsed three times and dried before returning to the field. The bottle lids were washed in a similar manner. After the first couple of sample sets were analyzed, it appeared that some contamination was occurring. It is believed that RWT was contaminating the samples by getting caught between the lid and a protective seal inside the lid. The contamination seemed to be reduced once the lids were rinsed 4 times.

The discrete samples from the ISCO™ samplers were analyzed in the Wet Chemistry Laboratory at the H.J. Andrews using a fluorometer with a 13mm cuvette holder. The sensitivity was set at FS = 67% of 90.00 µg/L at medium using a 20 µg/L standard. The calibration included using the same stream water used to calibrate the fluorometers in the beginning of the tracer experiment and a 20 µg/L standard. The samples were analyzed by ISCO™ sets, usually 24 samples long. Before and after each set run, a series of standards were measured to check the amount of drift that the fluorometer may have undergone. The check standards included a 50 µg/L, a 20 µg/L, a solid high, a solid low, and a blank. If significant drift occurred, the fluorometer was recalibrated.

Originally the bulk standard flasks were kept in the dark cupboard in the lab and replaced every 2 or 3 weeks. However, this method was flawed because the standards were at room temperature when analysis began and the samples, which were stored in the refrigerator, were at a cooler temperature. Figure 30 shows how this flaw in methodology may have affected the concentration results. The difference in temperature between calibration standards and discreet samples may have caused systematic shifts in concentrations observed in some of the first ISCO™ samples sets because RWT fluoresce is partially temperature dependent (Figure 30). In Figure 30 the flux breakthrough curve vs. the time from the LTT injection is shown in log-log space for the Above Cold Cr. site. The flux breakthrough curve is derived from the measured concentrations at a given time multiplied by the stream discharge of the stream at the same time. The black box in the graph highlights the flux readings that are out of sequence with the measurements before and after them due to the temperature sensitivity of RWT, as mentioned above. Once the temperature discrepancy was noticed, the methodology was changed to include storage of the standards with the samples so that both were at the same temperature when the analysis began.

Figure 30. Observed shifts in ISCO™ sample sets due to possible differing temperatures between standards and samples.

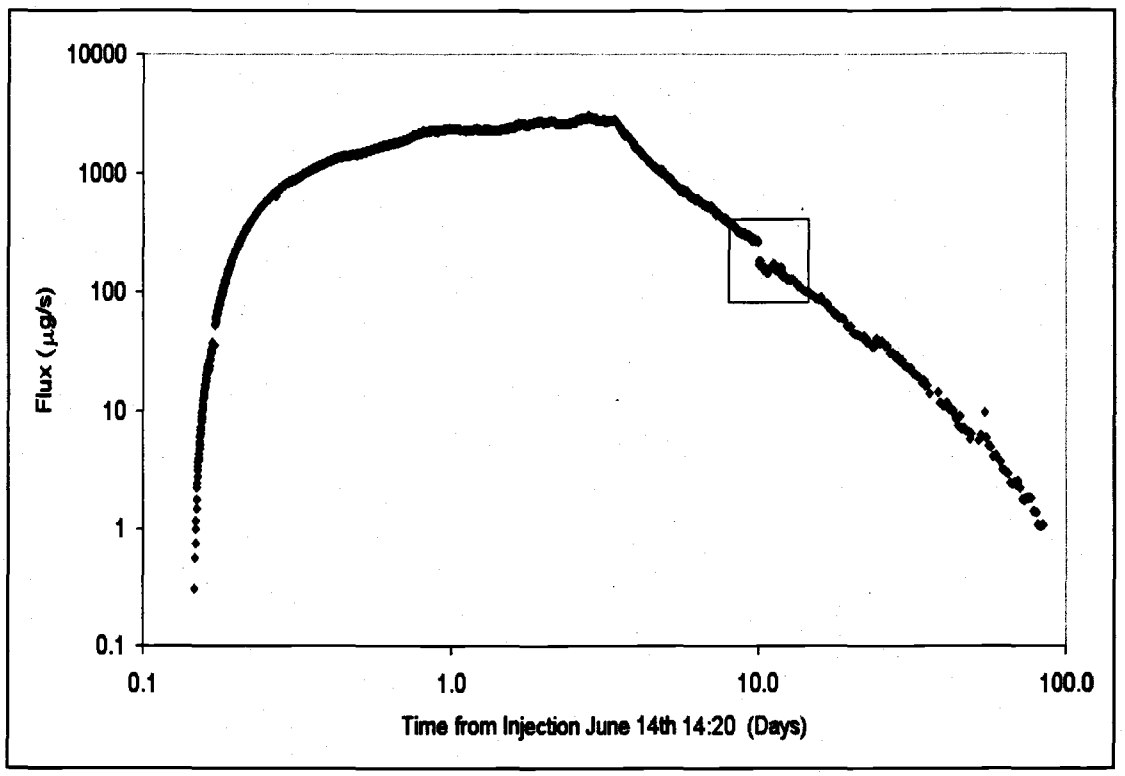

The discharge for Lookout Cr. was monitored during the tracer test for injection purposes. However it became apparent after the tests were over that discharge readings throughout the summer, covering all of the monitoring sites, was important. At the beginning of the tracer test there was an attempt to use capacitance rods to measure continuous discharge throughout the tracer test, however, technical difficulties prevented their use. During the tracer test stream discharge was measured six times at the injection site from June 14, 2003 to June 25, 2003 and once at each fluorometer site on June 25, 2003. Discharge information was later improved by acquiring data from Charles Frady of the Department of Fish and Wildlife, Oregon State University. Charles Frady measured stream discharge for the H.J. Andrews through June, July, and August of 2003.

Discharge measurements taken during the Inter-Order tracer test also helped to strengthen the hydrographic history of the summer stream flows. Discharge was measured using a Flo-Mate™ flow meter. The general stream discharge measuring

procedure was outlined in "The Open Channel Profiling Handbook" by Marsh-McBirney Incorporated (1994). This procedure included finding a reach that was fairly straight and uniform, lacked obstacles or eddies, and preferably was underlain by bedrock. These ideal features were not always met, but the best possible compromise was used for the measurement site. The width of the stream was measured and divided by 25. After dividing the stream into 25 segments, the depth and average velocity of each segment was measured. Using the width, average depth, and average velocity the discharge was estimated.

Equipment was supplied by a collaboration of research groups including the Geosciences Department Hydrogeology Lab, Jeff McDonnell's Hydrology Lab in the Forest Engineering Department, Steve Wondzell of the Pacific Northwest Forest Research Station, Mike Gooseff in the Department of Aquatic, Watershed, and Earth Resources of Utah State, Stan Gregory of the Fish and Wildlife Department, the H.J. Andrews Experimental Forest, John Selker of the Bioresources Engineering Department, and Jim Wigington of the Environmental Protection agency.

7.2. McRae Creek Intra-Order Tracer Test

The McRae Creek Intra-Order Tracer Test (IOTT) was conducted between the confluence of McRae Creek and the H.J. Andrews headquarters on the main stem of Lookout Cr. located in the Western Cascades of Oregon (Figure 31). The test was an extension of the LTT, to improve the study of the power-law behavior of hyporheic exchange within the hyporheic zone at multiple scales. This test was an independent comparison of the hyporheic behavior along the Lookout Cr. reach between McRae and the H.J. Andrews headquarters.

The test was conducted on July 8, 2003 after the stream below McRae Creek had returned to background fluorescence concentrations of ~0.05 μg/L following the LTT. This test involved injecting RWT into Lookout Creek below the confluence with McRae Creek and monitoring the concentration downstream at three locations (Figure 31). The monitoring sites included an injection ISCO™, a mid point site (Floodplain site), and a site at the H.J. Andrews headquarters. The

Universal Transverse Mercator (UTM) positions of all the sites are given in Table 3 and were established by the same methods described in the LTT methods section.

The McRae Cr. IOTT test reach is shown on a map in Figure 31. In Figure 31 the boundaries of the Lookout Cr. basin is outlined in black on a digital elevation map. The Lookout Cr. stream network, which includes McRae Cr., Mack Cr., Cold Cr. and many others, is shown in blue (Figure 31). The reach length along the main stem of Lookout Cr. that was encompassed by the tracer is shown in orange and gold. The locations of the injection site and monitoring sites are shown on the map with gold representing the reach upstream to the floodplain monitoring site and orange representing the reach from the floodplain monitoring site to the headquarters monitoring site (Figure 31).

Figure 31. Map of the H.J. Andrews Experimental Research Forest, Oregon. Illustrating the boundaries of the Lookout Creek Basin, the Lookout Cr. stream network, and the monitoring site locations for the McRae Creek IOTT.

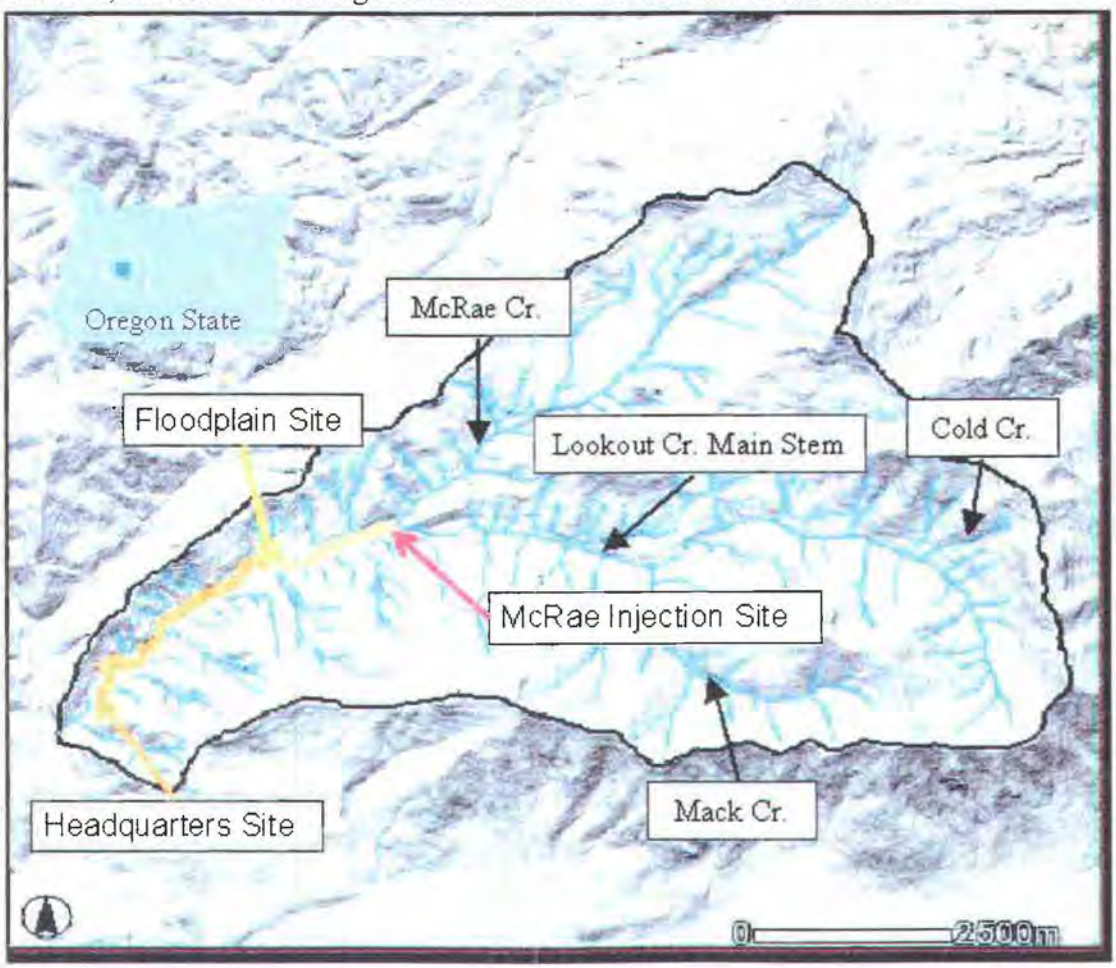

The methodology of the McRae Creek Tracer Test was the same as the LTT so only the differences will be noted. The McRae injection was planned to last for 24 h and was started on July 8, 2003 at 11:53:23. The injection site was located ~100 m downstream of the confluence and was ~50 m upstream of an obvious bedrock reach. The confluence of McRae and Lookout is the location where Lookout Cr. becomes a 5th order stream. The injection was powered solely by six 12 V deep-cycle batteries. A generator was not used to recharge the batteries in an attempt to hold the injection rate steady. The locations of the injection pump, RWT solution bucket, battery bank, multi-meter and RWT effluent release point at the injection site is shown in Figure 32.

Figure 32. Picture of the injection site set up for the McRae Cr. Intra-Order Tracer Test.

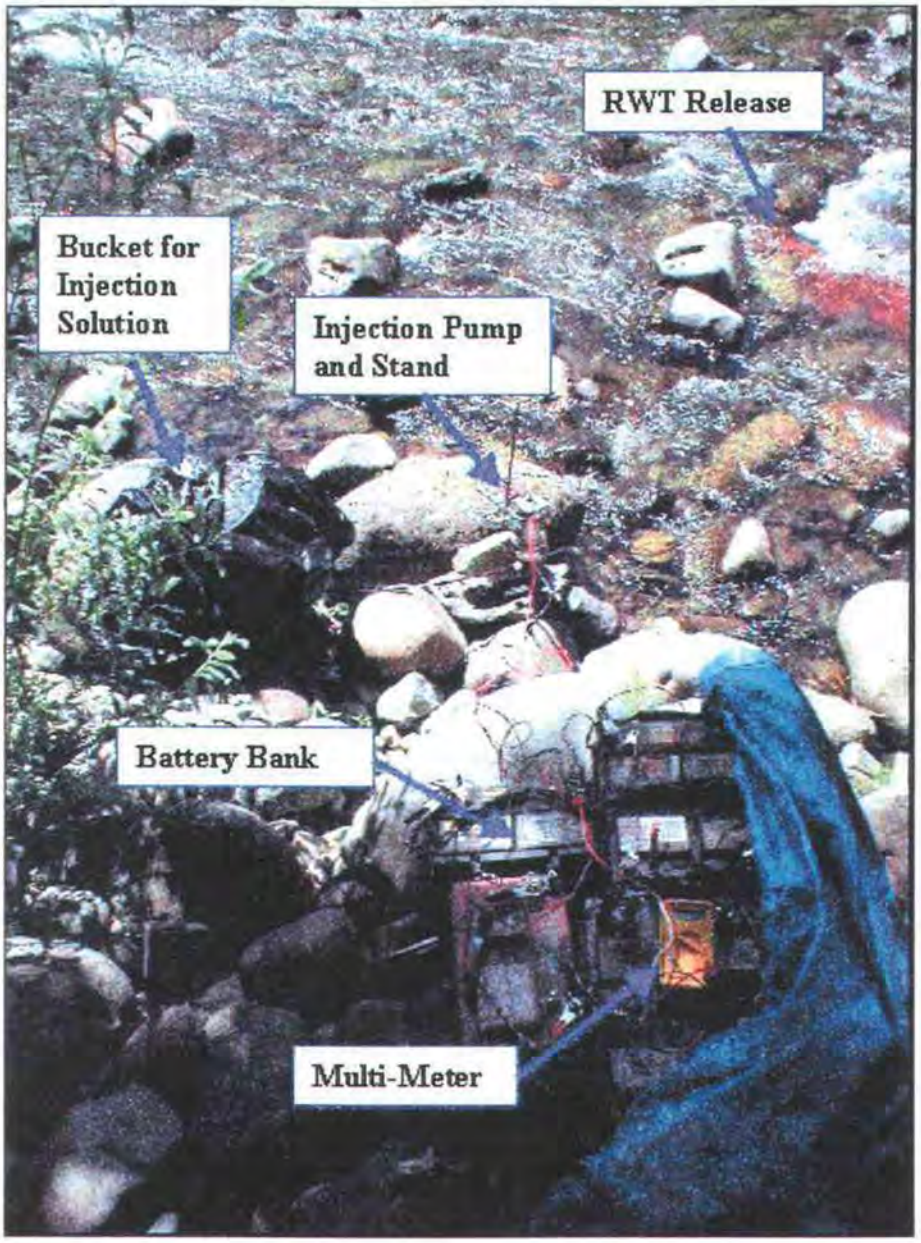

On the day before the injection, the discharge of Lookout Creek was 183.3 L/s, as measured 50 m downstream of the injection site using a Flo-Mate™ flow meter. Using this measured discharge we calculated that 225 g of RWT would be needed to achieve a target concentration of 15 µg/L for a 24 h injection. We mixed an injection solution that consisted of 4,500 mL of RWT and 18,000 mL of water

from the stream, resulting in a concentration of 10.0 g/L RWT. Next we calibrated the FMI pump to pump at a rate of 0.27 mL/s at 12.48 V. These rates should have created a 23.1 h injection at 15 µg/L. The injection solution was held in a 6-gallon bucket, with a garbage bag placed over the top to prevent dust from entering the solution.

This originally measured discharge is now believed to be erroneous. We believe our measure was incorrect because our discharge varied from the other source, including our own calculations from the breakthrough curve plateau and other scientist discharge measurement during the same time period. Using the concentration plateau we estimated that the discharge was 404 L/s and discharge measurements made by Charles Frady of the Fish and Wildlife Department near the same time above the injection site, found a discharge of 414 L/s. The error may have been derived from operator error, inherent error of the flow meter, significant underflow through alluvium, or a combination of the three.

The use of a large battery bank and no generator resulted in an injection that was steadier than the LTT, but had several unexplained dips and a general increase in measured concentrations (Figure 33). Figure 33 shows the concentration in Lookout Cr. 450 m below the McRae Cr. IOTT injection site during the test, represented by the black squares connected by a black line. The average concentration of 6.9 µg/L ± 1.8 µg/L is shown as a straight black line and a spill related spike is also shown and labeled (Figure 33).

Figure 33. Concentrations for the McRae Intra-Order Tracer Test taken from the injection site ISCO™.

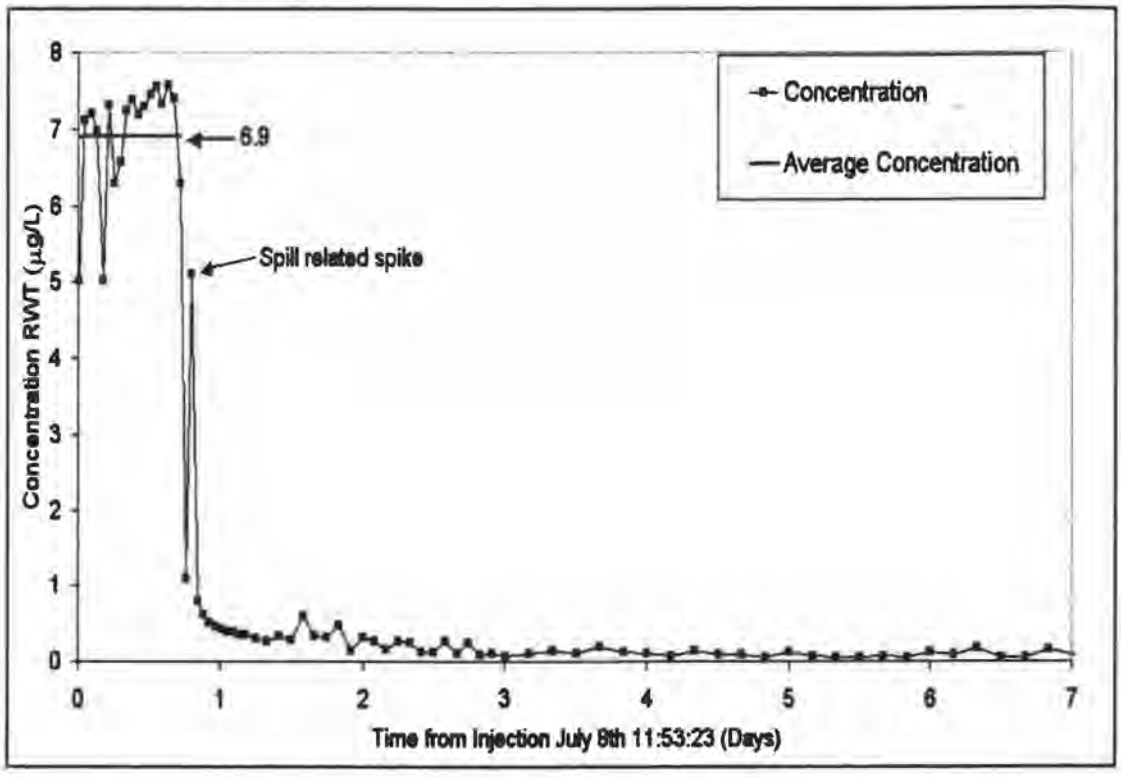

Despite the steadier injection rate of the injection, unforeseen problems arose that jeopardized the success of the McRae IOTT. During the tracer test the injection site was visited periodically throughout the day to monitor progress. The final check occurred at 20:00, at which point it was incorrectly estimated that the injection would last another 12 to 14 h. The first problem was discovered upon arriving at the injection site at 06:45, July 9,2003, four hours before the injection was calculated to end. We discovered that the injection had already run out and the FMI pump was melted from overheating. It appeared that the voltage of the batteries increased, which caused the FMI pumping rate to increase. Field notes indicate that the voltage, which began at 12.51 V at 12:00 rose to 12.55 V by 16:00, 12.57 V by 17:15, and 12.56 V by 19:30. The injection ISCO™ concentration also appears to show a gradual increase through time (Figure 33). We believe that the sun heated the batteries and rocks the batteries were sitting on. This solar heat is believed to have increased the batteries efficiency and voltage. It

is also possible that when the original pump calibrations were conducted, the batteries had not yet come into equilibrium and one or more batteries brought the average voltage above 12.51. After analyzing the injection ISCO™, it was determined that the injection most probably ended on July 9, 2003, between 04:40 and 05:00. The average time, 04:50, was assumed for analytical purposes. The RWT injection was estimated to have lasted for 17 hours and at the conclusion of the injection none of the RWT injection solution remained. A total of 224.3 g of RWT was injected into Lookout Creek during the McRae Cr. IOTT.

The second complication arose during clean up of the injection site. The RWT injection solution bucket, which still contained a small amount of leftover injection solution, was accidentally knocked into the stream. The spill occurred at the injection site at approximately 07:00, July 9, 2003 and the amount of the spill was estimated to be ~60 mL. A total of 22.5 L of 10.0 g/L RWT was therefore released into the stream during this tracer test. It is unknown if sediment was present in the bottom of the bucket after the injection, which may have increased the amount of RWT that was released into the stream.

The concentration of RWT was measured longitudinally at three locations using a fluorometer and two ISCO™ samplers (Figure 31). The fluorometer was calibrated using the standard solutions and techniques describe in the LTT. The fluorometer site was stationed on Lookout Cr. on a side bar located on the north bank of the stream, near the H.J. Andrews headquarters (Figure 31 and Table 2). The fluorometer was started 24 h before the injection and allowed to collect background information. The fluorometer was visited 2 to 5 times a day, depending on the state of the breakthrough curve and monitored for possible concentration range adjustments. The fluorometer was replaced with an ISCO™ sampler during the late time decline of the concentration curve. The replacement occurred on July 10, 2003 at 19:21. The ISCO™ samples continued to be collected until the concentrations were perceived to go below background fluorescence, below 0.1 µg/L on August 5, 2003.

Two ISCO™ monitoring sites were established from the beginning. The first ISCO™ monitoring site was 420 m below the injection site and the second was

located at a major constriction in the valley floor midway between the injection and the bottom of the monitored reach (Figure 31 and Table 2). The ISCO™ located in the middle of the test reach was located at the end of a broad floodplain that encompassed the entire test reach up to that point.

7.3. Mack Creek Intra-Order Tracer Test

The Mack Creek Intra-Order Tracer Test (IOTT) was conducted between the confluences of Mack Creek and McRae Creek on Lookout Creek, located in the Western Cascades of Oregon (Figure 34). The test was an extension of the LTT, in an effort to study the power-law behavior of hyporheic exchange within the hyporheic zone at multiple scales. This test was an independent comparison of the hyporheic behavior along the Lookout Cr. reach between Mack Cr. and McRae Cr.

The test was conducted on August 7, 2003 after the stream below McRae Creek had returned to a background fluorescence concentration of ~0.07 μg/L, following the LTT. The test involved injecting RWT into Lookout Creek below the confluence with Mack Creek and monitoring the concentration downstream at three locations (Figure 34). The monitoring sites include an injection ISCO™, a mid point site (Mid Mack site), and a site above the McRae Creek confluence. The UTM positions of all the sites are given in Table 3 and were established by the same methods described in the LTT methods section.

The Mack Cr. IOTT test reach is shown on a map in Figure 34. The boundary of the Lookout Cr. basin is outlined in black on a digital elevation map in Figure 34. The Lookout Cr. stream network, which includes McRae Cr., Mack Cr., Cold Cr. and many others, is shown in blue (Figure 34). The reach length along the main stem of Lookout Cr. that was encompassed by the tracer is shown in maroon and red. The locations of the injection site and monitoring sites are shown on the map with maroon representing the reach upstream to the middle tributary monitoring site and red represent the reach from there to the above McRae Cr. monitoring site (Figure 34).

Figure 34. Map of the H.J. Andrews Experimental Research Forest, Oregon State. Illustrating the boundaries of the Lookout Creek Basin, the Lookout Cr. stream network, and the site locations for the Mack Creek Intra-Order Tracer Test.

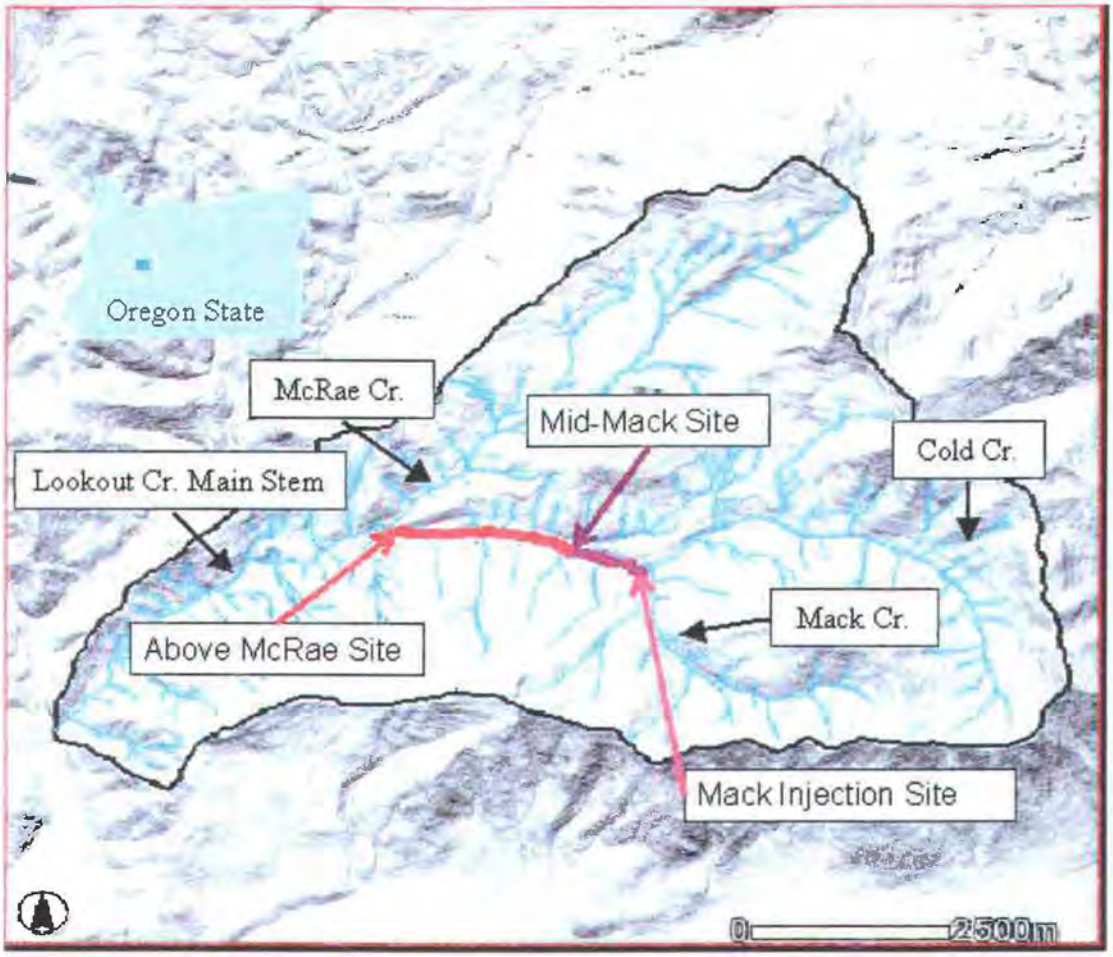

The methodology of the Mack Creek Tracer Test was the same as the LTT and only the differences will be noted. The Mack injection was planned to last for 24 h and was started on August 7, 2003 at 12:32:06. The injection site was located ~15 m downstream of the confluence between Mack Cr. and Lookout Cr. The confluence of Mack and Lookout is the location where Lookout Cr. becomes a 4th order stream. The injection was powered by five 12 V deep-cycle batteries. A generator was not used to recharge the batteries. After the FMI (model # RHB1) pump was damaged in the McRae tracer test a new system was installed.

The new pump was an AC injection pump (model # QG150) with a Q1CKC pump head, manufactured by Fluid Meter Inc. in Syosset, New York. The range of

pumping rates for the new FMI pump was 0-48 mL/min. We used a DC to AC 300 Watt Dual-Outlet Power Inverter by RadioShack™ in Fort Worth, Texas, to power the AC pump with DC batteries. This inverter method had the dual purpose of supplying power to the pump and regulating the power at a constant 115 VAC output. This constant power supply was shown in the laboratory to result in a constant pumping rate for the FMI pump.

The new AC FMI pump and power inverter resulted in an injection that was steadier than the LTT or the McRae IOTT, but irregular peaks were still observed (Figure 35). The reason for the spikes are unknown, but it is thought that attempts to remove air bubbles from the effluent line may have caused a flush of RWT into the stream and contributed to the rise in concentration. The black diamonds with a solid black line in Figure 35 shows the concentration in Lookout Cr. 25 m below the Mack Cr. IOTT injection site during the test and the average concentration of 14.6 µg/L ± 12.4 µg/L is shown with a straight black line (Figure 35). An error occurred in programming of the injection ISCO™ and only the first 3 hrs and the last 4 hrs of the peak injection period were captured with the sampler (Figure 35).

Figure 35. Concentrations for the Mack Intra-Order Tracer Test taken from the injection site ISCO™.

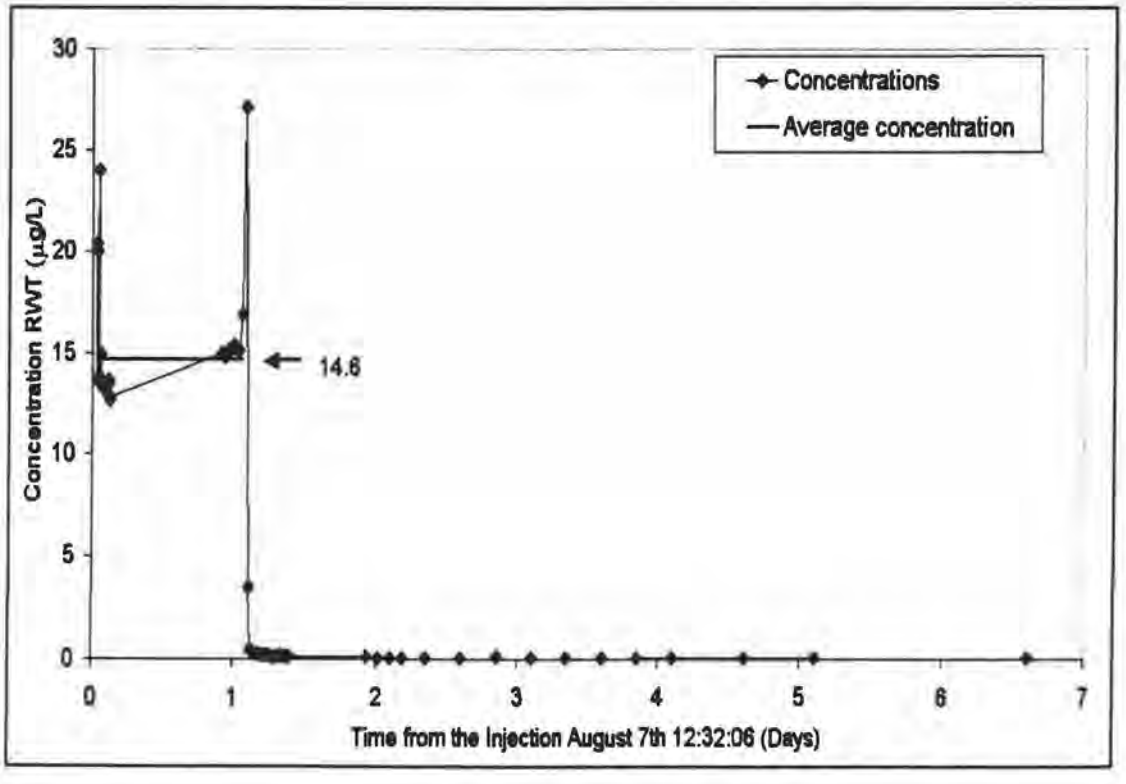

In an effort to prevent another accidental spill like the one that occurred during the McRae IOTT, several precautions were taken with the injection solution bucket. First of all, the bucket was fitted with a lid with two holes. The first hole was large enough to allow a stainless steel tube 7/16" in diameter to fit through. The intake hose to the injection pump was then fitted into the tube, which extended down 0.3 m and prevented the stiff plastic intake hose from curling away from the bottom of the bucket or getting stuck to the bottom. The second hole allowed the injection bucket to breath. The second precaution included placing the bucket in a 37.8 L Rubbermaid™ tub, manufactured in Fairlawn, Ohio, as a second level of spill protection.

The day before the injection we measured a discharge of 238 L/s, 10 m downstream of the injection site using a Flo-Mate™ flow meter. Using the 238 L/s discharge, we calculated that we would need 322.25 g of RWT to achieve a target concentration of 15 µg/L for a 24 h injection. We mixed an injection solution that consisted of 6,445 mL of RWT and 13,000 mL of water from the stream, resulting in a concentration of 16.57 g/L RWT. Next, we calibrated the FMI pump to pump at a rate of 0.21 mL/s at 115 V AC. The successful injection ended August 8, 2003 at 14:39:00 without incident, after running for 26.1 h. The injection site was visited periodically throughout the day and the final check occurred at 21:00. The remaining injection solution in the bucket after the injection totaled 79 mL. A total of 19.366 L of 16.57 g/L RWT, which was equivalent to 321.1 g of RWT, was therefore released into the stream during this tracer test. A small amount of residual sediment was present in the bottom of the bucket after the injection.

The original discharge measurement was found to be in error on November 11, 2003 and was corrected to 250 L/s. The error was noticed in the logbook, which had the stream incorrectly marked 3.6 m wide instead of 3.8 m. However, all of the injection calculations were based on the discharge estimate of 238 L/s. The estimated discharge using the concentration plateau was ~243 L/s and discharge measurements made by Charles Frady near the same time above the injection site was ~263 L/s.

The concentration of RWT was measured longitudinally at three locations using one fluorometer and two ISCO™ samplers (Figure 34). The fluorometer was calibrated using the standard solutions and techniques describe in the LTT. The fluorometer site was stationed on Lookout Creek on a side bar on the northern side of the stream, ~300 m upstream of the confluence with McRae Creek (Figure 29 and Table 2). The fluorometer was started 3.5 h before the injection and allowed to collect background information. The fluorometer was visited 2 to 5 times per day depending on the state of the breakthrough curve and monitored for possible concentration range adjustments. The fluorometer was replaced with an ISCO™ sampler during the late time decline of the concentration curve. The replacement occurred on August 10, 2003 at 13:22. The ISCO™ samples continued to be collected until the concentrations were perceived to go below background fluorescence at ~0.07 μg/L, and was finally shut down on August 23, 2003 at 03:30.

The two additional ISCO™ monitoring sites were established, 25 m below the injection site and at the largest tributary between Mack Creek and McRae Creek. This site was called the Mid Mack site because the stream was unnamed on the official 1986 H.J. Andrews Blue River Ranger District Map (Figure 34 and Table 2).

7.4. Cold Creek Intra-Order Tracer Test

The Cold Creek Intra-Order Tracer Test (IOTT) was conducted between the confluence of Cold Creek and Mack Creek on Lookout Creek located in the Western Cascades of Oregon (Figure 36). The test was extension of the LTT, which was an effort to study the power-law behavior of hyporheic exchange within the hyporheic zone at multiple scales. This test was an independent comparison of the hyporheic behavior along the Lookout Cr. reach between Cold Cr. and Mack Cr.

The test was conducted on September 11, 2003 after the stream below Cold Creek had returned to a background concentration of ~0.05 μg/L, following the

LTT. This test involved injecting RWT into Lookout Creek below the confluence with Cold Creek and monitoring the concentration downstream at three locations (Figure 31). The monitoring sites included an injection ISCO™, a mid point site at Longer Cr., and a site above the Mack Creek confluence. The UTM positions of all the sites are given in Table 3 and were established by the same methods described in the LTT methods section.

Figure 36. Map of the H.J. Andrews Experimental Research Forest, Oregon State. Illustrating the boundaries of the Lookout Creek Basin, the Lookout Cr. stream network, and the site locations for the Cold Creek Intra-Order Tracer Test.

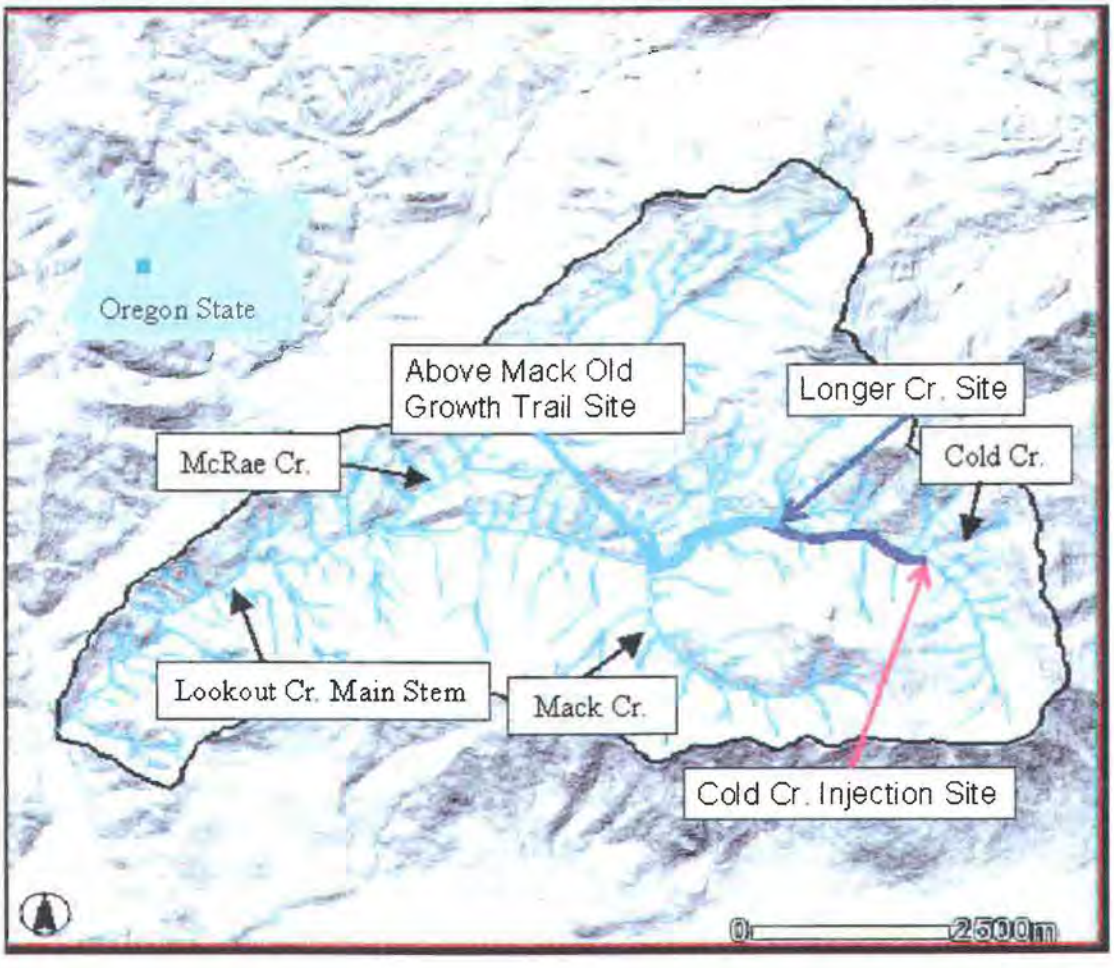

The methodology of the Cold Creek IOTT was the same as the Mack IOTT and so only the differences will be noted. The Cold Cr. injection was planned to last for 24 h and was started on September 11, 2003 at 10:30. The injection site was located ~10 m downstream of the Lookout Cr. confluence with Cold Cr. The

confluence of Cold and Lookout Creeks is the location where Lookout Cr. becomes a 3rd order stream. The injection was powered solely by five 12 V deep-cycle batteries and the power was converted to AC power for use in the same FMI injection pump that was used in the Mack Cr. IOTT. The injection pump was powered through a power inverter at a constant 115 VAC output.

The Cold Cr. IOTT injection was much steadier than the previous three tracer tests (Figure 37). It is believe that the Cold Cr. IOTT was steadier than the Mack Cr. IOTT because no attempts to clear bubbles out of the effluent line were made during the injection. Figure 37 shows, with the black diamond and solid black line, the concentration in Lookout Cr. 46 m below the Cold Cr. IOTT injection site during the test and in the straight black line, the average concentration of 49.8 µg/L ± 0.6 µg/L (Figure 37).

Figure 37. Concentrations for the Cold Intra-Order Tracer Test taken from the injection site ISCO™.

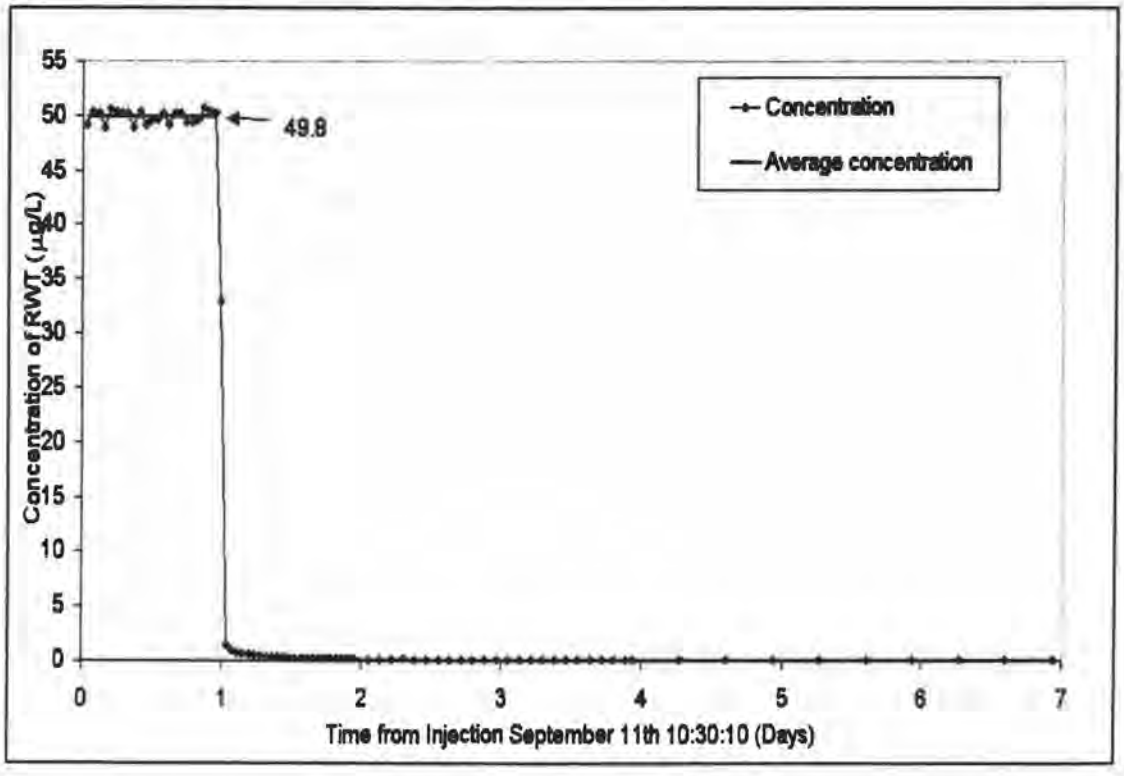

The day before the injection we measured a discharge of 85.6 L/s, 46 m downstream of the injection site, using a Flo-Mate™ flow meter. Using this

discharge we calculated that we would need 296.4 g of RWT to achieve a target concentration of 40 µg/L, for a 24 h injection. We then mixed an injection solution that consisted of 5,948 mL of RWT and 11,840 mL of water from the stream, resulting in a concentration of 16.71 g/L RWT. Next we calibrated the FMI pump to pump at a rate of 0.20 mL/s at 115 V AC. We found that we overestimated discharge after analyzing the injection ISCO™ samples because our actual concentration plateau reached 49.8 µg/L. The estimated discharge using the concentration plateau showed a discharge of ~67.5 L/s. Discharge measurements made by Charles Frady near the same time above the injection site was ~63 L/s.

The successful injection ended September 12, 2003 at 10:29:00 without incident after running for 23.9 h. The injection site was visited periodically throughout the day and the final check occurred at 19:17. The remaining injection solution in the bucket totaled 60 mL. A total of 17.788 L of 16.71g/L RWT, which was equivalent to 296.4 g of RWT, was released into Lookout Cr. during this tracer test. A small amount of residual sediment was present in the bottom of the bucket after the injection.

The concentration of RWT was measured longitudinally at three locations using one fluorometer and two ISCO™ samplers (Figure 36). The fluorometer was calibrated using the standard solutions and techniques described in the LTT. The fluorometer site was stationed on Lookout Creek on a side bar along the northern bank, 10m downstream of the lower old growth trail bridge and ~966 m upstream of the confluence with Mack Creek (Figure 36 and Table 2). The long distance above the confluence with Mack was determined to be the best site due to accessibility and resource limitations. The fluorometer was started 2.5 h before the injection and allowed to collect background information. The fluorometer was visited 2 to 5 times a day depending on the state of the breakthrough curve and monitored for possible concentration range adjustments. The fluorometer was replaced with an ISCO™ sampler during the late time decline of the concentration curve. The replacement occurred on September 15, 2003 at 9:44. The ISCO™ samples continually collected until the fluorescence concentrations were below a background fluoresce of 0.08 µg/L on October 26, 2003 12:00.

The two additional ISCO™ monitoring sites were established 46 m below the injection site and at Longer Creek, a large tributary between Cold Creek and Mack Creek (Figure 36 and Table 2).

7.5. Data Analysis Using the ArcHydro Data Model

A GIS Arc Hydro Data Model was created to spatially interpret physical features from the tracer tests and present the study reaches in map form. The ArcHydro data model allowed the calculations of the distances between each of the monitoring sites, the contributing drainage areas for each site, and several other exploratory calculations not included in this thesis.

The Arc Hydro Data Model was created using the steps outlined in "Arc Hydro Tools –Tutorial" (ESRI, 2003). As part of the setup process, the beginning of Lookout Cr. had to be determined. The tutorial recommended a stream threshold of 1% of the maximum flow accumulation area. The maximum flow accumulation area for H.J. Andrews Arc Hydro Data Model was determined to be 63.8 km^2. One percent of 63.8 km^2, the accumulation area, is 6.4 km^2. We found this value too high because it severely underestimated stream channel formation. After experimentation, and comparing the model to the known stream network, we found that a value of 0.128 km^2 was the best fit.

The UTM positions of all of the tracer sites and the synoptic sample sites were established using this Arc Hydro Data Model, as detailed in the LTT methods section. For details on the synoptic samples see Appendix IV: Synoptic Samples. Once the site positions were established on the GIS data layers, the ArcGIS snapping tool was used to place them directly on the drainage line layer. Using the Arc Hydro Data Model, all of the sites and synoptic sample locations were assigned to a sub-batch point. This process allows each point to be recognized by the data model and helps the model to conduct various spatial analyses and interpolations.

The first analysis conducted was the Arc Hydro tool for delineating sub-catchments, which allowed us to calculate the upslope contributing area of each of

the sites (Table 1 and Table 2). The sub-batch points that corresponded to a location just above a confluence had to be moved at least 7 m upstream from the confluence or else the Arc Hydro Model would include the downstream tributary in the sub-catchment calculations.

The second analysis was the estimation of the length between each site using the Arc Hydro data model. Using the ruler tool and measuring along the stream layer from one site to the next allowed the length of stream reach between each site to be measured. Other analyses are possible with this model but were unnecessary for this project.

7.6. Data Analysis Discharge Regressions

The mathematical equations used to analyze the concentration data from solute tracer tests operate under the assumption of constant discharge in the stream during the test. Many tracer tests are conducted over time periods that are short enough to assume that the discharge would not change or that the change was negligible. However, the LTT and IOTTs each lasted from 1 to 5 month long. Almost any natural stream system will undergo some fluctuations, declines, rises, and storm responses in time periods greater than one month, therefore the assumption that discharge does not change was not valid during the LTT and IOTTs.

The discharge of Lookout Cr. and its tributaries underwent a steady decline throughout the summer and experienced several storms during the LTT and IOTTs, which lasted from June 14, 2003 through November 15, 2003, (Figure 38). In Figure 38, the hydrograph in L/s for Lookout Cr. is shown vs. days from January 1, 2003. The hydrograph information was acquired through the U.S. Geological Survey and comes from their gauging station #14161500. The graph is displayed in semi-log space as a means to highlight the peaks and declines of the discharge. The locations of the beginning and endings of the LTT and the IOTTs are shown on Figure 38.

The reality that the stream discharge was changing necessitated that the change in discharge be accounted for in our mathematical analysis. As a means of

accounting for the changing discharge of the stream, the flux of RWT measured as μg/s was calculated and used as a surrogate for concentration. The flux was calculated by multiplying the tracer concentration at a monitoring site by the discharge at the same point and time.

The outlet of Lookout Cr. has a gauging station, however there are no other gauging stations directly on the main stem. Because of the lack of continuous discharge measurements above the outlet, several step were taken to estimate the discharge at the monitoring sites during the LTT and IOTTs. As mentioned earlier capacitance rods were originally going to measure continuous discharge throughout the tracer test, however technical difficulties prevented us from using them. In combination, we underestimated the importance of knowing the discharge throughout the longitudinal profile of Lookout Creek throughout the summer. As a result, we only measured discharge at the injection sites before and during individual injections and sporadically throughout the summer. Our discharge information was supplemented by information gathered by Charles Frady of the Department of Fish and Wildlife. Mr. Fardy's information was gathered throughout the H.J. Andrews in June, July, and August of 2003. The combination of Mr. Fardy's data and our own measured discharge data was necessary to create a continuous hydrograph for each site.

Figure 38. Hydrograph for Lookout Creek Catchment taken at the USGS gauging station from the last spring storm May 24th to November 20th, 2003.

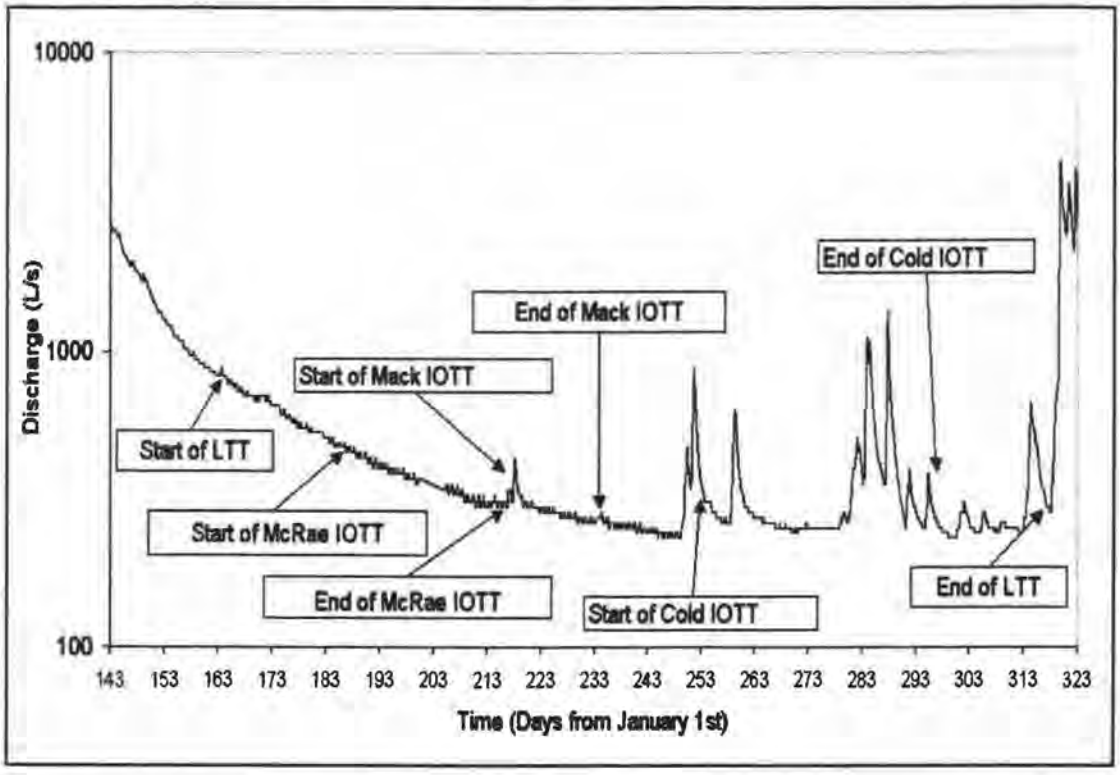

The H.J. Andrews offered a unique opportunity to offset the weakness in our discharge information. The H.J. Andrews is equipped with a USGS gauging station near the outlet of the basin as well as nine gauged sub-basins. Each of these stations has a continuous discharge record throughout 2003. The record provided by each of these stations was compared to the discrete discharge samples gathered at a given site. A linear regression between the discrete discharge samples and the different gauged basins was used to quantify which basin best fit the behavior at each monitoring site. An example is shown in Figure 39. The discrete discharge measurements taken below Cold Cr. are shown on the y-axis and the discharge measurements taken at the same time from the gauging station at Mack Cr. are shown on the x-axis in Figure 39. All of the gauging stations within the basin were compared by a linear regression to the discrete samples taken at each site. The regression with the highest r^2 value was chosen to represent the relationship between the specified basin and the site being evaluated. The best-fit

regression for the Below Cold Cr. site is shown in Figure 39 with an r^2 of 0.90. The regression equation was used to modify the specified basin's hydrograph to fit a monitoring site hydrograph. The fitted site hydrograph was used to adjust the concentration and estimate the flux. This process was carried out for each monitoring site for all of the tracer tests. The basin used for each site is included in Table 1 and Table 2.

A large amount of error was inherent in this hydrograph-transfer technique and some modifications were required. The modifications became apparent after examining the regression fits and comparing them to each other and the estimated flow rates from the concentration plateaus. A discharge vs. basin area relationship and a function to model to the discrete discharge measurements were also tried to create hydrographs for the monitoring sites. Despite the error involved in this regression technique, it was deemed the best possible way to evaluate the concentrations and fluxes given the information we possessed.

Figure 39. Hydrograph regression for the Below Cold Creek site's discrete discharges compared to the Mack Creek discharges at the same time during the summer of 2003.

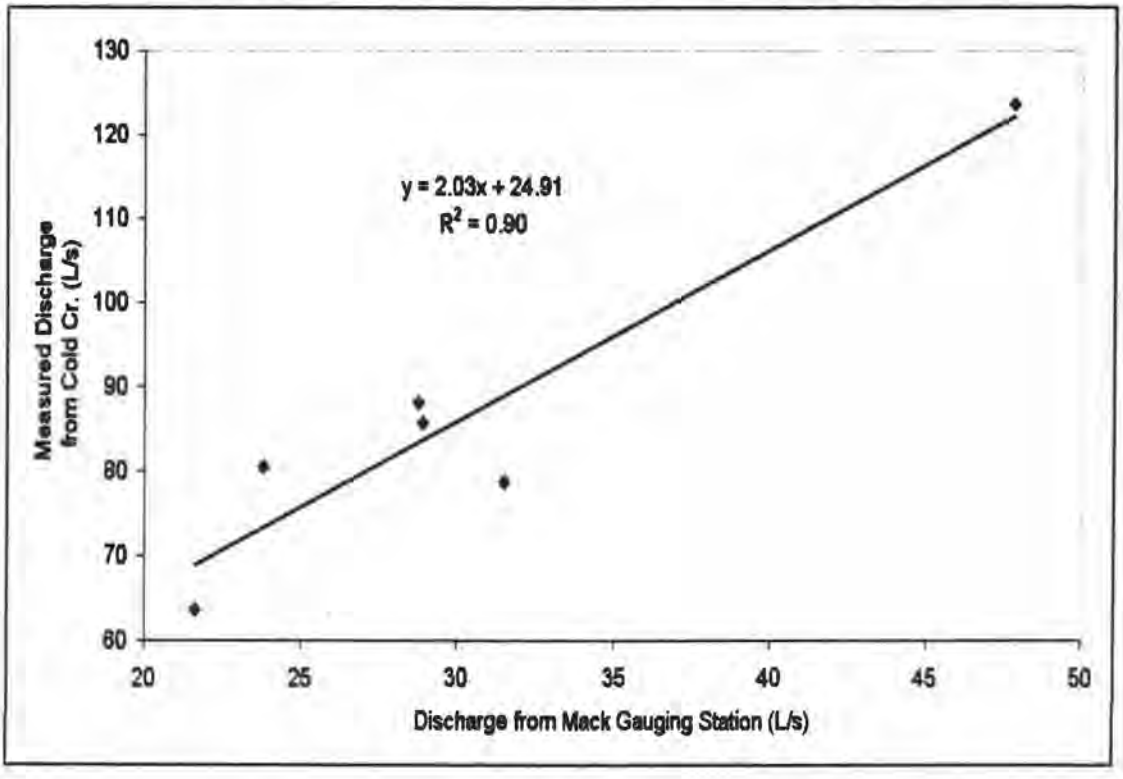

7.7. Data Analysis Parameter Modeling

The concentration breakthrough curve of a tracer test can be modeled using a semi-analytical solution to the mass transfer equation (Haggerty, 1995). The model used to derive the solution to this equation for our tracer tests was called Solute Transport and Multirate Mass Transfer-Linear coordinates (STAMMT-L). This model is based on the work reported in (Haggerty, 1995; Haggerty and Gorelick, 1995; Haggerty and Gorelick, 1998; and Haggerty et al., 2000a). STAMMT-L models solutions to the one-dimensional advective-dispersive mass transport equation and can include mass transfer between mobile and multiple immobile domains (Haggerty and Reeves, 2000). The immobile domain in this model can take on many forms including a single value or a distribution of diffusion rates or mass-transfer rates (Haggerty and Reeves, 2000). These different values or distribution of values can represent the variability in the diffusion coefficient, matrix size, or both (Haggerty and Reeves, 2000). STAMMT-L is particularly useful because it allows the user the ability to define the memory function and distributions of rate coefficients that will describe the behavior of the system being evaluated (Haggerty and Reeves, 2000).

The STAMMT-L model solution for a given breakthrough curve gave us information about the physical properties of the mobile and immobile domains of the stream length that the tracer test was conducted through. The information derived from the model runs included residence time distribution, mean velocity, dilution factor, dispersion coefficient, and the ratio between the area of the immobile domain to the area of the mobile domain (β_{tot}), as detailed in Section 5, Results of this thesis and Appendix II, Additional Parameter Information.

The STAMMT-L program was run by following a series of complex instructions detailed in the "STAMMT-L User's Manual Version 3.01" (Haggerty and Reeves, 2000). The model involved entering known physical characteristics about the tracer test. These characteristics included length of the test reach, total time of the injection, total time of monitoring, the concentration breakthrough curve, mass of the injection, type of injection, and a general residence time distribution function. The program then estimated the best-fit value for the

residence time distribution parameter, mean velocity, dilution factor, dispersion coefficient, and β_{tot}.

For this project, a square pulse injection was assumed with a constant injection and concentration for the duration of the injection time. This assumption was violated by the variance in the injection rate at most of the injection sites, except for the Cold Creek IOTT, however it was felt that this violation did not effect to overall conclusions in the thesis. The concentration breakthrough curve was replaced with the flux breakthrough curves to account for the changing discharge through the course of the tests. It was necessary for the program's algorithms to normalize the flux curves to the initial square pulse injection flux. This resulted in a ratio of measured flux over flux initial, which would give a value of 1 if the tracer test reached plateau at the monitoring site.

The general residence time distribution function was estimated to be a power-law function. This estimation came from observation of the late time behavior of the concentration and flux breakthrough curves. The breakthrough curves were shown to generally have a straight line on log-log graphs, which indicates a power-law decline of the curves in late time (Figures 4, 6, 8, 9, 11-16).

After giving STAMMT-L the information to estimate the solutions using a power-law residence time distribution, the program estimated the slope of the power-law as part of the parameters derived in the solution. Other residence time distributions functions, such as an exponential function, were also evaluated, however the results showed poorer fits, with lower root means square error (RMSE) and are discussed in Section 5: Results of this thesis. The STAMMT-L program used an optimization process to estimate the best-fit model parameters for each of the breakthrough curves. The result was a RMSE output. The fit with the lowest RMSE was used as the final parameter output. However, on some occasions, the output with the lowest RMSE also had unrealistic parameter values. For example sometimes the velocity would be estimated to be 100 times higher than the maximum velocity ever measured in the H.J. Andrews. When this problem occurred, measurements from the field were used to constrain the velocity

to a given value or a range of values and the best-fit parameters with the lowest RMSE in that range of values was used as the final output.

The power-law distribution function within STAMMT-L was found to be sensitive to its truncation input parameters. These truncation parameters α_{min} and α_{max} are estimated by the maximum and minimum exchange times observed during the test. Slight adjustments to the values of the parameters were found to improve the performance of the model fits (Table 4).

8.0 APPENDIX II: ADDITIONAL INFORMATION

8.1. Background

The longitudinal tracer test (LTT) and the intra-order tracer tests (IOTT) were conducted during the summer of 2003 on Lookout Creek in the H.J. Andrews, Oregon. The LTT consisted of a basin wide longitudinal tracer test on Lookout Creek. The IOTTs were smaller tracer tests conducted between the major confluences of Lookout Cr. The tests were conducted to study the behavior of hyporheic exchange and the distribution of exchange rates within the hyporheic zone at multiple scales. More specifically, this test was investigating whether the residence time distribution of the hyporheic zone behaved in a fractal manner.

The LTT and the IOTT were analyzed for several hyporheic parameters not discussed or only briefly discussed in the main section of this thesis. This section discusses those parameters and includes some graphic representations of the breakthrough curves not shown in the main body of the thesis.

The analyzes of the monitoring sites for each of the tests resulted in values for velocity, dispersion, dilution, β_{tot} (immobile area/mobile area), mass recovered, minimum exchange time, and maximum exchange time. The velocity measurement estimated by the STAMMT-L program was the mean velocity of the test reach throughout the testing period. The dispersion was the rate at which RWT exchange occurred between the immobile and mobile zones within the test reach. The dilution parameter measured how much water was gained over the reach or how much mass was not accounted for. The β_{tot} value was the parameter used to measure the area of the hyporheic zone compared to the active channel. In actuality, β_{tot} measures the area of the immobile zone to the area of the mobile zone. The immobile zone includes the hyporheic zone and the immobile zones in the stream such as pools, eddies, slews, etc. The mass recovered was the percent of the mass of RWT that was injected during a specific test and was later measured in the stream at a lower location during our stream monitoring. The minimum and maximum exchange times were required as parameters for the STAMMT-L model

and may be more relevant to the mathematics of the model than the actual physical flow paths.

8.2. Methods

The concentration and flux breakthrough curves of the LTT and the IOTTs for this section were gathered using the same methods and analytical tools outlined in Appendix I: Detailed Methods. The hydrographs used in the following parameter analysis were also derived using the same basin regression technique outlined in Appendix I: Detailed Methods. All of the monitoring sites for the LTT and the IOTTs were analyzed for hyporheic parameters. The analysis was conducted using the STAMMT-L modeling program and the same technique outlined in Appendix I: Detailed Methods.

The percent mass recovered was calculated directly from the concentration and discharge data. The concentration was first adjusted using the discharge to reflect the total flux of RWT in the stream at a given time. This adjustment was calculated by multiplying the concentration by the discharge at a given time. The flux breakthrough curve was integrated to calculate its first moment, which is equal to the mass recovered during the test.

The minimum and maximum exchange times were represented by α_{max} and $\alpha_{min,}$ respectively. Equation 7 and Equation 8 give the exact relationship between the minimum and maximum exchange times and the respective α values.

Equation 9 (minimum exchange time)

$$\frac{1}{Time_{\min imum}} = \alpha_{\max imum}$$

Equation 10 (maximum exchange time)

$$\frac{1}{Time_{\max imum}} = \alpha_{\min imum}$$

In order to calculate the in-channel and hyporheic volumes reported in Table 6, several steps and assumptions were used. First of all the length of the stream was known but the cross sectional area of the stream changes with longitudinal position and depending on discharge. The first assumption that was made was to assume that the cross sectional area changed linearly between monitoring sites. The discharge measurements taken at each of the monitoring sites throughout the summer were then used to calculate the cross sectional area at each site. The average area for all of the discharge measurements at a given site was then used as the cross sectional area value for that site. This method assumes that the average cross sectional area represents the changes in cross sectional between June 14, 2003 and November 15, 2003. This may not be a bad assumption for a tracer test because tracer test are an integration of values over the duration of the tracer test and they assume a constant discharge. After establishing a cross sectional area for each site standard calculus was then used to integrate the in-channel volume between each site (Table 6). Next the in-channel volumes were multiplied by the β_{tot} (immobile volume/mobile volume) values, estimated during the STAMMT-L parameter optimization, to yield an estimate for the hyporheic volume between each monitoring site (Table 4, 5 and 6). The total in-channel and hyporheic volume was also reported (Table 6).

8.3. Results

8.3.1. Additional McRae Creek. IOTT Information

The concentration and flux breakthrough curves of the McRae Cr. IOTT can be displayed using several different ways in order to highlight important characteristics of the curve itself. Throughout this thesis the primary method used to display breakthrough curves is using a log-log space. The log-log scale on the graph allows for easy recognition of power-law behavior, through the identification of straight line on the graph. Semi-log representation on a graph highlights exponential behavior and arithmetic scales will highlight linear features.

Figure 40 shows the concentration breakthrough curve of the McRae Cr. IOTT in arithmetic space. In Figure 40 the red squares represent the concentration

samples from the injection site 420 m below the injection site, the maroon squares represent data collected 1465 m downstream from the injection site at the floodplain site, and the blue squares are the data gathered 5367 m downstream at the headquarters site. The rising limb and the peak of the curve are clearly shown, however, the behavior of the tail is difficult to distinguish (Figure 40).

The flux breakthrough curve of the McRae Cr. IOTT in log-log space is shown in Figure 41. In Figure 41 the colored squares represent the same monitoring sites as in Figure 40, however, the injection site is not represented in this graph. The rising limb and the peak of the curve appear to be broader then in arithmetic space, however, the power-law behavior of the tail is easier to recognize (Figure 41). Smaller amounts of scatter are easier to observe in the log-log representation of the flux breakthrough curve.

Figure 40. Concentration BTC for the monitoring sites in arithmetic space during the McRae Creek IOTT.

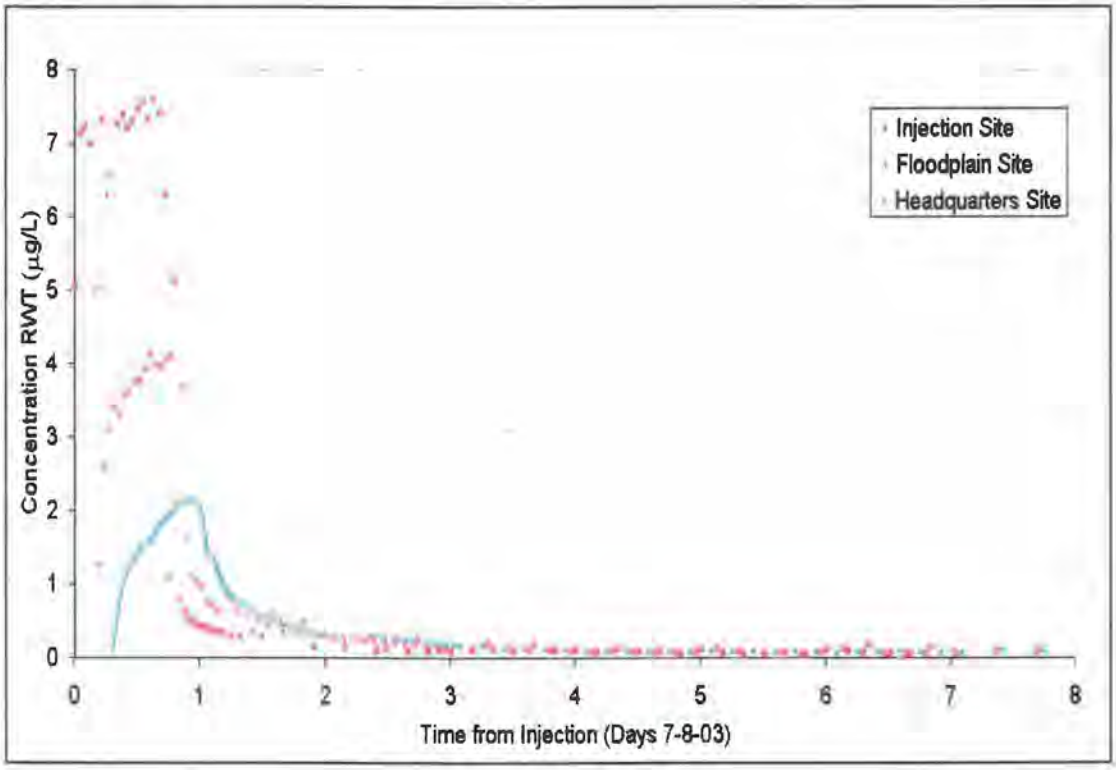

Figure 41. Flux breakthrough curves normalized to the average flux injection rate for the McRae Cr. IOTT monitoring sites in log-log space.

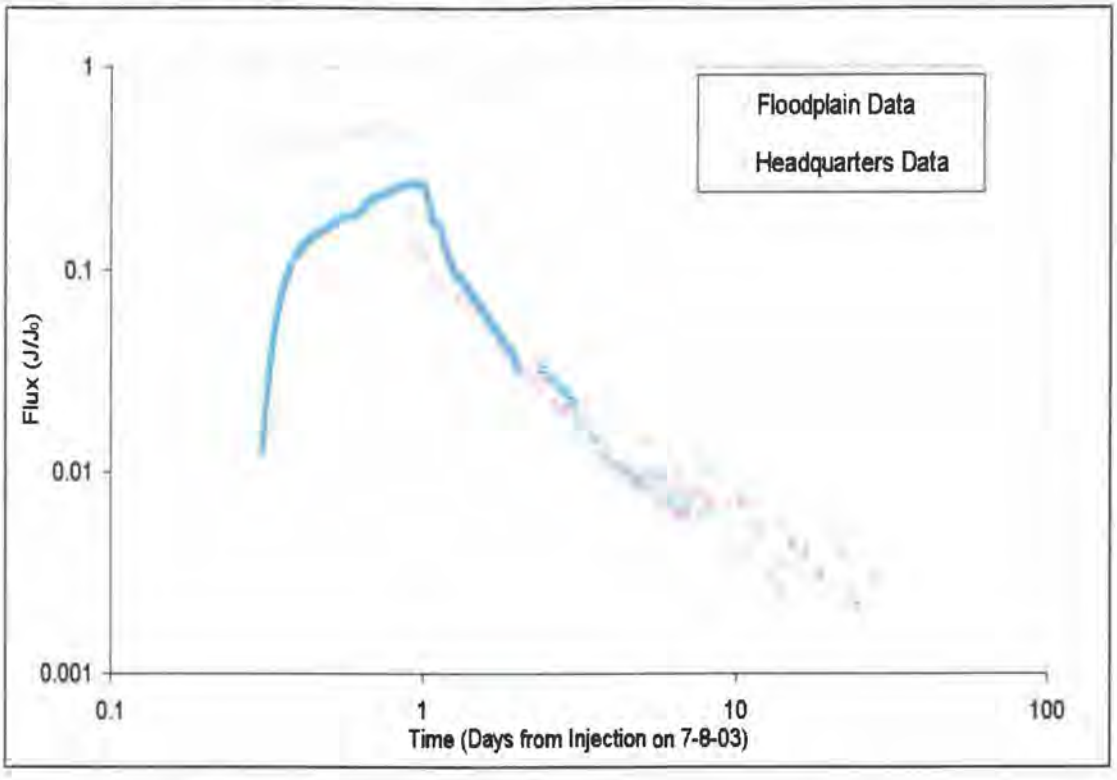

The flux breakthrough curve of the McRae Cr. IOTT in arithmetic space is shown in Figure 42. Figure 42 has the same labeling system as in Figure 41. The x-axis of Figure 42 is larger then Figure 40 and the difficulties of evaluating the behavior of the tail is more apparent.

Figure 42. Flux breakthrough curves normalized to the average flux injection rate for the McRae Cr. IOTT monitoring sites in arithmetic space.

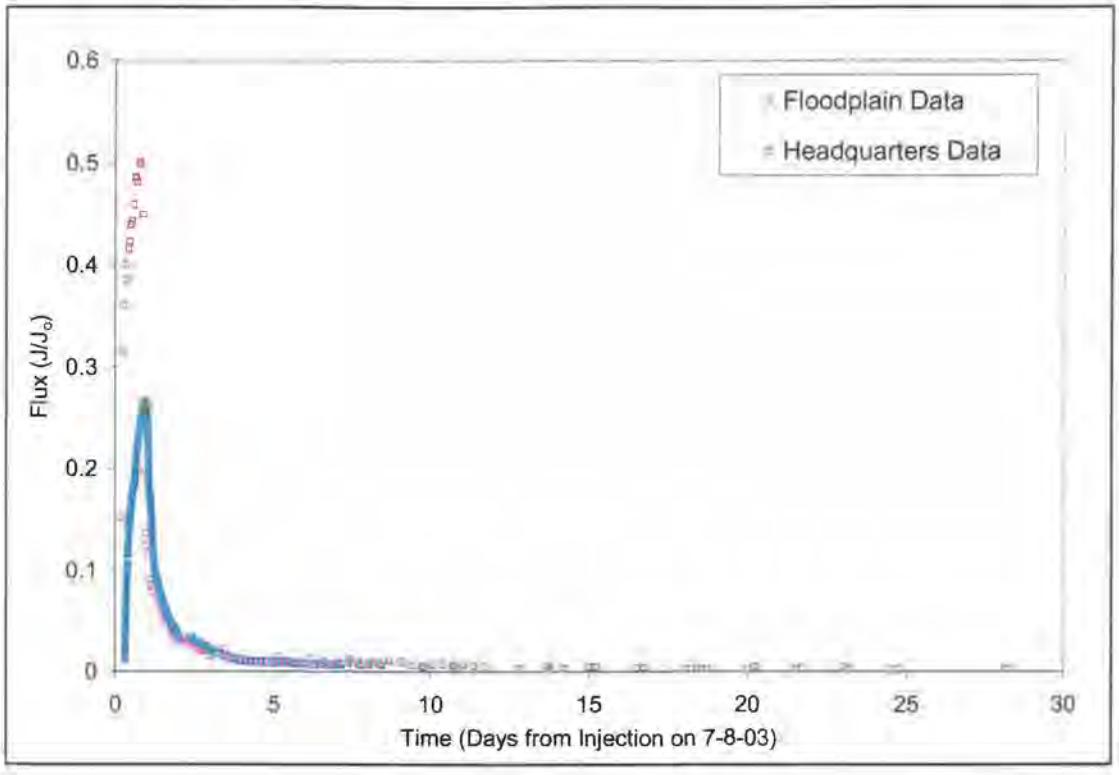

8.3.2. Additional Mack Creek. IOTT Information

The graphs in this section display the concentration and flux breakthrough curves of the Mack Cr. IOTT in several different ways as a means of highlight different important characteristics of the curve itself.

Figure 43 shows the concentration breakthrough curve of the Mack Cr. IOTT in arithmetic space. In Figure 43 the red squares represent the concentration samples from the injection site 25 m below the injection site, the gold squares correspond to data collected 1001 m downstream from the injection site at the middle tributary site, and the purple squares represent data gathered 3457 m downstream at the above McRae Cr. site. The injection site data points are poorly represented because of a sampling problem see Appendix I for details. The behavior of the tail is difficult to interpret from Figure 43 but the rising limb and

the peak of the curve show a gradual rise to the peak and a distinct drop after the end of the injections.

Figure 43. Concentration breakthrough curves for the monitoring sites in arithmetic space during the Mack Creek IOTT.

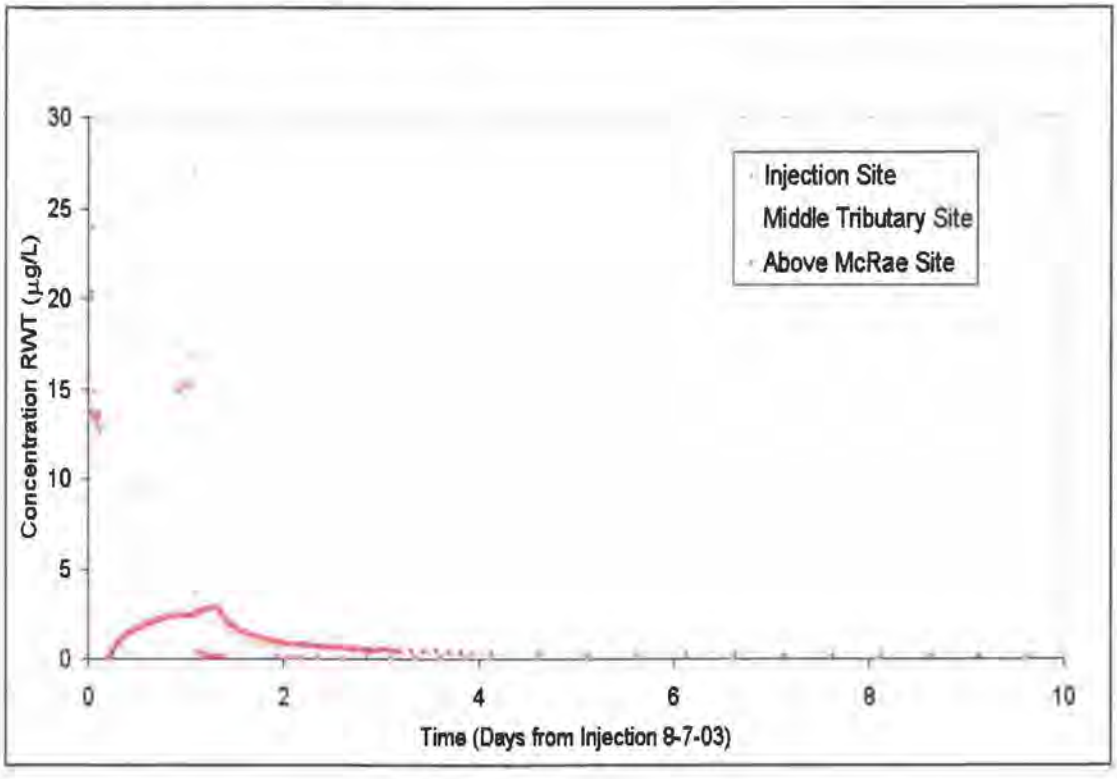

The Mack Cr. IOTT flux breakthrough curve in log-log space is shown in Figure 44. The colored squares of Figure 44 represent the same monitoring sites as in Figure 43, however, the injection site is not represented in this graph. The rising limb and the peak of the curve appear to be broader then in arithmetic space, however, the power-law behavior of the tail is easier to recognize (Figure 44). The rising limb of the flux breakthrough curve for the middle Mack site begins at a high initial reading with little lower values to create a rising limb. This behavior is partially due to interpreting from a log-log graph and also a result of not having a short enough sampling regime to capture the rise (Figure 44).

Figure 44. Flux breakthrough curves normalized to the average flux injection rate for the Mack Cr. IOTT monitoring sites in log-log space.

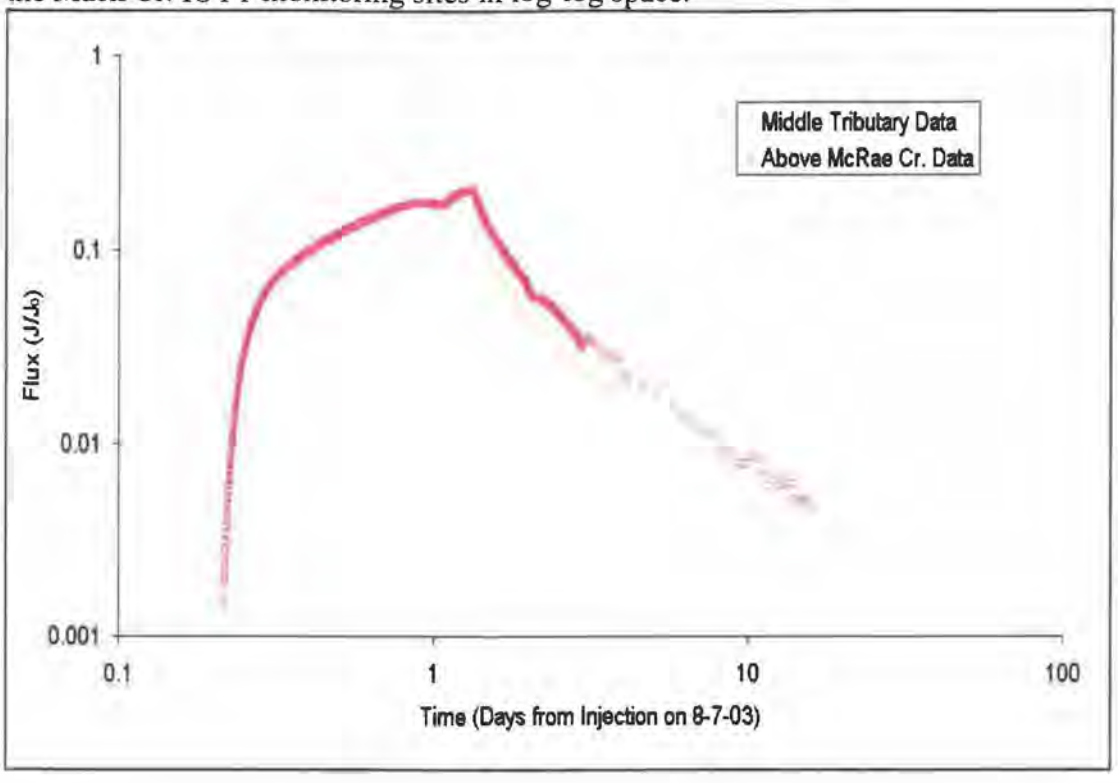

The flux breakthrough curve of the Mack Cr. IOTT in arithmetic space is shown in Figure 45. Figure 45 has the same labeling system as in Figure 44. The x-axis of Figure 44 is larger then Figure 43 and the difficulties of evaluating the behavior of the tail is more apparent.

Figure 45. Flux break through curves normalized to the average flux injection rate for the Mack Cr. IOTT monitoring sites in arithmetic space.

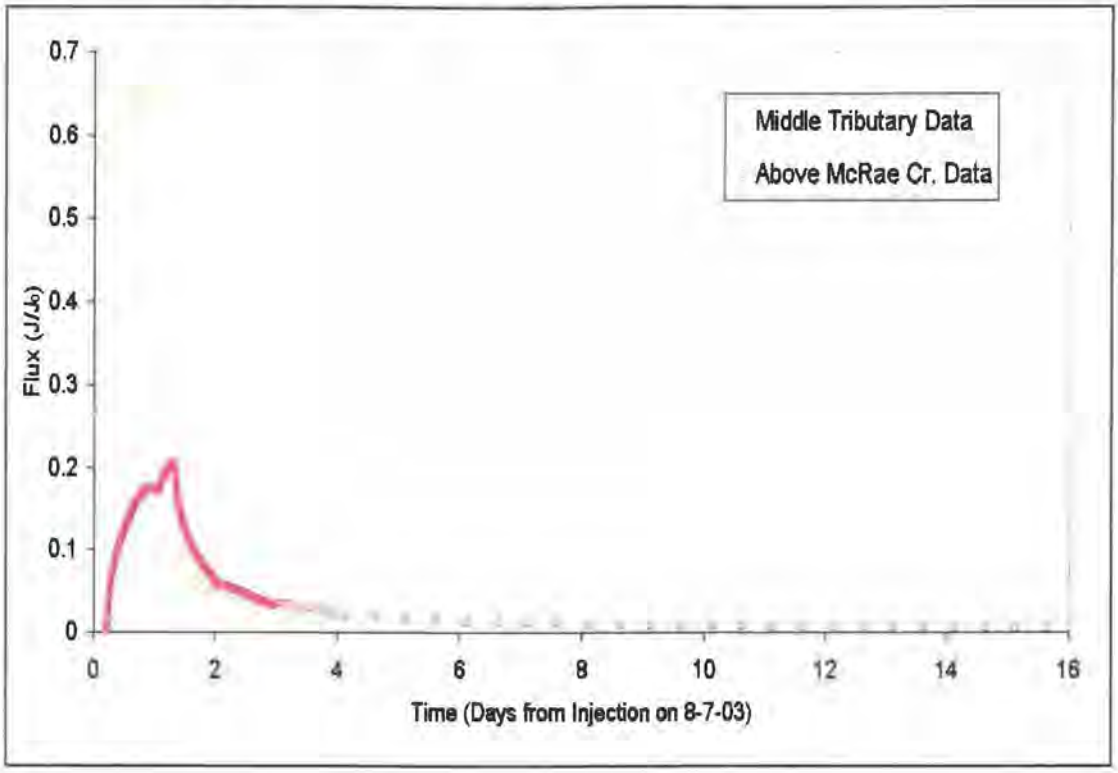

8.3.3. Additional Cold Creek. IOTT Information

The graphs in this section display the concentration and flux breakthrough curves of the Cold Cr. IOTT in several different ways as a means of highlight different important characteristics of the curve itself.

Figure 46 shows the concentration breakthrough curve of the Cold Cr. IOTT in arithmetic space. In Figure 46 the aqua squares represent the concentration samples from the injection site 46 m below the injection site, the dark blue squares correspond to data collected 2105 m downstream from the injection site at the Longer Cr. site, and the light blue squares represent data gathered 3054 m downstream at the above Mack Cr. site. The behavior of the tail is difficult to interpret from Figure 43 but the rising limb and the peak of the curve show a gradual rise to the peak and a distinct drop after the end of the injections.

Figure 46. Concentration breakthrough curves for the monitoring sites in arithmetic space during the Cold Creek IOTT.

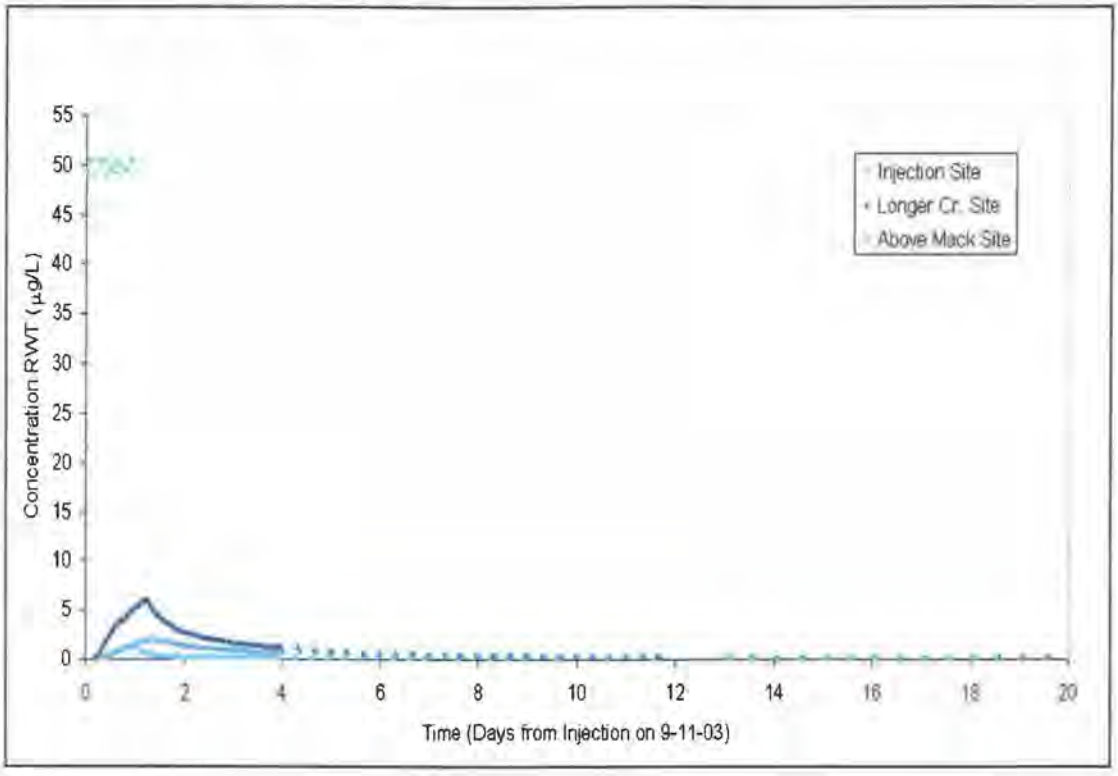

The Mack Cr. IOTT flux breakthrough curve in log-log space is shown in Figure 47. The colored squares of Figure 47 represent the same monitoring sites as in Figure 46, however, the injection site is not represented in this graph. The rising limb and the peak of the curve appear to be broader then in arithmetic space, however, the power-law behavior of the tail is easier to recognize (Figure 47). The power-law behavior of the declining tail is shown to begin immediately after the injection stops in Figure 47. Figure 47 shows a storm event on September 9, 2003 that was captured as a spike in the flux curves five days after the beginning of the injection.

The flux breakthrough curve of the Mack Cr. IOTT in arithmetic space is shown in Figure 48. Figure 48 has the same labeling system as in Figure 47. The x-axis of Figure 48 is larger then Figure 46 and the difficulties of evaluating the behavior of the tail is more apparent.

Figure 47. Flux breakthrough curves normalized to the average flux injection rate for the Cold Cr. IOTT monitoring sites in log-log space.

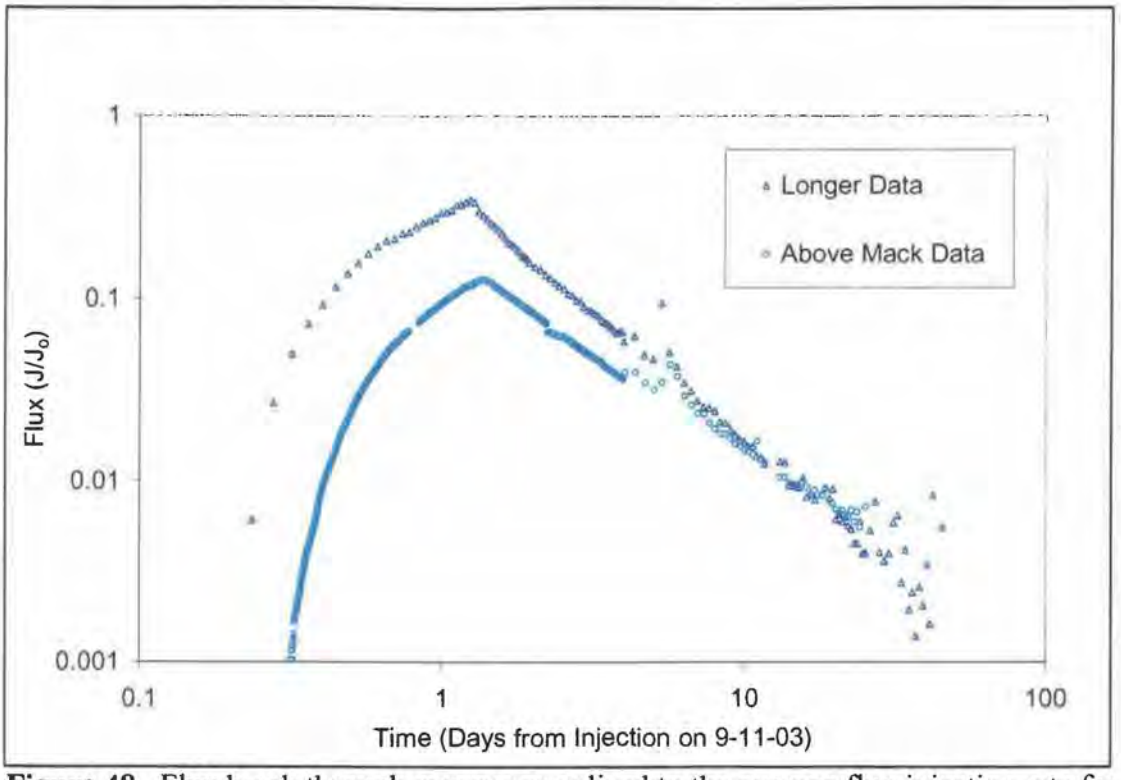

Figure 48. Flux break through curves normalized to the average flux injection rate for the Cold Cr. IOTT monitoring sites in arithmetic space.

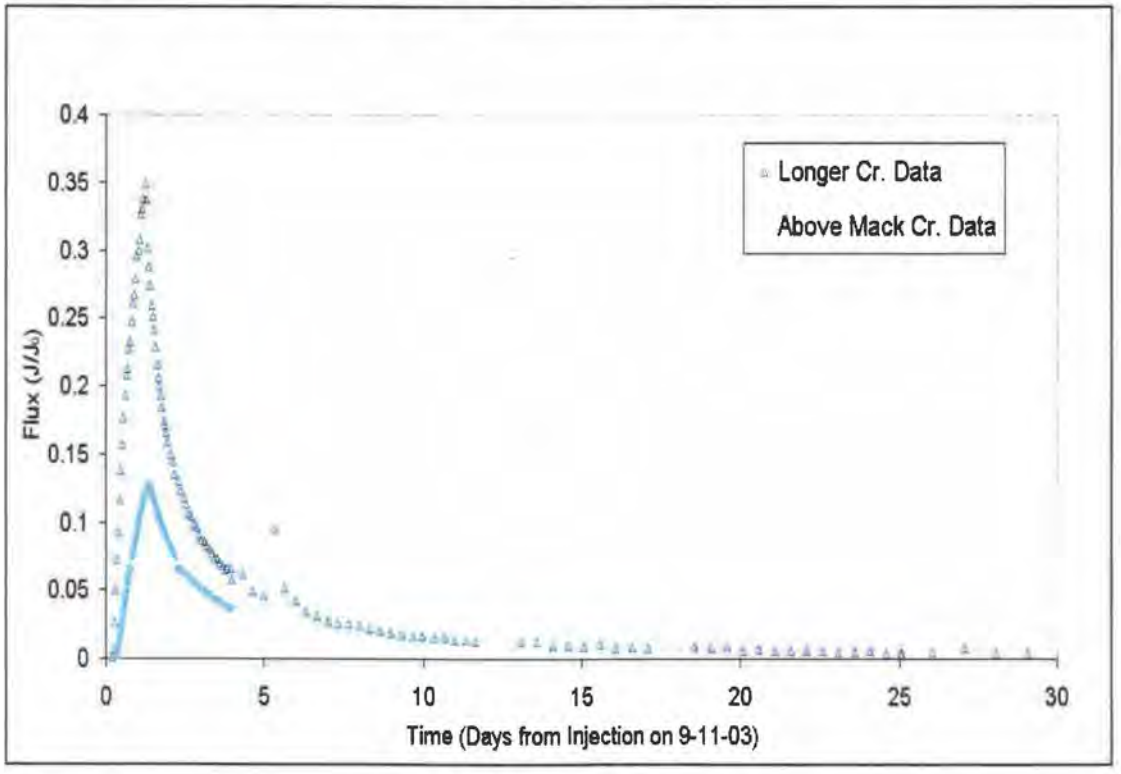

8.3.4. Additional Parameter Information

The LTT and the IOTTs were modeled for a variety of hyporheic parameters using the STAMMT-L mass transfer modeling program. The summary of results for the STAMMT-L estimated values for velocity, dispersion (D_L), dilution, β_{tot} (ratio of immobile area/mobile area), percentage of mass recovered, minimum exchange time, and maximum exchange time is given in Table 4 and Table 5.

The velocity estimates for the LTT compared to the IOTTs are distinctly different. Figure 49 shows the estimated velocities for the LTT and the IOTTs at each of the monitoring sites. The velocities for the LTT are represented by triangles and the velocities for the IOTTs are shown by squares (Figure 49). Both the LTT and the IOTT had a strong linear relationship within each group as shown by the linear regression in Figure 49. The velocity values in the IOTTs are lower and have a shallower trend for the same location on the river network (Figure 49). Both the LTT and the IOTT increase longitudinally downstream.

Figure 49. The STAMMT-L velocity estimates for the LTT and IOTTs.

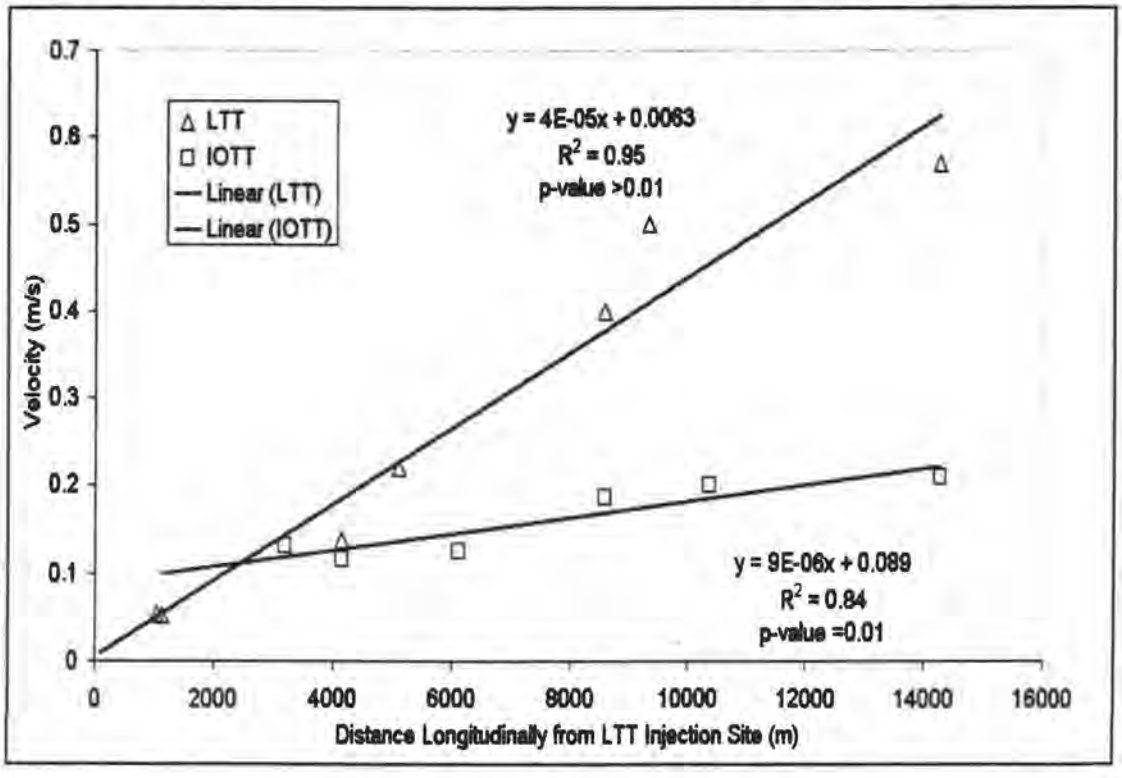

In Figure 50 the dispersion coefficient (D_L) estimated at each site for the LTT and IOTTs are shown relative to there longitudinal distance from the LTT injection site. The LTT estimates are shown by a triangle and the IOTT are shown by a square and individual tests are labeled. The arrows on the graph indicate the downstream direction. Dispersion (D_L) values show an increase longitudinally for the LTT and the Cold Creek IOTT, but decrease downstream for the Mack and McRae Creek IOTTs (Figure 50).

Figure 50. The STAMMT-L dispersion estimates for the LTT and IOTT shown in the longitudinal position relative to the LTT.

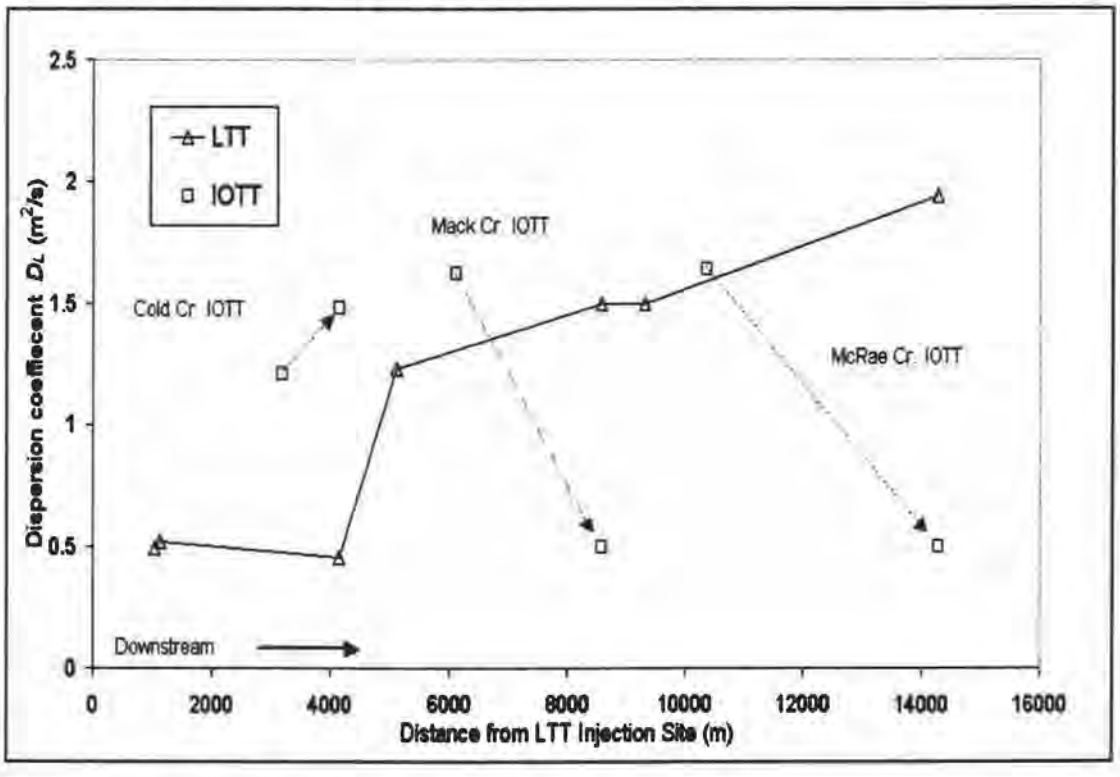

The dispersion coefficients (D_L) are shown in Figure 51 for the monitoring sites of the LTT and IOTTs relative to the distance from each tests injection site. The labeling system is the same as Figure 50 but values of each dispersion coefficient (D_L) is also shown in Figure 51. The dispersion values show a wide variance when compared to the distance from the injection site and may converge down at some larger distance from the injection site (Figure 51). The ambiguity in

the possibility of convergence arises from not having duplicate tracer tests at a scale greater then 6 km to compare with the LTT results.

Figure 51. The STAMMT-L dispersion estimates for the LTT and IOTT shown in distance from the individual injection sites, H.J. Andrews, summer, 2003.

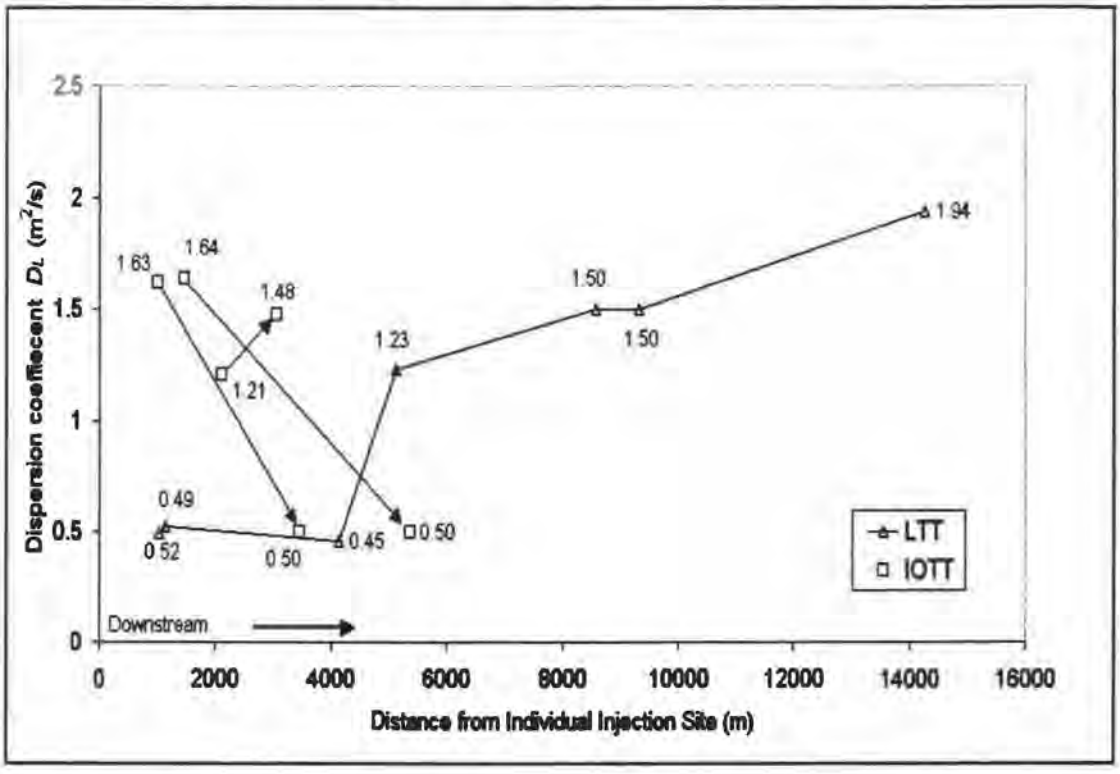

The dilution factor vs. longitudinal distance from the LTT injection site for the LTT and IOTTs are shown in Figure 52. The IOTT are labeled in Figure 52 and arrows indicate the downstream direction of each. Dilution is shown to be greater during the higher discharges of the LTT than the lower flows of the IOTT's for the same location on the river network (Figure 52).

The distance a tracer travels effects the estimate of the dilution factor as shown in Figure 53. In Figure 53 the dilution factor is displayed vs. the distance from individual test injection distance. The values of the LTT (triangles) and the IOTTs (squares) regress around a mean that increases with distance from injection (Figure 53).

Figure 52. The STAMMT-L dilution factor estimates for the LTT and IOTT shown in the longitudinal position relative to the LTT.

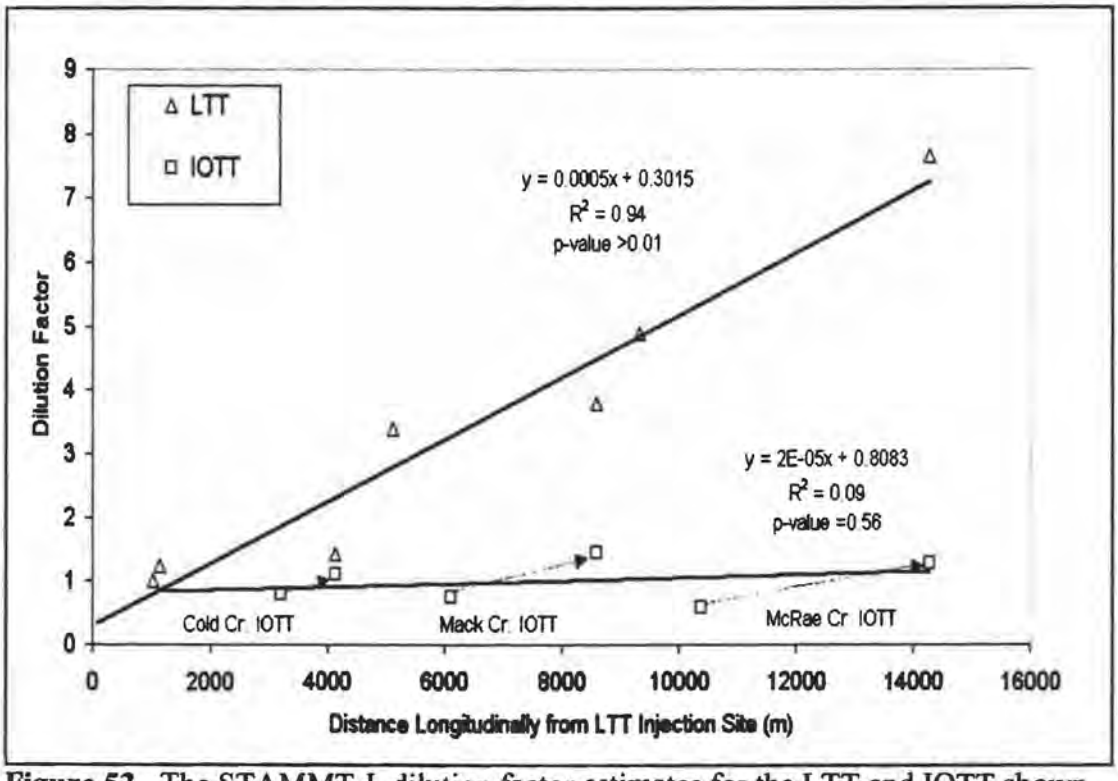

Figure 53. The STAMMT-L dilution factor estimates for the LTT and IOTT shown in distance from the individual injection sites.

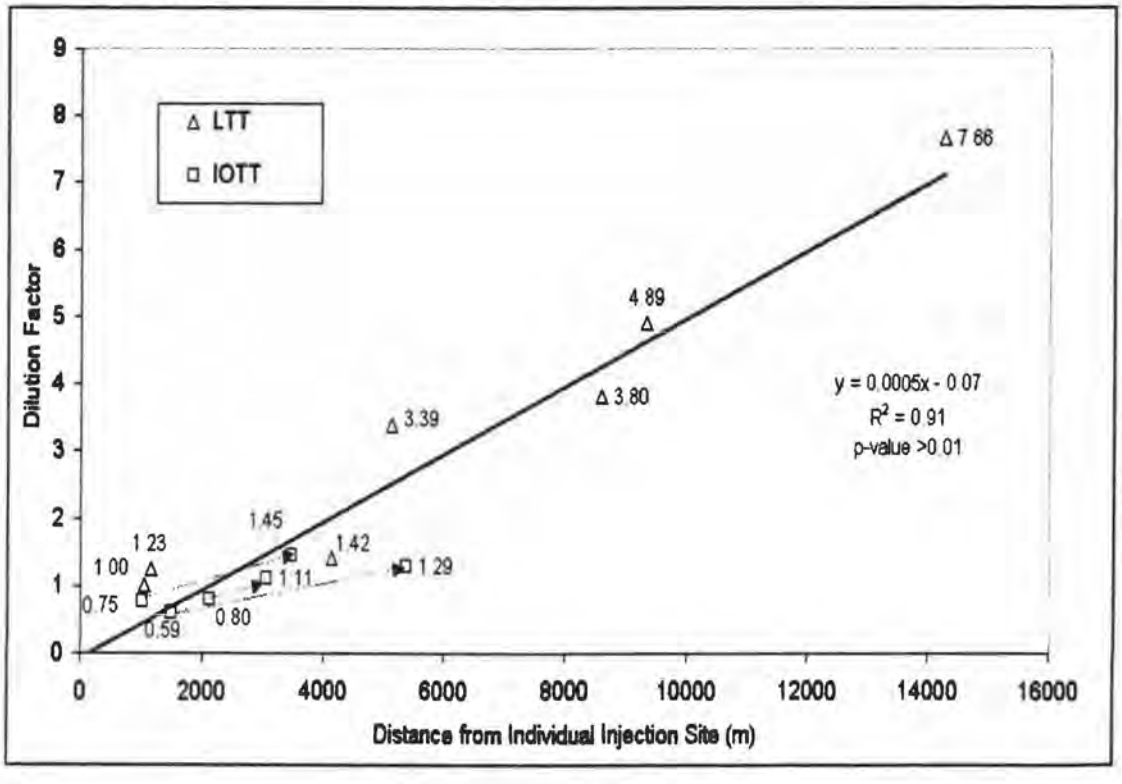

The STAMMT-L estimates for β_{tot} are shown in Figure 54 vs. the distance from individual test injection sites. A clear pattern does not seem evident with the LTT in triangles or the IOTTs in triangles (Figure 54). Distance from the individual injection sites showed wide variance below 6 km with a possible convergence after 6 km. A duplicate tracer test of 6 km was not conducted, so this trend cannot be verified (Figure 54).

Figure 54. The STAMMT-L β_{tot} estimates for the LTT and IOTT shown in distance from the individual injection sites.

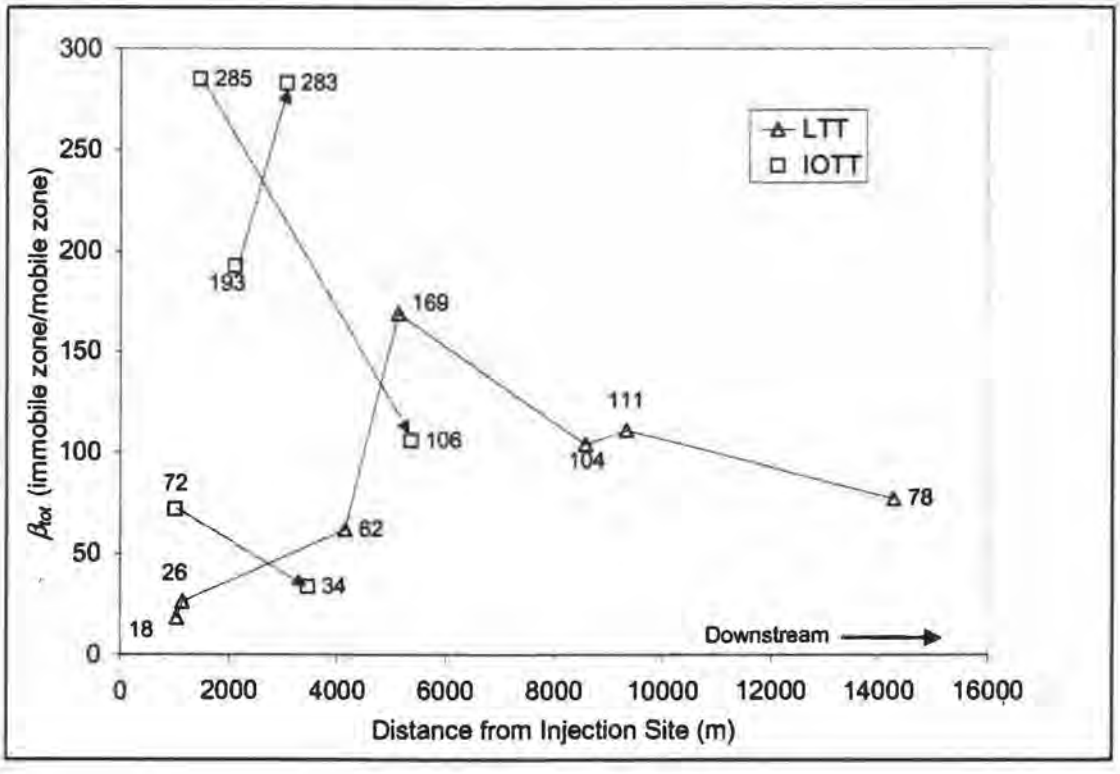

Figure 55 shows the behavior of the mass recovered vs. longitudinal distance from the LTT injection site for each of the tracer tests conducted during this study. In Figure 55 squares represent the LTT, triangles are shown for the Cold Cr. IOTT, circles display the Mack Cr. IOTT values, and diamonds represent the McRae Cr. IOTT. A best-fit regression has been calculated for each of the tracer tests and the corresponding equation is listed under the test label. Each test label has an arrow pointing to the line that corresponds to the regressed best fit. Mass recovered was

found to be dependent on the distance from the injection site and declined in the downstream direction for all the tests (Figure 55).

The above Cold Cr. site during the Cold Cr. IOTT registered a value of 101 % of RWT mass recovered (Figure 55). Since it is impossible to recover more mass then you injected it is believed that the discharge of the stream was overestimated, which resulted in a larger then possible estimate of percent mass recovered.

Figure 55. Percentage of RWT mass recovered for LTT and IOTT's as shown by longitudinal position relative to the LTT injections site.

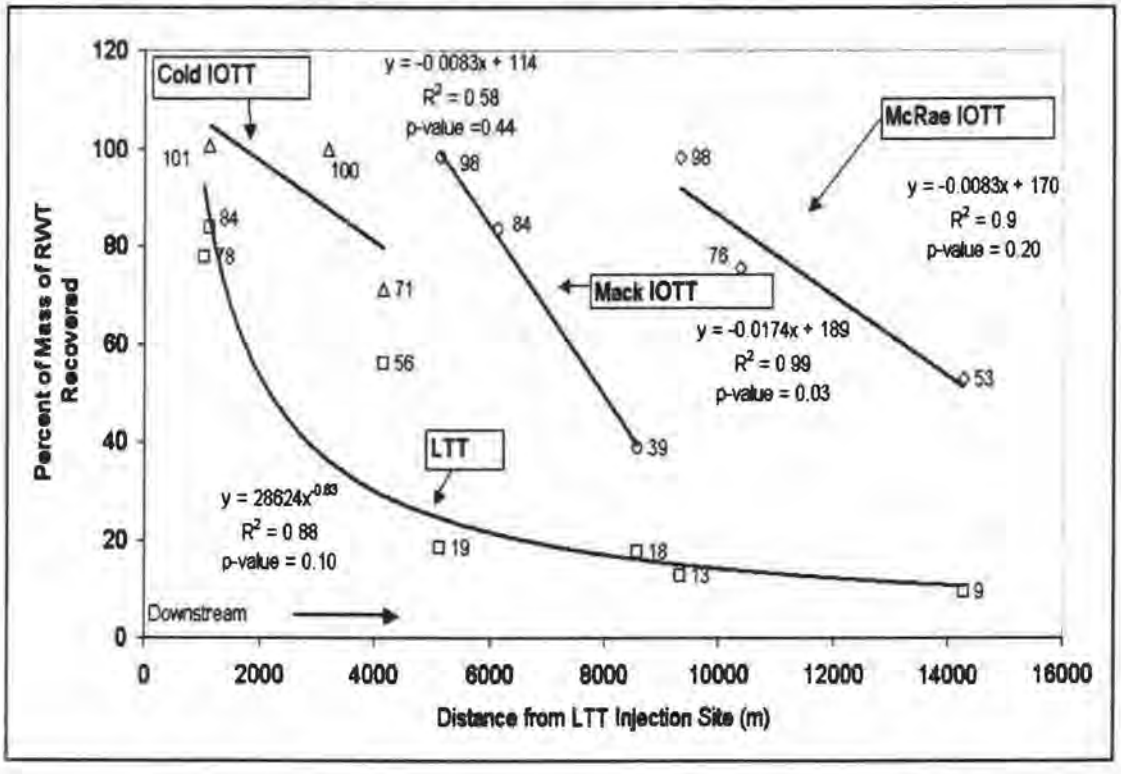

The relationship between the mass recovered and the total distance from the individual tracer test injection site is shown in Figure 56. The LTT percents are shown as squares and labeled and the IOTTs percents are shown as triangles and labeled (Figure 56). By analyzing the four tracer tests together there appears to be a relationship between percent of RWT recovered and the distance from the injection. Mass recovered appeared to decline exponentially with distance from the injection site (Figure 56).

Figure 56. Percentage of RWT mass recovered for LTT and IOTT's as shown in distance from individual injections sites.

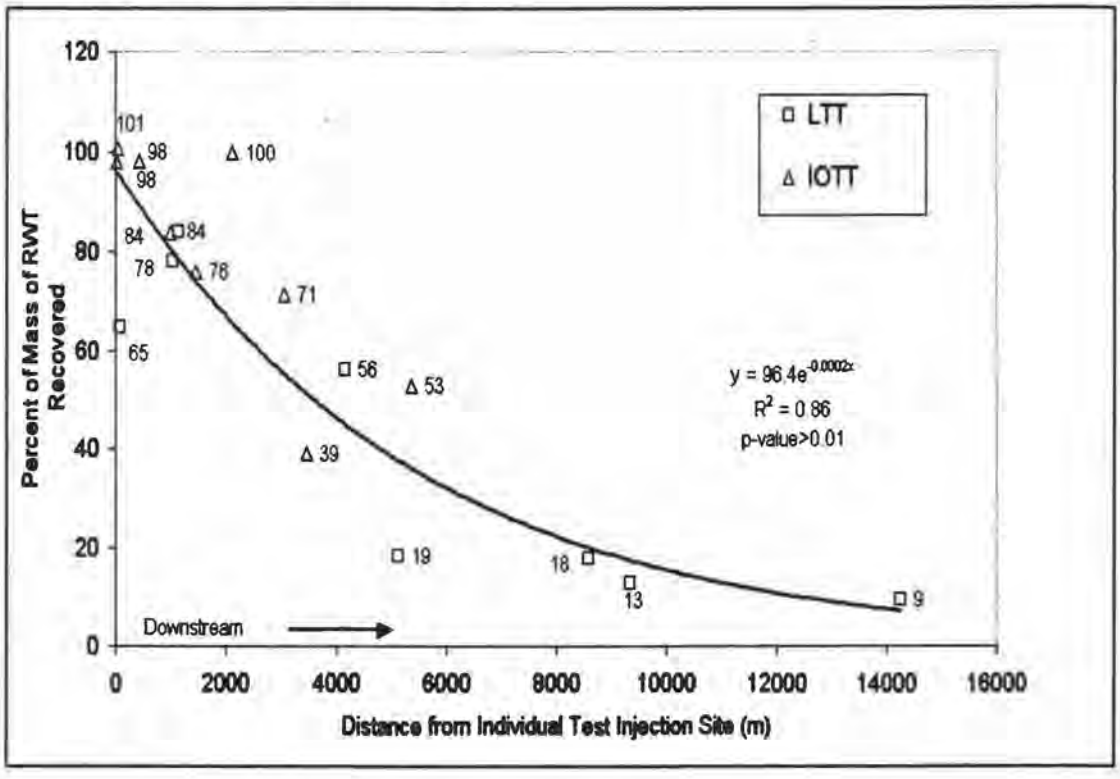

Figure 57 shows the maximum exchange time (α_{min}) on the left y-axis and the minimum exchange time (α_{max}) on the right y-axis with distance from the LTT injection site on the x-axis. Squares represent the maximum exchange time and the minimum exchange time of the LTT (Figure 57 and Figure 58). Triangles represent the maximum exchange time and the minimum exchange time of the IOTTs, (Figure 57 and Figure 58). Solid symbols with a dashed line represent maximum exchange time (α_{min}) of the tests (Figure 57 and Figure 58). Open symbols with a solid line represent minimum exchange time (α_{max}) of the tests (Figure 57 and Figure 58). In Figure 58 black represents the LTT, blue shows the Cold Cr. IOTT, maroon stands for the Mack Cr. IOTT, and orange represents the McRae Cr. IOTT. The estimated minimum and maximum exchange times for the LTT and IOTTs showed wide variance with respect to distance from the injection site and position on the longitudinal profile (Figure 57 and Figure 58). The majority of the variability was observed in the IOTT's, not the LTT (Figure 57 and

Figure 58). The minimum exchange time (α_{max}) was noted to have a wider spread of variance when compared to the maximum exchange time (α_{min}) (Figure 57 and Figure 58). Variability increased with distance from individual IOTT injection sites (Figure 57 and Figure 58).

Figure 57. Longitudinal variability of minimum exchange times and maximum exchange times as estimated by STAMMT-L.

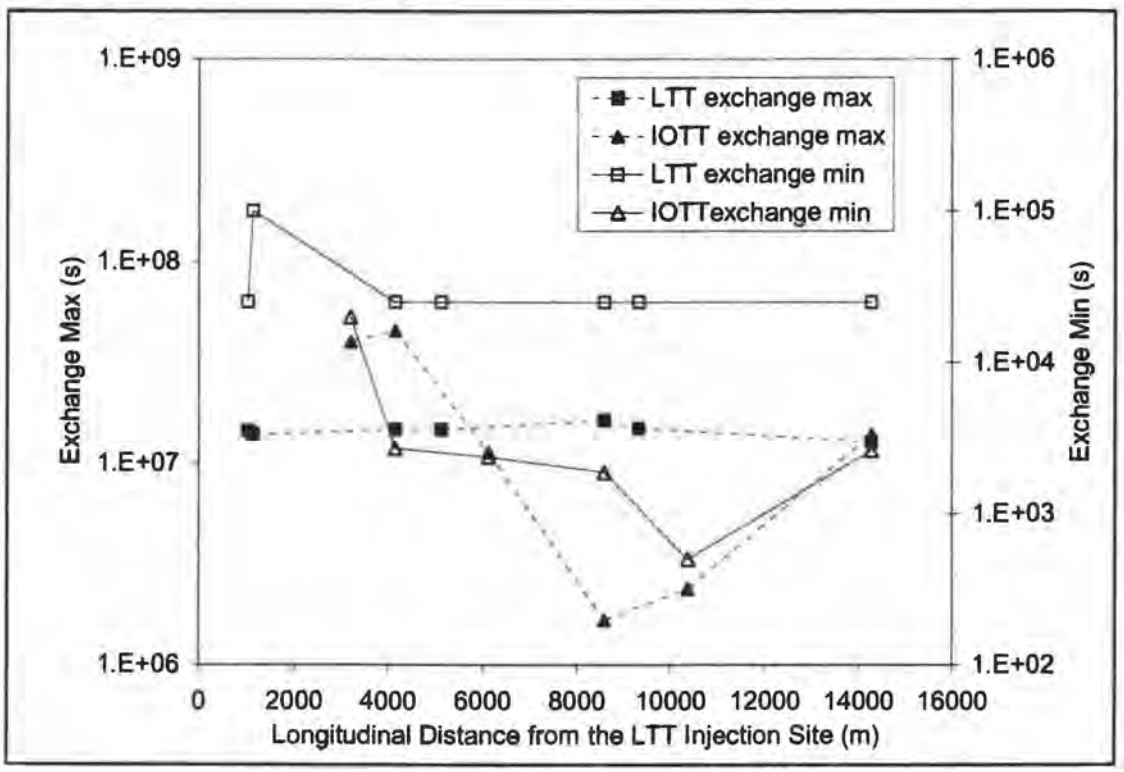

Figure 58. Variability of minimum exchange times and maximum exchange times as shown in distance from individual injections sites and estimated by STAMMT-L.

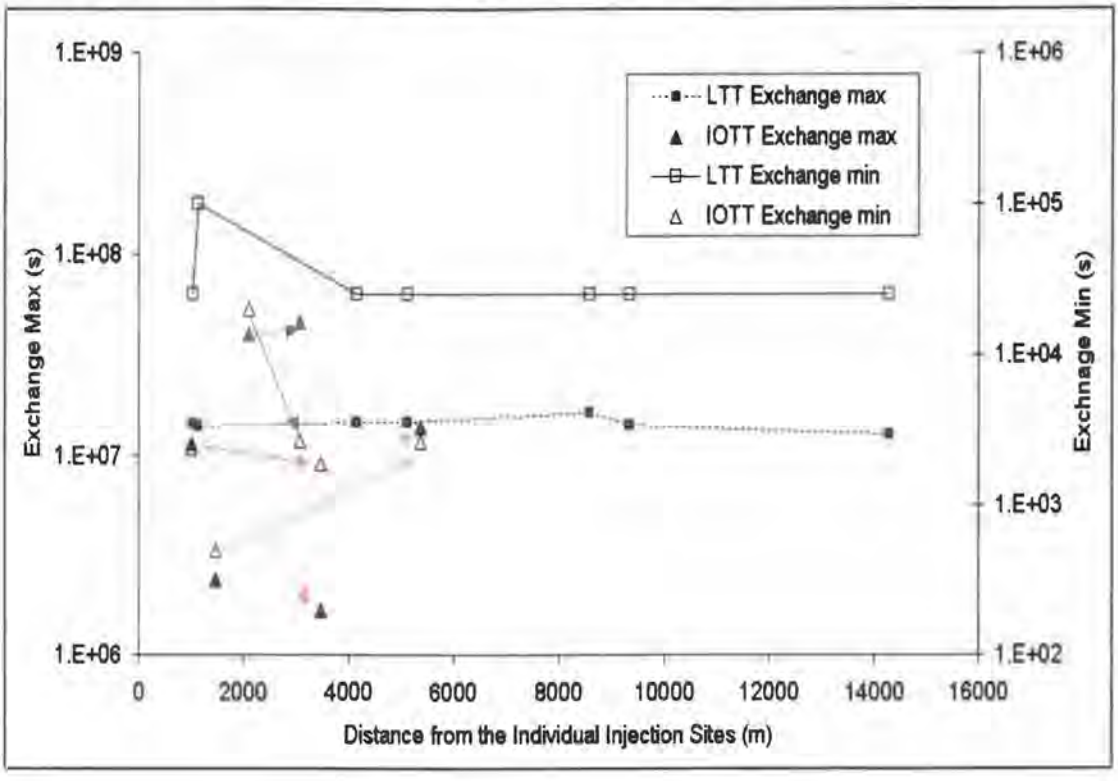

8.4. Discussion

8.4.1. Velocity

The melting of the snow pack and the draining of the mountain hillslope and soil reduced the stream recharge, which caused the declining hydrograph. The trend of higher stream velocity during the LTT compared to the IOTT was a result of the natural hydrograph decline throughout the summer (Figure 38 and Figure 49).

The increase of velocity longitudinally within each of the tracer tests was also expected. Generally as the stream network increases the discharge increases and increases in discharge are accompanied by increase in velocity as well as width and depth of the stream channel.

8.4.2. Dispersion (D_L)

During the LTT and the Cold Cr. IOTT dispersion increased in the downstream direction but the dispersion decreased downstream in the Mack Cr. and McRae Cr. IOTTs (Figure 50). The dispersion modeled in the stream does not show a clear pattern (Figure 50 and Figure 51). The dispersion parameter D_L is likely sensitive to both the distance from the injection site and the types of geomorphology that the test is conducted in. The different values of dispersion observed at the same location during different tests indicate that large variability can be observed in the same stream. Factors that affect this variability include geomorphology, discharge, and tracer test reach length. The decline in variability observed in the LTT is likely a product of not having similarly large duplicate tests (Figure 51). However, a characteristic threshold length may exist where that variability collapses down to a basin wide value.

8.4.3. Dilution Factor

The higher discharges of the LTT and the associated larger volume of stream recharge from the stream's source aquifer may have caused a larger degree of dilution during the first test. Later in the summer, during the IOTTs, there was less recharge to the stream and therefore, the degree of dilution was reduced. These factors may have contributed to the pattern seen in Figure 52 were the LTT was shown to be consistently more diluted than the IOTTs. The length of the tracer test was another factor that may have contributed to the differences in the dilution between the LTT and the IOTTs (Figure 53). A longer test reach allows a larger volume of influx of fresh recharge water to enter the stream and hence dilute the concentration of RWT in the stream. Figure 53 shows a clear relationship of increased dilution with increased distance that the solute tracer travels for the injection site.

An additional reason for the observed increase in dilution with distance from the injection sites could be the influences of sorption of RWT to clays minerals, iron minerals, and organic materials. The increase in distance from the respective injection sites is accompanied by an increase in the probability that the RWT will

have been exposed to substance that will cause sorption. Normally RWT sorption is linear within the Lookout Cr. basin and would be expected to be gradually release in the late time. However, with the decline in discharge in the stream and the accompanying lowering of the stage, it maybe that some of the RWT was attached to particles that were dried up and left out of the stream system. The abandon RWT was then left unaccounted for in the tracer test and will remain there until the stream stage raises enough to reactivate it. The modeling program may have accounted for the absorbed RWT by adjusting the dilution factor to match the concentration with the stream discharge.

8.4.4. Ratio of Hyporheic Volume to Stream Volume: β_{tot}

During the LTT, the β_{tot} increased down stream until below Mack Cr. after which the value declines from 169 to 77 (Figure 54 and Table 4). This change in trend may be a result of the geomorphic change from a boulder/log jam step pool geomorphology to a regime dominated by less large steps, more cascades, wider flood plains, and more secondary channels. The large step pool geomorphology, which is characterized by a large impoundment of sediments with high hydraulic potential, provides a large volume of sediment for flow paths to occupy. Additionally, the stream in these upper step pool regimes is comparatively smaller in total discharge, which allows for the ratio of immobile zones and mobile zones to become large. The lack of a defined pattern in the β_{tot} during the LTT and the IOTT indicates that the β_{tot} is not dependent on the distance from the injection sites rather the tests are sensitive to sub-reach geomorphological changes and the accumulated effect from the above reaches (Figure 54).

The argument that the β_{tot} is influence by geomorphic characteristics may be further supported by looking at the changes in β_{tot} along the longitudinal profile of Lookout Cr. (Figure 19). Looking at the general trend of increasing or decrease β_{tot} among individual tracer tests the trends seems to be consistent between tests over the same stream reach (Figure 19). For example, the Cold Cr. IOTT showed an increase in the β_{tot} in the downstream direction and the Mack and McRae Cr. IOTT showed a general decline downstream, which matches the pattern that β_{tot} took

during the LTT (Figure 19). The pattern may indicate an expansion and contraction of the hyporheic zone along the longitudinal profile of Lookout Cr. The change in the size of the hyporheic zone is heavily influenced by changes in the geomorphic characteristics of the stream.

Looking at the values of β_{tot} from the LTT and the IOTTs it is apparent that the values vary between tests for the same longitudinal monitoring sites, but the meaning of this variation is not clear (Figure 19). For example, the values of β_{tot} during the IOTTs at Cold Cr. and McRae Cr. were higher than the values of β_{tot} at the same locations during the LTT (Figure 19). However, the Mack Cr. IOTT had lower β_{tot} values than the LTT values (Figure 19). These observed differences may be a result of the interplay between the reach length, geomorphology, injections time, and discharge. The physical hyporheic conditions in certain reaches such as between Cold Cr. and Mack Cr. and below McRae Cr. may accommodate a larger percentage of hyporheic flow during summer low flows. For example, as the stream discharge decreases through summer some geomorphic features may allow the same amount of stream water to utilizing the same amount of hyporheic zone. If the same amount of hyporheic flow is traveling through the same amount of hyporheic volume then the modeling program would register a larger ratio between the stream and hyporheic zone, because the stream volume would have decrease with decreasing discharge.

Another factor that could be influencing the changes in β_{tot} could be groundwater recharge. For example, a stream reach like Mack Cr. to McRae Cr. could be influenced by groundwater recharge. Assuming that the groundwater recharge stays constant throughout the summer then as the discharge of a reach declines through summer the ground water recharge would have a greater influence on the β_{tot} as the summer progressed. The greater influence of groundwater recharge would then reduce the amount of hyporheic zone sensed by the tracer test.

Finally the last influence on the STAMMT-L estimates of β_{tot} that must be considered is sorption. The sorption of RWT to clay minerals, iron minerals and organic matter causes the RWT to become trapped in the hyporheic zone for an

unspecified amount of time and as a result acts as a retardation factor. The retardation of RWT by sorption is increased as the distance from the injection site increase due to the increased probability that the RWT will become sorbed to a surface. The shift in the breakthrough curve that is a result in the retardation of RWT causes our estimates of β_{tot} to be over estimates, further more the error in the estimates increases with increasing distance from the injection sites.

The values of stream volume and hyporheic volume estimated from stream cross sectional area and β_{tot} values are reported in Table 6.

8.4.5. Mass Recovery

The longer time the tracer spent in the stream system, the greater the potential that the RWT was exposed to sorption from clay minerals, iron silicates, organic matter, and photochemical decay. It was expected that some tracer would be lost over a given reach and that loss would increase with distance downstream. In fact the decline in the mass of RWT recovered with distance from the injection site was observed in all the tracer tests (Figure 55).

Tracer sorbed by the materials in the stream may be reactivated by diffusion at a later time in the test and reenter the stream. This released RWT would be recorded in the late time breakthrough curve as a long residence time pathway. This sorption caused long residence time pathways would eventually be recorded. However, a possible explanation for the lack of test recognition of the longest pathways and some of the lost amount of tracer could be the monitoring duration. Because the concentration tails decline as a power-law, a large amount of tracer mass is accounted for in the tail. The shallower the slope of the power-law tail the larger the amount of mass in the tail.

Monitoring duration and sensitivity became an important issue as the RWT concentration declined. The longer the stream is monitored, the greater the amount of tracer would be recovered in the tail. The power-law tail theoretically continues to lower and lower concentrations into infinite time. Based on this assumption, 100% recovery is not possible for any finite experiment and incredibly sensitive machines would be necessary to record low concentrations of

really late arrival times. However, practically speaking, a time can be reached when the concentrations becomes undetectable and are obscured by the natural background before all of the mass is recovered. The time it takes to return to background concentration levels is directly related to the slope of the power-law in that reach. This phenomenon is described as the distribution of residence times for that reach. The time to background is also dependent on the concentration of the injection, the injection time, and the length of the reach that is being monitored.

Another possible explanation for the loss of RWT during the LTT and the IOTTs is the abandonment of sorbed RWT on particles as the stream stage declines through the summer. Once the stage of the stream declines the RWT that is abandoned until the rain events cause the stage to rise again.

A relationship is observed by looking at all of the monitoring sites for all of the tracer tests together and evaluating there mass recovered by the distance from there injection sites. This relationship is shown to be an exponential decline in mass recovery with distance from individual injection sites (Figure 56).

8.4.6. Minimum exchange time (α_{max}) and Maximum exchange time (α_{min})

The sensitivity of STAMMT-L and the tracer tests to α_{min} and α_{max}, maximum and minimum exchange times respectively, was a surprise and a challenge. In order to use STAMMT-L to model power-law behavior of concentration curves, the α_{min} and α_{max} were needed to set boundaries on the behavior, because of the finite time of the tracer tests. Originally we thought that as long as α_{min} and α_{max} were set at values significantly greater than or less than maximum and minimum exchange times respectively, then the program would function and the values would have an insignificant effect on the real solutions. We found that during our long tracer test, the STAMMT-L solutions were affected by the α_{min} and α_{max} truncation values. The values seemed to vary the greatest between tests. The LTT had very little change in values over the entire longitudinal profile (Figure 57 and Figure 58). However, the IOTTs each had their own independent values, which seemed to grow farther apart with distance downstream (Figure 58).

9.0 APPENDIX III: STORM RESPONSE

9.1. Background

The longitudinal tracer test (LTT) and the Cold Creek intra-order tracer test (IOTT), conducted during the summer of 2003 on Lookout Creek in H.J. Andrews, Oregon resulted in an observed solute behavior that is not completely explained. The LTT was commenced on June 14, 2003 and continued through November 15, 2003. The Cold Cr. IOTT was commenced on September 11, 2003 and continued through October 5, 2003. During this time interval, the fall storm season in the Western Cascades began. This allowed a unique opportunity to observe the solute tracer response to several storm events at differing residence time distributions.

Throughout the summer of 2003 there was little or no precipitation, with the first rain event occurring on August 6, 2003 (Figure 21). From the start of the LTT to the first rain event the Lookout Cr. hydrograph steadily declined (Figure 38). Between August 6, 2003 and November 15, 2003 there were ~11 different rain events and after each event the hydrograph decline towards base flow (Figure 21). Many of these storm events increased the stream hydrograph 2 to 7 times were as little or no change in the concentration of RWT was observed (Figure 21, Figure 22, and Figure 23).

9.2. Methods

The concentration breakthrough curves for this section of the LTT and the Cold Cr. IOTT were gathered using the same tests and methods outlined in Appendix I: Detailed Methods. The hydrographs used in this storm analysis were also derived using the gauged basin regression technique outlined in Appendix I: Detailed Methods. The monitoring sites that captured the concentration and hydrographic response to the early fall storm events included the Above Cold Cr. Site #2, Below Cold Cr. Site #4, Longer Cr. Site #5, and Above Mack Cr. Site #6.

9.3. Results

The main storm events that were observed during the LTT and the Cold Cr. IOTT occurred on August 6, September 7, 9, 16, October 8-10, 11, 15, 19, 22, 29, and November 12, 2003 and are labeled in Figure 21.

The concentration decline during the LTT at the above cold Cr. site is shown in Figure 59 along with the hydrograph for that site during the same time. In Figure 59 the discharge of the above Cold Cr. site is shown by a solid line and the values are given on the left y-axis. The in stream RWT concentrations are shown by a open squares and their values are given on the right y-axis in Figure 59. In Figure 59 the best fit regressions equation for the decline of the RWT concentrations after several of the rain events are shown with boxes and arrows pointing to the segment of the curve that they correspond to.

The decline of the RWT concentration in the stream does not appear to be significantly effected by the increase in the hydrograph after many of the storms. The 1st, 5th, 7th, 8th, 9th, and 10th storm events do not show any increase in decline in concentration at the above Cold Cr. LTT site, Longer Cr. IOTT site, or the above Mack IOTT site (Figure 22, Figure 23, and Figure 59). The 2nd, 3rd, 4th, 6th, and 11th storm events do show some decline, but the decline does not appear to be proportional to the increase in the stream hydrograph (Figure 59).

The decline that is observed in the LTT site after the 2nd, 3rd, 4th, 6th, and 11th rain events may be shown by changes in the rate of decline expressed as different exponential or power-law functions that best characterize their decline (Figure 59).

The concentration decline during the Cold Cr. IOTT at the Longer Cr. site and Above Mack Old Growth site are shown in Figure 22 and Figure 23 along with the hydrograph for that site during the same time. The 4th storm event on September 16, 2003 at both the Longer Cr. site and Above Mack Old Growth sites, appears to have a slight decline in concentration that was not proportional to the amount of the observed hydrographic rise (Figure 22 and Figure 23). The 5th thru 9th storm

events seem to have little or no effect on the concentration (Figure 22 and Figure 23).

Figure 59. Concentration at the above Cold Cr. site responses after rain events during the LTT.

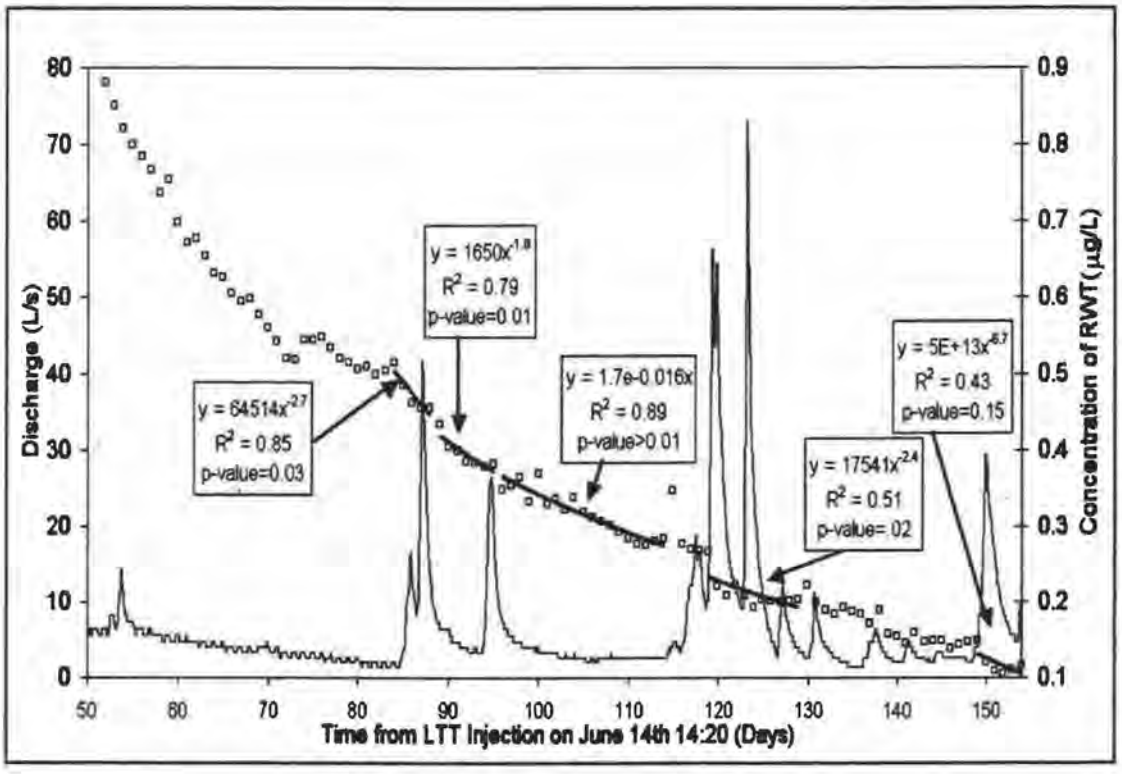

Figure 60 shows the concentration at the injection site ISCO™ during the Cold Cr. IOTT. The hydrograph is shown by a solid line with the values of discharge displayed on the left y-axis of Figure 60. The RWT concentration of at the injection monitoring site are shown by solid triangles with a dotted line connecting them (Figure 60). The RWT concentrations are given on the right y-axis in Figure 60 and the x-axis is the time from the Cold Cr. IOTT injection. The concentration at the injection site during the decline of the Cold Creek IOTT breakthrough curve was very sporadic and shows a behavior not observed elsewhere. The injection site concentrations increased after the 4th storm event and then fluctuated upward during period of no storms (Figure 11 and Figure 60).

Figure 60. The concentration and the hydrograph at the Injection site during the Cold Cr. IOTT.

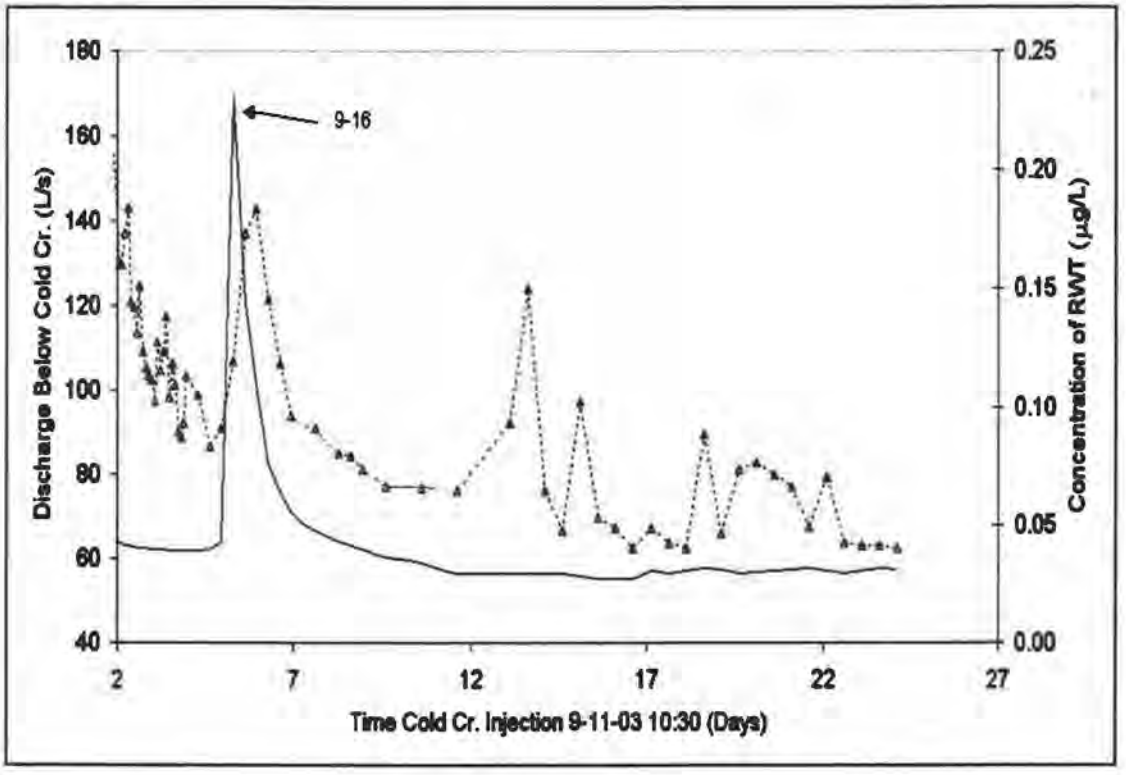

9.4. Discussion

There are two main issues concerning the solute tracer response to fall rain events. The first issue is the small or no change in concentration during proportionally large rain events for three different monitoring sites involving the LTT and the Cold Cr. IOTT. The second issue is the large response and sporadic spikes observed at the Cold Cr. IOTT injection ISCO™ site, which is in the middle of the sites that showed no change in concentration.

The lack of a major decline in the concentration in response to the increase in the stream hydrograph must mean that the water added to the stream during rain events is entering the stream as RWT labeled water. One possible explanation is that this labeled water entering the stream during early fall storm events is coming from the hyporheic zone and may be derived from flow paths that are as much as 5 months old. The change in the saturated zone and the stage level of the stream may

be causing the hydraulic gradients within the stream to increase enough to activate or increase the rate of exchange within the hyporheic zone. This increased activity of the hyporheic zone may then deliver labeled water to the stream at levels that allow the concentration in the stream to stay constant even though the volume of water has increase substantially. The surprising aspect of this scenario is that it appears to activate just enough RWT to keep the concentration near steady and it does not activate more RWT and cause a rise.

Another possible mechanism for the steady concentration during rain events could be coming from interplay between sorption and stage level increases. During the higher stage levels of the summer when the LTT was showing high concentrations in the upper levels of Lookout Cr. sorption may have stranded RWT out of the stream. The addition of the rain activated stream water causes the stream stage to rise back to earlier levels and then may mobilize the stranded RWT. However, again this does not explain the exact balance achieved between RWT and discharge that allowed the concentration to remain constant and not increase.

The fact that the decline after the first couple of storms appears to continue at either a exponential decay or a power-law decay may be due to the RTDs of the reach. Figure 59 shows that after each storm the decline in concentration behaves slightly differently, as represented by the different exponential and power-law equations that characterize the decline. These different equations may represent different RTDs and may indicate that the each storm activates slightly different flow paths within the hyporheic zone. Another possible explanation is that the observed decline may also be a remnant of the previous decline and may only experience a small drop in concentration before continuing back to the original declining behavior.

It appears that the hyporheic zone may have strong controls on the origin of water being released during the first storms of the fall season. As the storm season progresses it appears that the amount of decline increases. This may be a result of fresh rainwater from the earlier storm working through the medium range flow paths within the flow path distributions. The two lower IOTT sites may have had

no response in the late time concentration of RWT because they had lost sensitivity to small concentration changes due to the already low concentrations.

The observed increase in concentration at the injection site during the Cold Creek IOTT may be explained by the reoccupation of abandoned immobile zones. The LTT may have filled immobile zones during high discharges from the June injection. Throughout the summer the discharge slowly dropped and may have isolated high concentrations of water in pools or pockets. The dropping discharge may have left rocks and substrate with RWT that was absorbed to them isolated from the hydrological system. The first storm in the upper reach may have reactivated the abandoned immobile zones and RWT absorbed substrate. The reactivated area then caused a pulse of higher concentration of RWT to be observed at the monitoring sites. This response may be indicative to headwater streams where the system is flashy and experiences rapid rises and falls in the stage of the stream relative to the in stream discharge. A pulse of RWT may only have been sense by a monitoring site that is close enough to the trapped pools to see the pulse and dispersion could spread the pulse out enough that the lower monitoring site, which is 2059 m downstream, may not register the increase.

10.0 APPENDIX IV: SYNOPTIC SAMPLES

10.1. Background

The longitudinal tracer test (LTT) conducted on Lookout Creek, Oregon within the boundaries of the H.J. Andrews during the summer of 2003, presented unique opportunities to evaluate solute transport and water quality characteristics within a stream network. The main purpose of conducting a RWT dye tracer test was to monitor the concentration at a given location downstream of the injection site and establish a concentration breakthrough curve.

The breakthrough curve can then be analyzed to convey information about the physical characteristics of that stream reach. The breakthrough curve presents a temporal picture of how the concentration changes through time at one location. Another way of viewing the same system is to take a spatial perspective of the same tracer test. Gathering RWT concentrations at spaced intervals longitudinally along the stream network at the same time gives a spatial view of a tracer test. This spatial analysis technique of the RWT concentration during the LTT injection was attempted by conducting a synoptic sampling procedure.

10.2. Methods

Roy Haggerty and Mike Gooseff gathered synoptic samples on June 17, 2003 during the last day of the RWT tracer injection for the LTT. The gathering procedure involved walking down Lookout Creek and taking grab samples of the stream water approximately every 100 m to 150 m. Other information gathered at each sampling site included, time, GPS position, and electric conductivity. The most affective synoptic sampling is to sample at various longitudinal sites all at the same time, however because of limited personnel the samples were collected as a team walked down the stream over the course of 9 h.

The GPS locations of the sample sites were entered into the H.J. Andrews Arc Hydro Data Model described in detail in Appendix I: Detailed Methods, and converted to Universal Transverse Mercator (UTM) coordinates. Some of the sample sites did not have GPS positions and coordinates were estimated using

evidence of distance downstream and physical observations about location given in the field notes. Additionally, the entire set of GPS positions was shifted 20 to 40m off the stream channel. This shift implied that a systematic positioning error occurred throughout the data set. We adjusted for the error by using waypoints 20, 39, and 51 to spatially reorient all of the waypoints closer to the river layer. The waypoints were linked to the known locations of the Cold Creek, Longer Creek, and Mack Creek confluences. After adjustment, some points were still off of the drainage line stream layer. The field note evidence was then used to adjust most of the waypoints that corresponded to known locations (i.e. head of a previous test known as 410 and bottom another test known as 411). In some cases, points had to be moved onto the drainage line without evidence. In these cases, the points were moved directly perpendicular to the drainage line stream location. In all cases, the snapping tool was used to put the point on the line. The positions of each of the synoptic samples are shown in Figure 61, Table 7, and Table 8.

Figure 61 shows a digital elevation map of the upper reaches of Lookout Cr. The main stem of Lookout Cr. is labeled as well as the LTT injection site, Cold Cr., Longer Cr., and Mack Cr. (Figure 61). In Figure 61 the locations of the synoptic samples are shown as yellow circles.

The synoptic samples were collected between 9:03 and 17:33. The total collection time was 8 h and 30 min. Samples were collected over a distance of 5,378 m (Figure 61).

Figure 61. The positions of the synoptic samples take on June 17, 2003 during the injection of the LTT.

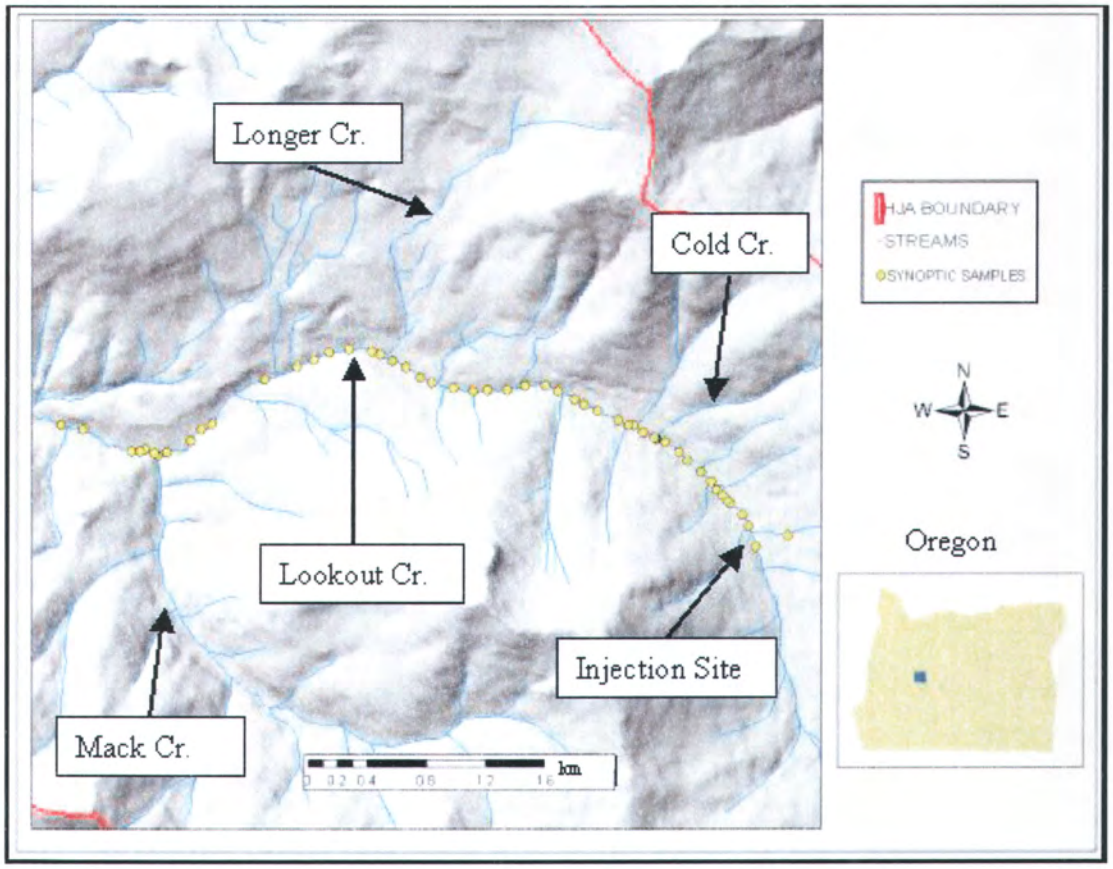

Table 7. Summary of synoptic samples taken during the LTT on June 17, 2003 between 9:03 and 17:34.

Sample #	Cumulative Distance (m)	Upslope Area (km^2)	Time (h:min)	Concentration w/blank subtracted	Waypoint No.	UTM (x)	UTM (y)
1	0	3.81	9:03	137.4	7	570389	4897004
2	90	4.14	9:09	142.6	8	570321	4897068
3	200	4.28	9:15	104.8	9	570241	4897141
4	236	4.53	9:20	93.4	10	570229	4897182
5	274	4.54	9:25	83.2	11	570274	4897241
6	326	4.56	9:31	77.0	12	570180	4897285
7	398	4.82	9:38	64.4	13	570100	4897284
8	495	4.98	9:41	63.0	14	570042	4897361
9	610	5.23	9:48	56.4	15	569974	4897457
10	686	5.34	9:54	55.6	16	569901	4897497
11	810	5.39	10:10	52.4	17	569795	4897556
12	882	6.18	10:19	54.5	19	569723	4897574
13	971	6.26	10:32	21.1	21	569640	4897607
14	1087	7.38	10:43	15.1	23	569558	4897685
15	1164	7.71	10:49	14.4	24	569487	4897707
16	1284	7.84	10:56	14.0	NA	NA	NA
17	1415	7.95	11:10	13.4	26	569285	4897827
18	1492	8.06	11:19	13.3	27	569198	4897835
19	1616	8.89	11:26	11.9	28	569127	4897931
20	1713	8.93	11:35	11.8	29	569039	4897947
21	1852	8.98	11:45	11.4	30	568907	4897901

Table 8. Summary of synoptic samples taken during the LTT on June 17, 2003 between 9:03 and 17:34.

Sample #	Distance from above site (m)	Upslope Area (km^2)	Time (h:min)	Concentration w/blank subtracted	Waypoint No.	UTM (x)	UTM (y)
22	120	9.63	12:13	11.31	31	568794	4897896
23	136	9.71	12:22	10.71	32	568683	4897887
24	94	9.75	12:29	10.61	33	568589	4897916
25	139	9.95	12:39	9.71	34	568478	4897931
26	150	10.57	12:46	8.88	35	568356	4897943
27	80	10.61	12:55	7.97	36	568243	4897942
28	118	10.68	13:04	6.90	37	568157	4898022
29	105	10.95	13:11	6.67	38	568071	4898099
30	156	13.74	13:28	3.48	40	567946	4898178
31	161	13.95	1337	3.20	41	567806	4898204
32	132	14.00	13:48	3.29	42	567678	4898188
33	115	14.13	13:59	3.07	43	567579	4898142
34	128	14.18	14:06	3.29	44	567477	4898084
35	98	14.29	14:18	2.88	NA	NA	NA
36	136	14.98	14:31	2.82	45	567478	4897973
37	80	15.01	14:51	2.53	NA	NA	NA
38	78	15.02	15:18	2.27	NA	NA	NA
39	73	16.12	15:25	2.12	NA	NA	NA
40	79	16.14	15:34	2.17	NA	NA	NA
41	101	16.26	15:42	2.24	NA	NA	NA
42	108	16.36	15:51	2.21	NA	NA	NA
43	148	16.43	15:59	2.21	48	566696	4897626
44	121	16.50	16:10	2.20	NA	NA	NA
45	89	16.52	16:18	2.22	49	566498	4897515
46	74	16.53	16:26	2.00	50	566439	4897459
47	26	25.15	16:35	1.26	51	566427	4897460
48	105	25.20	16:59	1.50	53	566376	4897551
49	53	25.22	17:06	1.53	54	566301	4897507
50	101	25.26	17:12	1.63	NA	NA	NA
51	106	25.31		1.47	NA	NA	NA
52	317	26.17	17:34	1.43	56	565893	4897736

10.3. Results

The concentrations of the synoptic samples are shown in Figure 62. The concentrations declined steadily with distance from the injection site (Figure 62). Sharp declines in sample concentrations were noticed at all of the major tributaries (Figure 62). In Figure 62 the concentrations of the monitoring sites are shown in open triangles and the synoptic sample concentrations are shown by solid

triangles. The concentration of the monitoring sites are generally in agreement with the synoptic samples. However, the above Cold Cr. site had a higher concentration 87.6 µg/L then the synoptic sample 54.5 µg/L gather at the same time and location.

Figure 62. The concentrations of the synoptic samples and concentration at the upper monitoring sites take during the injection of the LTT in semi-log space, June 17th 2003.

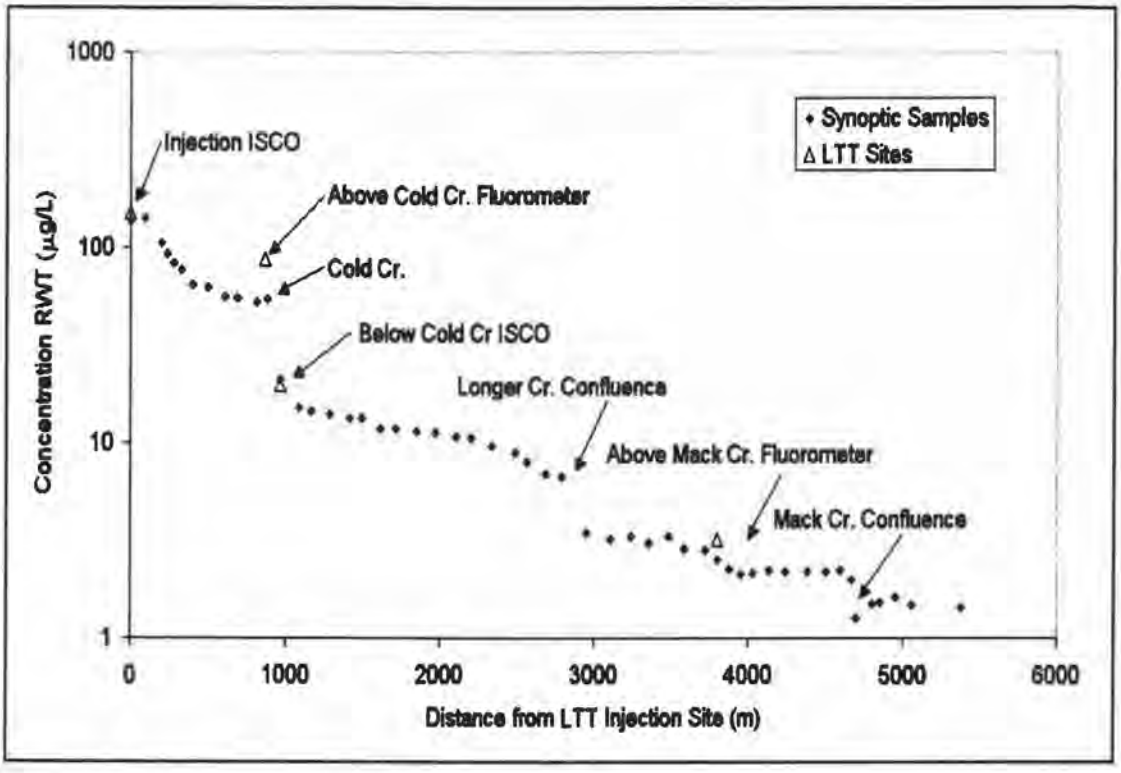

In Figure 63 the concentration of the synoptic samples vs. upslope contributing area is shown in log-log space. The concentrations of the monitoring sites are represented as open triangles and the synoptic sample concentrations are shown by solid triangles. A power-law fit has been shown to represent the declining sample concentrations with increasing basin size with an $r^2 = .96$ and a p-value >.01 (Figure 63).

Figure 63. The concentrations of the synoptic samples and concentration at the upper monitoring sites vs. the contributing basin area take during the injection of the LTT in semi-log space, June 17th 2003.

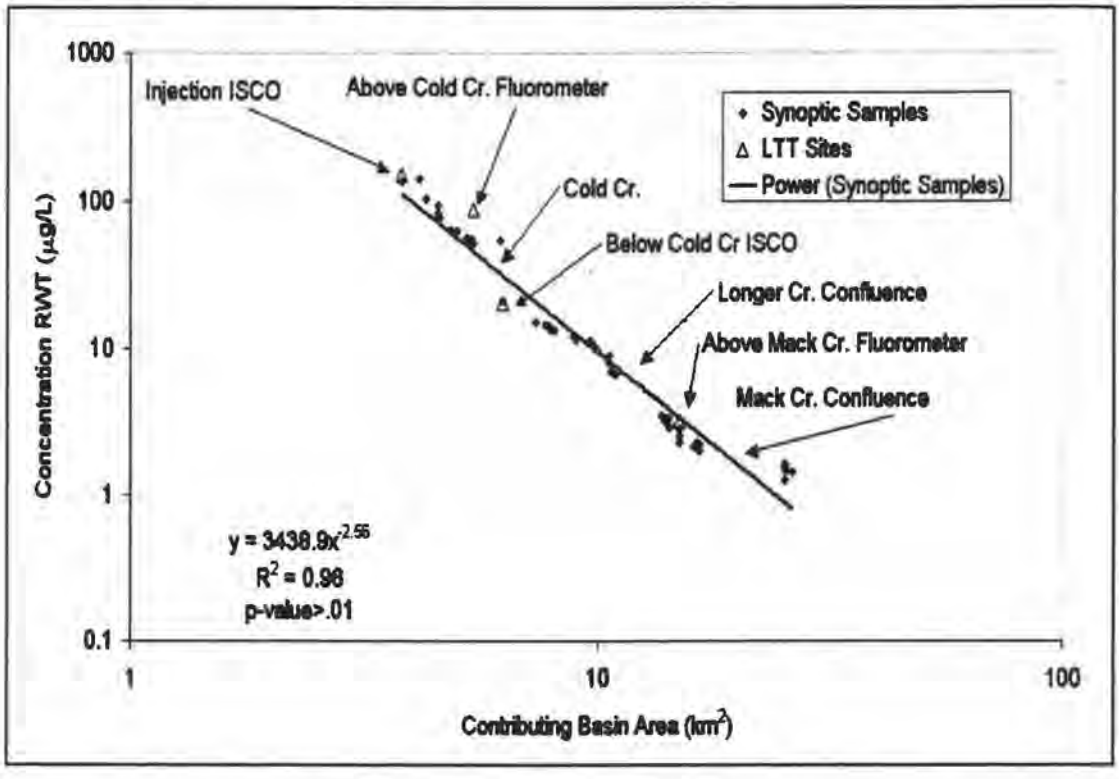

10.4. Discussion

The addition of unlabeled water from the tributaries along Lookout Cr. was expected to dilute the concentrations of RWT within the stream. The synoptic samples confirm that the major confluences contribute enough additional discharge to decrease the measured concentration of RWT in the stream by dilution.

A closer look at the declines in concentration associated with the Cold Cr., Longer Cr., and the Mack Cr. confluences illustrates the differences between Cold Cr. and the other tributaries. The decline in concentration below the Cold Cr. confluence is larger then the decline at Longer Cr. and Mack Cr. even though the increase in contributing basin area is much smaller at Cold Cr. This observation leads to the conclusion that Cold Cr. has a larger apparent contributing area then is

represented by the in-basin contributing area. In other words the Cold Cr. basin has inputs from outside of its delineated basin presumably by groundwater transfer.

The decline in concentration with increasing basin area follows a power-law decline. The reasons for this decline are unknown.

The reasons for the higher concentration at the fluorometer monitoring site above Cold Cr. compared to the synoptic samples is unknown. Laboratory analytical error remains a possibility but the samples were run several times with a insignificant difference between the runs.

REFERENCES

Andrews Experimental Forest, H. J. (2003). H.J. Andrews Experimental Forest, USDA Forest Service Pacific Northwest Research Station, Oregon State University and the Willamette National Forest. www.fsl.orst.edu/lter.

Bencala, K. E., R.E. Rathbun, A.P. Jackman, V.C. Kennedy, G.W. Zellweger, and R.J. Avanzino (1983). "Rhodamine wt dye losses in a mountain stream environment." Water Resources Bulletin 19(6): 943-950.

Bencala, K. E., and R.A. Walters (1983). "Simulation of solute transport in a mountain pool-and-riffle stream: A transient storage model". Water Resources Research 19: 718-724.

Bencala, K. E., J.H. Duff, J.W. Harvey, A.P. Jackman, and F.J. Triska (1993). "Modeling the stream-catchment continuum." Modeling Change in Environmental Systems. A. J. Jakeman, M.B. Beck, M.J. McAleer. New York, NY, John Wiley and Sons, Inc.

Benda, L. E., D.J. Miller, T. Dunne, G.H. Reeves, and J.K. Agee (1998). "Dynamic landscape systems". River Ecology and Management: Lessons from the Pacific Coastal Ecoregion. R. J. N. and R. E. Bilby. New York, Springer-Verlag.

Bloschl, G., and M. Sivapalan (1995). "Scale issues in hydrological modeling: a review." Hydrological Processes 9: 251-290.

Bond, B. J., J.A. Jones, G. Moore, N. Phillips, D. Post, and J.J. McDonnell (2002). "The zone of vegetation influence on baseflow revealed by diel patterns of streamflow and vegetation water use in a headwater basin." Hydrological Processes. 16: 1671-1677.

Bond, B. 2003. "Hydrology and ecology meet--and the meeting is good." Hydrological Processes. 17: 2087-2089.

Choi, J., J.W. Harvey, and M.H. Conklin (2000). "Characterizing multiple time scales of stream and storage zone interaction that affect solute fate and transport in streams." Water Resources Research 36(6): 1511-1518.

Cirmo, C. P. and. J. J. McDonnell (1997). "Linking the hydrologic and biogeochemical controls of nitrogen transport in near-stream zones of temperate-forested catchments: a review." Journal of Hydrology 199: 88-120.

Cvetkovic, V. and. R. Haggerty (2002). "Transport with multiple-rate exchange in disordered media." Physical Review 65(5):051308-1 - 051308-9

Environmental Systems Research Institute, Inc. (ESRI) "Arc Hydro Tools- Tutorial." Redlands, California, USA. Environmental Systems Research Institute, Inc., May 2002.

Feder, J. "Fractals." New York: Plenum, (1988).

Fernald, A., D. Landers, and P.J. Wigington (2000). "Water quality effects of hyporheic processing in a large river." American Water Resources Association Technical Publication Series TPS-00-2: 167-172.

Fernald, A.G., P.J. Wigington Jr., and D. H. Landers (2001). "Transient storage and hyporheic flow along the Willamette River, Oregon: Field measurements and model estimates." Water Resources Research 37(6): 1681-1694.

Findlay, S. (1995). "Importance of surface-subsurface exchange in stream ecosystems: The hyporheic zone." Limnology and Oceanography 40(1): 159-164.

Franken, R.J., R.G. Storey, and D.D. Williams (2001). "Biological, chemical and physical characteristics of downwelling and upwelling zones in the hyporheic zone of a north-temperate stream." Hydrobiologia 444: 183-195.

Gooseff, M. N., S.M. Wondzell, R. Haggerty, and J. Anderson (2003). "Comparing transient storage modeling and residence time distribution (RTD) analysis in geomorphically varied reaches in the Lookout Creek basin, Oregon, USA." Advances in Water Resources 26(9): 925-937.

Gooseff, M. N., J. LaNier, R. Haggerty, and K. Kokkeler (in press). "Determining in-channel (dead zone) transient storage by comparing solute transport in a bedrock channel - alluvial channel sequence, Oregon, USA " Water Resources Research.

Gooseff, M. N., J. Anderson, J. LaNier, R. Haggerty, and S.M. Wondzell (in press). "A modeling study of hyporheic exchange pattern and the sequence, size, and spacing of stream bedforms in mountain stream networks, Oregon, USA." Hydrological Processes.

Grant, G. E., F.J. Swanson, and M.G. Wolman (1990). "Pattern and origin of stepped-bed morphology in high-gradient streams, western Cascades, Oregon." Bulletin of the Geological Society of America 102: 340-352.

Haggerty, R. (1995). "Aquifer remediation in the presence of rate-limited mass transfer." Ph.D. dissertation, Stanford University, Stanford, California.

Haggerty, R., and S.M. Gorelick (1995). "Multiple-rate mass transfer for modeling diffusion and surface reactions in media with pore-scale heterogeneity." Water Resources Research 31:2383-2400.

Haggerty, R., and S.M. Gorelick (1998). "Modeling mass transfer processes in soil columns with pore-scale heterogeneity." Soil Science Society of America Journal 62(1), 62-74.

Haggerty, R., S.A. McKenna, and L.C. Meiges (2000). "On the late-time behavior of tracer test breakthrough curves." Water Resources Research 36(12): 3467-3479.

Haggerty, R., and P. Reeves (2002). STAMMT-L version 1.0 user's manual, Sandia National Laboratories, Albuquerque, New Mexico.

Haggerty, R., S.M. Wondzell, and M.A. Johnson (2002). "Power-law residence time distribution in the hyporheic zone of a 2nd -order mountain stream." Geophysical Research Letters 29(13).

Haggerty, R., C.F. Harvey, C.F. von Schwerin, and L.C. Meigs (accepted to WRR 2003). " What controls the apparent timescale of solute mass transfer in aquifers and soils? A comparison of experimental results." Water Resources Research.

Harvey, J. W., and K.E. Bencala (1993). "The effect of streambed topography on surface-subsurface water exchange in mountain catchments." Water Resources Research 29(1): 89-98.

Harvey, J. W., B.J. Wagner, and K.E. Bencala (1996). "Evaluating the reliability of the stream tracer approach to characterize stream-subsurface water exchange." Water Resources Research 32(8): 2441-2451.

Harvey, J. W., B.J. Wagner, and K.E. Bencala (1996). Quantifying hydrologic interactions between streams and their subsurface hyporheic zones. Streams and Ground Waters. J. A. and P. J. M. Jones. San Diego, Academic Press: 425.

Harvey J.W., B.J. Wagner, J.H. Thorp (2000). " Quantifying hydrologic interactions between streams and their subsurface hyporheic zones." Streams and ground waters Academic Press, San Diego, CA, USA.

Henry, K. S., H.M. Valett, J.A. Morrice, C.N. Dahm, G.J. Wroblicky, M.A. Santistevan, and M.E. Campana (1994). Ground water-surface water exchange in two headwater streams. Second International Conference on Ground Water Ecology, Altanta, Georgia, American Water Resources Association.

Hinkle, S. R., J.H, Duff, F.J. Triska, A. Laenen, E.B. Gates, K.E. Bencala, D.A. Wentz, and S.R. Silva (2001). "Linking hyporheic flow and nitrogen cycling near the Willamette River- a large river in Oregon, USA." Journal of Hydrology 244: 157-180.

Jackman, A. P., R.A. Walters, V.C. Kennedy (1984) " Low-flow transport models for conservative and sorbed solutes; Uvas Creek, near Morgan Hill, California Pagination: 82." Water-Resources Investigations - U. S. Geological Survey.

Jackson, C. R., and C.A. Sturm (2002). "Woody debris and channel morphology in first and second order forested channels in Washington's coast ranges." Water Resources Research 38(9): 1177.

Jones, J. A., and G.E. Grant (1996). "Peak flow responses to clear-cutting and roads in small and large basins, western Cascades, Oregon." Water Resources Research 32(4): 959-974.

Jones, J. A., F.J. Swanson, B.C. Wemple, K.U. Snyder (2000). "Effects of roads on hydrology, geomorphology, and disturbance patches in stream networks." Conservation Biology. 14(1): 76-85.

Jones, J. A. (2000). "Hydrologic processes and peak discharge response to forest removal, regrowth, and roads in 10 small experimental basins, western Cascades, Oregon." Water Resources Research. 36(9): 2621-2642.

Jones, J.B., S.G. Fisher, and N.B. Grimm (1995). "Vertical hydrologic exchange and ecosystem metabolism in a sonoran desert stream." Ecology. 76(3): 942-952.

Kasahara, T., and S.M. Wondzell (2003). "Geomorphic controls on hyporheic exchange flow in mountain streams." Water Resources Research 39(1): 3-1 to 3-14.

Kirchner, J.W., X. Feng, and C. Neal (2001). "Catchment-scale advection and dispersion as a mechanism for fractal scaling in stream tracer concentrations." Journal of Hydrology 254: 82-101.

Knighton, A. D. (1984). The adjustment of channel form. Fluvial forms and processes. A. D. Knighton. Baltimore, MD, Edward Arnold.

Laenen, A., and K.E. Bencala (2001). "Transient storage assessments of dye-tracer injections in rivers of the Willamette basin, Oregon." Journal of the American Water Resources Association 37(2): 367-377.

Langbein, W. B., and L.B. Leopold (1964). "Quasi-equilibrium states in channel morphology." American Journal of Science 262(June): 782-794.

Leopold, L. B., and T. Maddock Jr. (1953). "The hydraulic geometry of stream channels and some physiographic implications." U.S. Geological Survey Professional Paper 252 252: 57.

Leopold, L. B., and W.B. Langbein (1962). "The concept of entropy in landscape evolution." U. S. Geological Survey Professional Paper (1962): A1-A20.

Mandelbrot, B.B. (1967). "How Long is the Coast of Great Britain? Statistical Self Similarity and Fractional Dimension," *Science*, 155: 636-638.

Mandelbrot, B.B. "The fractal geometry of nature." New York: W. H. Freeman and Co., (1982).

Malcolm, I. A., C. Soulsby, and A.F. Youngson (2002). "Thermal regime in the hyporheic zone of two contrasting salmonid spawning streams: ecological and hydrological implications." Fisheries Management and Ecology 9: 1-10.

Marion A., M.Bellinello, I. Guymer, A. Packman (2002). "Effect of bed form geometry on the penetration of non reactive solutes into a streambed." Water Resources Research 38(10): 1209.

Marsh-McBirney Incorporated (1994). "Open Channel Profiling Handbook." Fredrick, Maryland. P/N105 0030 01 REV2.

McDonnell, J.J. (1990). "A rationale for old water discharge through macropores in a steep, humid catchment." Water Resources Research 26(11): 2821-2832.

McDonnell, J.J. (2003). "Where does water go when it rains? Moving beyond the variable source area concept of rainfall-runoff response." Hydrological Processes 17: 1869-1875.

McGuire, K.J., D.R. DeWalle and W.J. Gburek (2002). " Evaluation of mean residence time in subsurface waters using oxygen-18 fluctuations during drought conditions in the mid-Appalachians." Journal of Hydrology 261: 132-149.

Meakin, P. "Fractals, scaling and growth far from equilibrium." Cambridge: Cambridge University Press, (1998).

Merigliano, M. F. (1997). "Hydraulic geometry and stream channel behavior: an uncertain link." Journal of the American Water Resources Association 33(6): 1327-1336.

Montgomery, D. R., and J.M. Buffington (1997). "Channel-reach morphology in mountain drainage basins." Geological Society of America Bulletin 109(5): 596-611.

Nakamura, F., F.J. Swanson, and S.M. Wondzell (2000). "Disturbance regimes of stream and riparian systems- a disturbance - cascade perspective." Hydrological Processes 14: 2849-2860.

Neuman, S. P. (1990). "Universal scaling of hydraulic conductivities and dispersivities in geologic media." Water Resources Research 26(8): 1749-1758.

Pickens, J. F., and G.E. Grisak (1981). "Scale-dependent dispersion in a stratified granular aquifer." Water Resources Research 17(4): 1191-1211.

Poff, N. L., J.D. Allen, M.B. Bain, J.R. Karr, K.L. Prestegaard, B.D. Richter, R.E. Sparks, and J.C. Stromberg (1997). "The natural flow regime." Bioscience 47(11): 769-784.

Sanchez-Cabeza, J., and L. Pujol (1999). "Study on the hydrodynamics of the Ebro river lower course using tritium as a radiotracer." Water Research 33(10): 2345-2356.

Schumm, S. A., and R.W. Lichty (1965). "Time, space, and causality in geomorphology." American Journal of Science 263(February): 110-119.

Schummer, R., D.A. Benson, M.M. Meerschaert, and B. Baeumer (2003). " Fractal mobile/immobile solute transport." Water Resources Research 39(10): 13-1 -13-12.

Seibert, J, K. Bishop, A. Rodhe and J. McDonnell (2003). " Groundwater dynamics along a hillslope: A test of the steady-state hypothesis." Water Resources Research 39(1): 2-1-2-9.

Snyder, K. U. (2000). Debris flows and flood disturbance in small, mountain watershed. Department of Forest Science. Corvallis, Oregon State University.

Stanford, J. A., and J.V. Ward (1993). "An ecosystem perspective of alluvial rivers: connectivity and the hyporheic corridor." Journal of North American Benthological Society 12(1): 48-60.

Stanley, E.H., and A.J. Boulton (1993). "Hydrology and the distribution of hyporheos: perspectives from a mesic river and a desert stream." Journal of North American Benthological Society 12(1): 79-83.

Storey, R. G., K.W.F. Howard, D.D. Williams (2003). "Factors controlling riffle-scale hyporheic exchange flows and their seasonal changes in a gaining stream: a three dimensional groundwater flow model." Water Resources Research 39(2): 8-1 to 8-17.

Strahler, A.N. (1964). "Quantitative geomorphology of drainage basins and channel networks" section 4-2, Handbook of Applied Hydrology. Ed. Ven te Chow, McGraw-Hill, New York.

Swanson, F. J., and M.E. James (1975). "Geology and geomorphology of the H.J. Andrews Experimental Forest, western Cascades, Oregon." U.S. Forest Service Pacific Northwest Paper PNW-188: 14.

Swanson, F. J., L.E. Benda, S.H. Duncan, G.E. Grant, W.F. Megahan, L.M. Reid, and R.R. Ziemer (1986). Mass failure and other processes of sediment production in Pacific Northwest forest landscapes. Streamside Management: Forestry and Fishery Interactions, Seattle, WA, University of Washington.

Swanson, F. J., and J.A. Jones (2002). "Geomorphology and Hydrology of the H.J. Andrews Experimental Forest, Blue River, Oregon." Field Guide to Geologic Processes in Cascadia: Oregon Department of Geology and Mineral Industries Special Paper 36.

Triska, F. J., Vance C. Kennedy, Ronald J. Avanzino, Gary W. Zellweger, and Kenneth E. Bencala (1989). "Retention and transport of nutrients in a third-order stream: channel processes." Ecology 70(6): 1877-1892.

Turner Designs. "Fluorometer user manual: Model 10-AU-005-CE." Sunnyvale, California, USA. Turner Designs, April 1999.

Valett, H. M., C.C. Hakenkamp, and A.J. Boulton (1993). "Perspectives on the hyporheic zone: integrating hydrology and biology. Introduction." Journal of North American Benthological Society 12(1): 40-43.

Valett, H. M., J.A. Morrice, C.N. Dahm, M.E. Campana (1996). "Parent lithology, surface-groundwater exchange, and nitrate retention in headwater streams." Limnology and Oceanography 41(2): 333-345.

Vannote, R. L., G.W. Minshall, K.W. Cummins, J.R. Sedell, and C.E. Cushing (1980). "The River Continuum Concept." Canadian Journal of Fisheries and Aquatic Sciences 37: 130-137.

Vitar, T., D. Burns, G. Lawrence, J.J. McDonnell and D. Wolock (2002). " Estimation of baseflow residence times in watersheds using the runoff recession hydrograph." Hydrological Processes 16: 1871-1877.

Wagner, B. J., and J.W. Harvey (1997). "Experimental design for estimating parameters of rate-limited mass transfer: analysis of stream tracer studies." Water Resources Research 33(7): 1731-1741.

Weiler, M., B.L. McGlynn, K.J. McGuire, and J.J. McDonnell (in press). " How does rainfall become runoff?: A combined tracer and runoff transfer function approach." Water Resources Research.

Wemple, B. C., F.J. Swanson, and J.A. Jones (2001). "Forest roads and geomorphic process interactions, Cascade Range, Oregon." Earth Surface Processes and Landforms 26: 221-234.

Wemple, Beverley C.; Jones, Julia A.; Grant, Gordon E. 1996. "Channel network extension by logging roads in two basins, western Cascades, Oregon." Water Resources Bulletin. 32(6): 1195-1207.

White, D.S. (1990). "Biological relationships to convective flow patterns within stream beds." Hydrobiologia 196: 149-158.

White, D.S. (1993). " Perspectives on defining and delineating hyporheic zones." Journal of North American Benthological Society 12(1):61-69.

White, D. S. (2002). "Biological relationships to convective flow patterns within stream beds." Hydrobiologia 196: 149-158.

Williams, D.D. (1993). "Nutrient and flow vector dynamics at the hyporheic/groundwater interface and their effects on the interstitial fauna." Hydrobiologia 251: 185-198.

Wolman, M. G., and J.P. Miller (1960). "Magnitude and frequency of forces in geomorphic processes." Journal of Geology 60: 54-74.

Wondzell, S.M. (Submitted to Hydrological Processes). Effect of channel and valley floor morphology, and of changing discharge, on hyporheic exchange flows in two small mountain streams,.

Wondzell, S. M., and F.J. Swanson. (1996). "Seasonal and storm dynamics of the hyporheic zone of a 4th order mountain stream. I: Hydrologic processes." Journal of North American Benthological Society 15(1): 3-19.

Wondzell, S. M., and F.J. Swanson. (1996). "Seasonal and storm dynamics of the hyporheic zone of a 4th order mountain stream. II: Nitrogen cycling." Journal of North American Benthological Society 15(1): 20-34.

Wondzell, S. M., and F. J. Swanson. (1999). "Floods, channel change, and the hyporheic zone." Water Resources Research 35(2): 555-567.

Wörman, A., A.I. Packman, H. Johansson, and K. Jonsson (2002). "Effect of flow-induced exchange in hyporheic zones on longitudinal transport of solutes in streams and rivers." Water Resources Research 38(1): 2-1 to 2-15.